

**ECOLE POLYTECHNIQUE FEDERALE DE LAUSANNE
SCHOOL OF LIFE SCIENCES**



Master project in Life Sciences Engineering

**AN INTRACRANIAL EEG STUDY ON HUMAN SHORT-TERM
MEMORY**

Carried out in the Kreiman Lab
At Harvard Medical School in Boston
Under the supervision of Prof. Gabriel Kreiman and PhD Yuchen Xiao

Done by

PAULA SÁNCHEZ LÓPEZ

Under the direction of
Prof. Silvestro Micera
Translational Neural Engineering Laboratory

EPFL

External Expert Prof. Gabriel Kreiman

LAUSANNE, EPFL 2022

Summary

Short-term memory (STM) is an essential brain capacity in our everyday live. STM allows us to store and maintain information in our memory for a short period of time. To study STM, we analyzed human intracranial EEG (iEEG) recordings of 20 epileptic patients while playing a classic matching card memory game. The memory game was a highly dynamic task in which subjects were initially presented with covered images on a board and were instructed to flip any two images each time, until all matching pairs were found. Hence, subjects had to keep track of the tiles' information in STM, allowing us to study how neural activities may track STM processes. We used the gamma band power as a proxy of neural activity, and we leveraged generalized linear models to simultaneously assess the relative contribution of multiple parameters to the neural responses. We found neural activities that contained information about non-associative or associative STM processes. Neural responses involved in non-associative memory encoded whether a tile was novel or familiar to the participants. Associative-memory neural activities could predict the correct retrieval from memory of a tile's pair location. Our analysis also revealed brain locations involved in object-category recognition. We found neural responses that encoded both the image category of the visualized tile and novelty or familiarity with the tile. In contrast, most of the electrodes that encoded successful retrieval of the tile's pair were not selective to specific image categories. To our knowledge, it is the first time that human neural responses involved in both subtypes of STM processes and object recognition have been studied under the same experimental paradigm.

Acknowledgements

I would like to express my sincere gratitude to Prof. Gabriel Kreiman for giving me the opportunity to complete my Master's work in his lab. Thanks for our weekly meetings in which I learned a lot from him and his inspiring comments and suggestions. I would also like to thank Yuchen Xiao, a Ph.D. in the lab with whom I work on the memory project, for all she taught me about intracranial EEG recording and our insightful discussions. Gabriel and Yuchen were excellent mentors and scientists, and I am thankful to have had the chance to work with them. I would also like to thank Silvestro Micera for supervising my project from Europe.

I am grateful to all the incredible friends I made during my Master's journey. Thanks to my friends in Lausanne, for all our weekend adventures and studying days, for making Lausanne feel like home. Thanks for making those two difficult years two of my most beautiful years. I would like to thank my dear friends in Boston, both inside and outside the lab, that made this year an unforgettable experience. Thanks for the places we discovered and for our stimulating conversations about science.

I would like to thank the Bertarelli Foundation for all the support this year. Thanks for giving me the opportunity to complete my Master's Thesis at Harvard Medical School and living in Boston. I would also like to thank La Caixa Foundation for giving me the chance to complete my Master's degree at EPFL. It has been a dream come true. Thanks to both foundations for making it possible, I could not be more grateful.

My deepest thanks to my family for always believing in me. Thanks for bringing me into the world of science and for the unwavering support. I feel very lucky.

Paula Sánchez López

Abbreviations

AMS	Associative Memory Selective
AUC	Area Under the Curve
BCH	Boston Children's Hospital
BWH	Bringham and Women's Hospital
CT	Computed Tomography
DVA	Degree of Visual Angle
EBA	Extrastriate Body Area
ECoG	Electrocortigraphy
EEG	Electroencephalography
EPFL	École Polytechnique Fédérale de Lausanne
FFA	Fusiform Face Area
GLM	Generalized Linear Model
HMS	Harvard Medical School
iEEG	Intracranial EEG
IT	Inferior Temporal cortex
LOF	Lateral orbitofrontal
MRI	Magnetic Resonance Images
MTL	Medial Temporal Lobe
NAMS	Non-associative Memory Selective
NSLC	n-since-last-click
NSP	n-since-pair
PPA	Parahippocampal Place Area
RT	Reaction Time
SEEG	Stereo-electroencephalography
SEM	Standard Error of the Mean
STM	Short-Term Memory
VIF	Variation Inflation Factor
VS	Visual Selective
WM	Working Memory

Contents

Summary	i
Acknowledgements	ii
Abbreviations	iii
List of Figures	vi
List of Tables	viii
1 Introduction	1
1.1 Short-term memory	1
1.1.1 Non-associative memory	2
1.1.2 Associative memory	3
1.1.3 Note on recollection and familiarity	3
1.1.4 STM versus Working Memory	4
1.2 Visual category selectivity	4
1.3 Feedback signals	5
1.4 Intracranial electroencephalography	5
1.5 Thesis contribution	6
2 Methods	7
2.1 Task Paradigm	7
2.2 Epilepsy patients and recording procedure	8
2.3 Electrodes' location	9
2.4 Behavioral analyses	10
2.5 Pre-processing of intracranial field potential data	10
2.6 Time-frequency decomposition	11
2.7 Generalized Linear Model	11
2.7.1 Groups of behavioral parameters	13
2.8 Equalization of match and mismatch trials	13
2.9 Latency study	14
2.10 Gamma band and lower frequencies interplay	14
2.11 Eye-tracking experiment	15
3 Results	16
3.1 Behavior	16
3.2 Eye-tracking experiment	18

3.3	First tile memory-selective electrodes	20
3.3.1	Non-associative memory: <i>first-click</i> and <i>n-since-last-click</i>	21
3.3.2	Associative memory: <i>match</i> and <i>n-since-pair*match</i>	24
3.4	Second tile memory-selective electrodes	29
3.4.1	Non-associative memory: <i>first-click</i> and <i>n-since-last-click</i>	29
3.4.2	Associative memory: <i>next-match</i>	31
3.5	Feedback: <i>match</i> after the second tile	32
3.6	Visual selective electrodes	34
3.7	Visual selective vs. memory selective electrodes	37
3.7.1	Latency of visual selective and memory selective electrodes	38
3.8	Gamma band and lower frequencies interplay	40
3.9	Other predictors: <i>distance</i>	44
4	Discussion	45
5	Conclusion	52
	Appendices	60
A	Methods and behavior tables	60
B	Gray matter tables	63
C	Gray matter figures	73
D	White matter tables	78
E	White matter figures	86

List of Figures

2.1	Experimental paradigm.	8
2.2	Locations of electrodes in the gray matter.	9
2.3	Latency estimation example	14
2.4	Representation of the time-wise correlation between gamma and alpha/beta band power for an example trial.	15
3.1	Comparison of behavioral parameters for match and mismatch trials across all subjects.	17
3.2	Correlation between behavioral parameters	17
3.3	Average number of clicks per tile before the exact tile was match, for tiles belonging to each image category.	18
3.4	Participants' gaze movements during match and mismatch trials.	19
3.5	Multi-collinearities across predictors.	20
3.6	An example of a LOF electrode where <i>first-click</i> was a significant predictor for gamma activities during the 1st tile.	22
3.7	An example of a pars opercularis electrode where gamma activities increased for <i>first-click</i> and larger <i>n-since-last-click</i> tiles.	23
3.8	An example electrode in the right LOF gyrus where <i>match</i> was a significant predictor for gamma activities during the 1st tile	25
3.9	An example electrode located in the left middle temporal gyrus where <i>match</i> and <i>n-since-pair*match</i> were significant predictors	27
3.10	An example electrode located in the precunes where <i>match</i> and <i>n-since-pair*match</i> were significant predictors.	28
3.11	An example of a LOF electrode where <i>n-since-last-click</i> was a significant predictor for gamma activities after the 2nd tile.	30
3.12	Example <i>next-match</i> electrode during the 2nd tile, located in the left precuneus	31
3.13	An example electrode in the insula where <i>match</i> was a significant predictor for gamma activities after the 2nd tile	33
3.14	An example electrode in the middle temporal cortex where <i>match</i> was a significant predictor for gamma activities for both the 1st the 2nd tiles	34
3.15	Visual selective electrodes' location.	35
3.16	Examples of visual selective electrodes.	36
3.17	Example of a VS and NAMS electrode located in the fusiform.	38

3.18	Comparison of the latency between VS, NAMS and AMS brain regions.	39
3.19	Comparison of the latency between VS fusiform, NAMS pars opercularis and AMS LOF electrodes.	40
3.20	Example of a LOF and pars opercularis electrode that showed gamma-alpha anti-correlation.	42
3.21	Example of a LOF and insula electrode that showed gamma-alpha anti-correlation.	43
3.22	Example of an IT electrode selective for <i>distance</i>	44
C.1	An example of a pars opercularis electrode where gamma activities decreased for <i>first-click</i> and larger <i>n-since-last-click</i> tiles.	73
C.2	An example electrode located in the lateral orbitofrontal cortex where <i>match</i> and <i>n-since-pair*match</i> were significant predictors.	74
C.3	An example electrode in the insula where <i>match</i> was a significant predictor for gamma activities after the 2nd tile	75
C.4	An example electrode in the LOF cortex where <i>match</i> was a significant predictor for gamma activities after the 2nd tile	76
C.5	An example electrode in the lateral orbitofrontal cortex where <i>match</i> was a significant predictor for gamma activities for both the 1st the 2nd tiles	77
E.1	Locations of electrodes in the white matter	86
E.2	An example of a white matter electrode located close to the lateral orbitofrontal cortex that presented <i>first-click</i> and <i>n-since-last-click</i> as significant predictors.	87
E.3	An example white matter electrode located close to the entorhinal cortex where <i>match</i> was a significant predictor for gamma activities during the 1st tile	88
E.4	An example white matter electrode located close to the parsopercularis where <i>n-since-pair*match</i> was a significant predictor for gamma activities during the 1st tile	89
E.5	An example white matter electrode located close to the LOF where <i>n-since-pair*match</i> was a significant predictor for gamma activities during the 1st tile	90
E.6	An example white matter electrode located close to the the lateral orbitofrontal cortex where <i>match</i> was a significant predictor for gamma activities after 2nd tile	91
E.7	An example white matter electrode located close to the the fusiform gyrus that was selective for images containing animals and persons.	91

List of Tables

2.1	Frequency bands and multi-taper parameters.	11
2.2	Behavioral parameters	12
3.1	Percentage of VS, NAMS and AMS electrodes that are also VS, AMS and NAMS.	37
3.2	Proportion VS, AMS and NAMS electrodes showing gamma and slower frequency interactions for the 1st tile	41
A.1	Epileptic subjects.	60
A.2	Electrodes' location.	61
A.3	Comparison for each subject of the number of clicks before a tile was matched. Tiles were grouped by image category.	62
B.1	Number of gray matter electrodes that presented each predictor as significant for the 1st tile GLM.	63
B.2	Number of gray matter electrodes that presented each predictor as significant for the 2nd tile GLM.	64
B.3	First-tile GLM results of gray matter electrodes that presented n-since-last-click and/or first-click as significant predictors.	65
B.4	First-tile GLM results of gray matter electrodes that presented match and/or n-since-pair*match as significant predictors.	66
B.5	Gamma responses of electrodes that presented n-since-pair*match as a significant predictor could predict familiarity to the tile's pair only for match trials.	67
B.6	Second-tile GLM results of gray matter electrodes that presented n-since-last-click and/or first-click as significant predictors.	67
B.7	Second-tile GLM results of gray matter electrodes that presented match as significant predictors.	68
B.8	Second-tile GLM results of gray matter electrodes that presented next-match as significant predictors.	69
B.9	First-tile GLM results of visual selective electrodes in the gray matter.	69
B.10	Second-tile GLM results of visual selective electrodes in the gray matter.	70
B.11	Percentage of electrodes in each brain that are VS, NAMS or AMS.	70
B.12	Proportion VS, AMS and NAMS electrodes showing gamma and slower frequency interactions after the 2nd tile	71
B.13	Proportion of electrodes in each brain region showing gamma and slower frequency interactions after the 1st tile	71

B.14	Proportion of electrodes in each brain region showing gamma and slower frequency interactions after the 2nd tile	72
D.1	Number of white matter electrodes that presented each predictor as significant for the 1st tile GLM.	78
D.2	Number of white matter electrodes that presented each predictor as significant for the 2nd tile GLM.	79
D.3	First-tile GLM results of white matter electrodes that presented n-since-last-click and/or first-click as significant predictors.	80
D.4	First-tile GLM results of white matter electrodes that presented match and/or n-since-pair*match as significant predictors.	81
D.5	Second-tile GLM results of white matter electrodes that presented n-since-last-click and/or first-click as significant predictors.	82
D.6	Second-tile GLM results of white matter electrodes that presented match as significant predictors.	83
D.7	Second-tile GLM results of white matter electrodes that presented next-match as significant predictors.	84
D.8	First-tile GLM results of visual selective electrodes in the white matter.	84
D.9	Second-tile GLM results of visual selective electrodes in the white matter.	85

1 Introduction

What are the brain mechanisms involved when playing a board game? How are these mechanisms coordinated? To address these questions, we analyzed intracranial recordings of epileptic patients while playing a classic matching card memory game (Figure 2.1). During this game, participants had to find pairs of images from image matrices of different sizes. We refer to each unique location and image in the game as a tile; thus, two tiles were matched if they displayed the same image. At each trial, participants had to flip any two tiles on the board until all matching pairs were found. Different brain mechanisms involved included: recognizing the image on the tile, storing the tiles' information in short-term memory (STM), recalling by association the tile's pair, and finally processing the feedback of whether the tile was matched. The main brain mechanism studied in this project is memory, more specifically STM, which is the cognitive system necessary to store the tiles' information in a readily available and active state for a short period of time. In this section, we present a literature review of the two main subtypes of memory studied, as well as object recognition and reward processing (feedback) in the human brain. We also justify using the gamma-band power as a key frequency band to study cognitive processes.

1.1 Short-term memory

STM is a cognitive system with limited capacity that stores information temporarily. Items held in STM can be readily available for mental manipulations like calculation, reordering, and retrieval. An example of STM task is remembering a verification code sent to one's phone which is immediately forgotten after inputting the numbers. Intracranial recordings, through their superior spatiotemporal resolution, have significantly advanced the understanding of the STM mechanisms [1, 2]. Researchers have characterized and continue to discover the spatial and temporal neural signatures underlying mnemonic processes. These results will collectively be indispensable to formulate the theoretical foundation of the human memory system, guiding and restraining biologically-based computational models, and developing neural intervention techniques to treat memory dysfunctions [1, 2, 3].

In this project, we considered two subtypes of memory retrieval: associative and non-associative recognition memory. In non-associative memory, a previously encoded item or information can be recognized as novel or familiar. Alternatively, in associative memory, one item can cue recall of other components, which reactivate the memory about an item's matching or associated items.

1.1.1 Non-associative memory

Non-associative recognition memory refers to the ability to recognize as familiar previously encountered events, objects, people, scenes, and others. Three main processes support recognition memory: recollection, familiarity and novelty [4, 5]. Recollection is an all-or-nothing retrieval of a previously encountered event, while familiarity is a graded strength signal that indicates confidence in previous occurrence [4]. Novelty refers to the first exposure to new information. It remains unclear whether recollection, familiarity, and novelty are neurally distinct processes. Several paradigms have been developed to study recognition memory in humans [6]. In the *yes/no recognition test*, subjects are first presented with a series of stimuli. After a delay period, they are presented with a new list of previously presented stimuli mixed with new ones (novel), and they have to indicate whether they can recognize the stimuli (*yes*) or not (*no*). Another popular test is the *forced choice recognition memory test*, where subjects are presented with both a previously encountered stimuli and a new one, and they have to decide which one is the new item [6]. *Yes/no* paradigms can only test for successful or failed retrieval of the information (recollection), but not familiarity. Hence, more recent paradigms included an arbitrary scale where subjects could indicate their confidence level in remembering the stimulus, thus allowing them to study the strength of the memory, i.e., familiarity [7, 8, 9, 10].

Several studies have reported brain regions or single neurons that are selective to familiarity or novelty [5, 8, 10, 11, 12, 13, 14, 15, 16, 17] and those that code for different degrees of familiarity or memory strength [7, 8, 9, 10]. These studies have focused mainly on the role of the medial temporal lobes (MTLs) -hippocampus, amygdala, and parahippocampal regions- in recognition memory, where distinct activity patterns have been found. Two types of neurons involved in non-associative memory were described in the MTLs: novelty and familiarity detectors, which show a selective increase in firing for new and old stimuli, respectively [13]. Selective firing patterns have also been found between the hippocampal, parahippocampal, or perirhinal cortex [7, 10, 16].

Taken together, a piece of information can constantly change its status in STM. The first exposure to new information can trigger a novelty recognition signal and the mechanisms necessary to encode this information in STM. If correctly encoded, there would be a new and strong mental representation of this information in STM. However, as more information feeds in or memory load increases, that particular information may fade away, and its memory trace becomes gradually weaker. When that information re-emerges, it can be recognized as familiar and have a fresh memory status again. Nevertheless, if a long time has elapsed since its last emergence, it may have faded away from STM and reappear as entirely novel. How neural activities embody such dynamics of STM is poorly understood. In the present study, we study non-associative STM in a highly dynamic setting. As opposed to traditional experimental paradigms in recognition memory [6], subjects in this project did not provide feedback about whether they consider a previously visualized tile as novel or not. Instead, we used different behavioral parameters to study familiarity and novelty. We hypothesize that electrodes' locations showing differential neural responses for first-time versus previously encountered tiles could detect novelty, while neural responses encoding familiarity would be modulated by how recently the information (tile) was visualized the last time. We refer to electrodes whose signals are selective to novelty or familiarity as *non-associative memory selective* (NAMS) electrodes.

1.1.2 Associative memory

Associative memory is another subtype of STM, which refers to the ability to associate or link two items. Associative memory can also be a form of long-term memory, such as learning to associate a person's name and face and being able to recall such association after many years. Many task paradigms have been developed to study associative memory. One standard paradigm is the *delayed paired associate*. During training, subjects are presented with a set of item-item pairs (e.g. face-name pairs). During test, subjects are presented with one of the items in the pair (e.g. face), and they have to cue-recall the paired stimulus (e.g., the name) [18, 19]. Thus, subjects used the encountered item, i.e., the cue, to recall its associated item from memory. We refer to the associated item as the *pair*.

A key neural phenomenon under associative memory is that neurons can learn associations and be selective to different elements within an association [2, 19, 20, 21, 22]. Even a single neuron can respond to both entities of a learned association [2, 20, 21]. Neural responses can also signal successful associative memory retrieval and may also be selective to the content of the cue's pairing information rather than the cue itself [18, 19, 22, 23, 24]. Research has substantiated the importance of the MTL in the formation of associative memories [20, 25]. Many neurophysiological studies have reported enhanced activity in the hippocampus during associative memory retrieval [18, 19, 23]. As for non-associative recognition, associative memory is mediated by recollection and familiarity [25]. Recollection signals imply only the successful recall of the cue's pair, while familiarity signals can also contain information about the memory status or familiarity with the pair, i.e. memory strength.

Associative recognition memory is a necessary mechanism to play the matching card memory game: the visualization of one tile has to cue-recall the location of its matching pair. Successful or failed retrieval of the pair would result in a match or a mismatch trial, respectively. Thus, we hypothesize that different neural responses for match versus mismatch trials could encode associative recollection signals. Like non-associative memory, familiarity with the cue's pair would be modulated by how recently the tile's pair was seen. In this project, we refer to electrodes whose signals can predict successful recollection and familiarity with the tile's pair as *associative memory selective* (AMS) electrodes.

1.1.3 Note on recollection and familiarity

Recollection and familiarity are two important mechanisms in both associative and non-associative recognition memory [4, 5]. Recollection reflects a threshold process whereby information about a study event is retrieved or not, whereas familiarity reflects a graded strength signal of the information retrieved about the event, i.e., memory strength. There is a long-lasting debate over whether familiarity and recollection are neurally distinct [26, 27, 28]. Several studies showed that familiarity and recollection are not functionally dissociable [14, 29, 30, 31, 32]. These studies support a continuous strength model, in which brain activity involved in retrieval can track both recollection and familiarity. Alternatively, other studies support a dual-process model, in which recollection and familiarity involve different brain structures [5, 26, 28, 33, 34]. These studies highlight the role of the hippocampus in recollection, while familiarity is mediated by other structures such as the perirhinal cortex and the temporal lobes [33], or the parahippocampal gyrus [5]. Although

familiarity and recollection have been commonly discussed under the context of long-term recognition and episodic memory, recollection- and familiarity- like processes may also serve short-term recognition and STM [26, 34, 35, 36].

1.1.4 STM versus Working Memory

In the literature, there has been considerable discrepancies about the differences between STM and working memory (WM). WM has been defined in three main distinct ways: as a multi-component system that manipulates information in STM, as STM applied to cognitive tasks, and as the use of attention to manage STM [37]. The memory game consisted of a cognitive task that required the manipulation of STM information, in e.g. making the associations between tiles and their pairs. Hence, we could consider that in this project we analyze both STM and WM processes. To avoid discrepancies in the literature, we use the term STM.

1.2 Visual category selectivity

Brain activity can also reflect the type of information that is being visualized or held in memory. Neuroimaging studies have identified subregions in the ventral visual pathway that selectively responded to different categories of objects. In humans, widely studied visually selective regions include the fusiform face area (FFA) for human faces, the extrastriate body area (EBA) for human bodies, and the parahippocampal place area (PPA) for building and scenes [38, 39, 40, 41, 42, 43]. These brain regions' response was stronger when subjects visualized the *preferred* stimuli versus the *non-preferred* stimuli. Invasive physiological recordings have also indicated that the macaque and human ventral object recognition system is divided into discrete regions selective to different object categories. The inferior temporal (IT) cortex, the highest area in the ventral pathway, is a key structure in object recognition [44, 45, 46, 47]. Neurons in the human MTLs also showed visual selectivity to different image categories, including buildings, animals, famous people and faces [11, 48, 49]. We refer to such neurons selective to visual categories as *category selective* neurons [48], or more broadly, *visually selective* (VS) neurons [15]. In our implementation of the matching card memory game, each tile's image belonged to one of five image categories: animal, food, indoor, person, or vehicle. We consider VS electrodes' locations those that showed increased neural responses for one or more image categories.

As opposed to neurons encoding associative or non-associative recognition memories, i.e. *memory-selective* (MS) neurons, the response of VS neurons was found to be insensitive to whether a stimulus was familiar or novel. Moreover, most neurons involved in memory retrieval in the MTL did not show category selectivity, and so they did not encode information about the identity of the retrieved item [2, 15]. Research also showed that VS neurons' activity happened earlier than NAMS neurons [15].

1.3 Feedback signals

Findings from human and animal studies point out different brain regions responsive to reward delivery. These studies highlight the importance of the orbitofrontal cortex [50, 51], the anterior cingulate cortex [52], the insula, the striatum [53] and the thalamus [54] for the processing of reward stimuli. Paradigms used to study reward-related neural responses include games in which subjects could receive either positive or negative feedback by receiving a monetary or other non-monetary rewards if they successfully achieved a task [55, 56, 50]. An example of such a paradigm is a gambling task, where subjects have to guess if the value of a card is lower or higher than the number 4, and they receive a monetary reward for correct guesses. Several studies have also found that the brain reward system can be activated not only during reward delivery but also during reward anticipation [57, 58].

In the matching card memory game, the outcome of a trial could be a match or a mismatch, and thus a successful or failed trial, respectively. Since the game's end goal was to match all pairs of tiles, we hypothesize that distinct neural responses after a match (positive feedback) or mismatch (negative feedback) could encode reward-related signals.

1.4 Intracranial electroencephalography

In the present study, we analyze intracranial field potentials recorded from epileptic patients implanted with intracranial-electroencephalography (iEEG) electrodes for clinical purposes. iEEG consists of intracerebral electrodes used in presurgical evaluations in order to anatomically define the localization of an epileptic focus. The ultimate clinical goal is to perform a resection of the cortical region causing epilepsy for each patient [59]. We analyzed two types of iEEG recordings: (1) electrocorticography (ECoG), which uses electrodes' grips implanted in the cortical surface; (2) stereo-electroencephalography (sEEG), which consists of wires that penetrate in the brain and reach deeper sites [59]. Human iEEG can record the response of a population of neurons with high spatiotemporal resolution, thus bringing unique new information about the human brain.

iEEG records field potentials that capture the average activity of large and diverse populations of neurons. The information carried by iEEG signals can be encoded in different frequency bands, such as gamma (30-150 Hz), beta (14-30 Hz), or alpha (8-14 Hz) [60]. In particular, we focused on the gamma frequency band (30-150 Hz) given that a large number of studies have suggested that the neuronal activities in this high-frequency band reflect synchronous firing of ensembles of neurons, as well as cortical activations [61, 62]. Research has shown that gamma band activities correlate with neural spiking activities [63, 64, 65] and can encode rich information about motor control, language, memory, and others [64, 66, 67, 68].

Literature has reported that different modes of WM (STM in this study) could be reflected by the interplay between gamma and lower frequency activities, like those in the beta [64, 69, 70], and alpha band [71, 72]. A push-pull relationship has been proposed for the prefrontal cortex: turning up beta activity would turn down gamma activity, and vice versa [64]. In this model, beta activities are considered to have an inhibitory role in WM that regulates gamma activities, gating the access of information to STM and controlling its maintenance. During encoding and decoding,

the *default* state reflected with beta oscillations is interrupted: beta activities decrease while gamma activities increase to allow the access of information to STM. This push-pull-like relationship was also reported between the alpha band and spiking activities [71] over the somatosensory and motor cortices, as well as between alpha and gamma power over the visual cortex [72]. These results were from monkey studies, while how such cross-frequency coupling orchestrates memory processes in humans is not fully understood.

1.5 Thesis contribution

We constructed generalized linear models (GLM) to characterize how neural responses in the gamma band were modulated and predicted by behavioral parameters that have implications in both non-associative and associative memory mechanisms. We analyzed gamma activities that could capture and encode a wide range of constantly changing STM statuses of a viewing tile, including novelty and familiarity. We also studied neural responses that were indicative of successful recall of pair but not failed recall, which could also contain information about the recency or familiarity of the pair. Moreover, the GLM allowed us to analyze brain locations that responded selectively to one or more preferred image categories and thus encoded information about the items visualized. We also compared whether MS neural responses could encode item-specific information about a tile, and vice versa. Finally, we computed the interactions between gamma and slower frequency bands to study different frequency modulation patterns involved in STM processes.

2 Methods

2.1 Task Paradigm

Participants performed an implementation of the classical memory matching game (Figure 2.1). The game involves remembering the location and content of a set of tiles to find all the matching pairs. A square board containing $n \times n$ tiles was shown throughout each session. In the beginning, all tiles were in black. In each trial, participants chose first one tile, then a second one, by clicking on them in a self-paced fashion. Upon clicking, the tile revealed a common object like a cat or a train. At the end of each trial, either the two tiles revealed the same image (match) or not (mismatch). If the tiles matched, those tiles turned green 1,000 ms after the second click and could not be clicked again for the remainder of the session. If the tiles did not match, they turned black again 1,000 ms after the second click. When all tiles had turned green, i.e., all matches had been found, the block ended and another block began. During each session, the map between positions and objects was fixed. The game always started with a block of size 3×3 and progressed to more difficult blocks (4×4 , 5×5 , 6×6 , and finally 7×7). Blocks that held an odd number of tiles (3×3 , 5×5 , and 7×7) contained one distractor object (a human face) with no corresponding pair. For each session, except for the 3×3 board, subjects had a limited time to match all tiles (2 minutes for 4×4 , 3.3 min for 5×5 , 4.8 min for 6×6 , 8.2 min for 7×7). If a participant did not complete a session within this time limit, the session ended, and a new, easier session started. The session became easier by reducing n by 1, except when $n=7$, where it was reduced by 2. Conversely, when participants completed a session with a board of size n within the allotted time limit, they moved on to a more challenging session by increasing n by 1. When participants completed an $n=7$ session, they would do further $n=7$ sessions. There was no image repetition across sessions.

All the object images were from the Microsoft COCO 2017 validation dataset [73] and were rendered in grayscale and square shape. The game included a balanced number of images from five categories: person, animal, food, vehicle, and indoor scenes. All the images were rendered on a 13-inch Apple MacBook Pro laptop. The size of each tile was 0.75×0.75 inches (2×2 degrees of visual angle, DVA) and the separation between two adjacent tiles was 0.125 inches (0.33 DVA) for board size $n=7$ and 0.25 inches (0.67 DVA) for the others. The game implementation was written and presented using the Psychtoolbox extension [74, 75] in MATLAB_2016b (Mathworks, Natick, MA). **The task paradigm was designed by Yuchen Xiao and Professor Gabriel Kreiman, and implemented by Yuchen Xiao.**

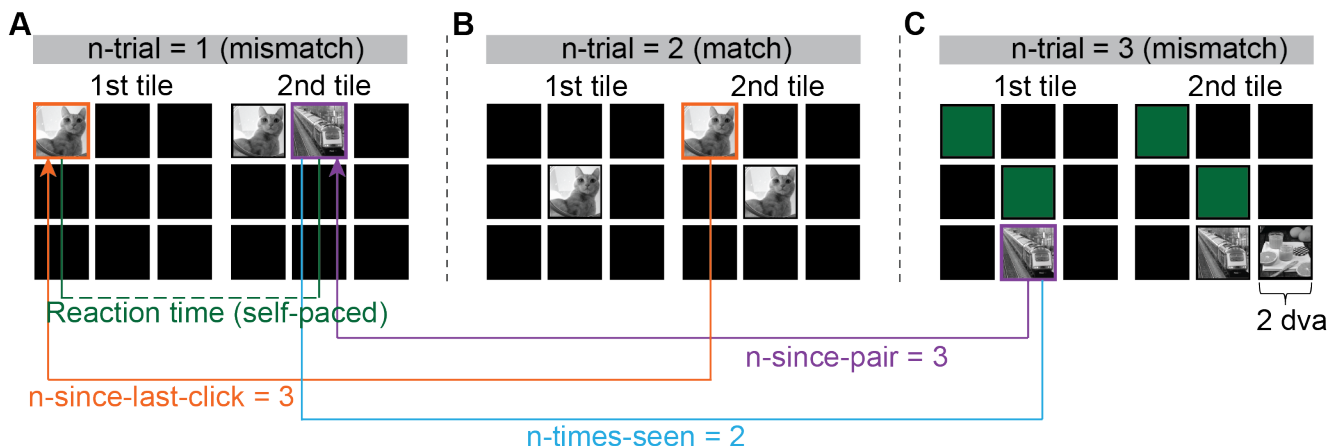


Figure 2.1: Experimental paradigm. Subjects performed the memory matching game during intracranial neurophysiological recordings with sEEG or ECoG electrodes. Subjects started with a 3×3 board and progressed to more difficult blocks (4×4 , 5×5 , 6×6 , and finally 7×7). If the subject could not complete the current block of board size $n \times n$ ($n \geq 4$) within a time limit, it would end immediately, and a new block of reduced n started. Subjects would remain at 7×7 boards if completed it within the time limit. **A-C** illustrate three consecutive trials in a 3×3 board. In each trial, two tiles were flipped sequentially and self-paced. If the two tiles contained different images (**A**, **C**, mismatch), both tiles reset to their original active states after one second. If both tiles contained the same image (**B**, match), they turned green and became fixed after one second. Three behavioral predictors used in the generalized linear models are defined here: *reaction time* (the time between the first and second tile within a trial), *n-since-pair* (the number of clicks elapsed since the last time a given tile’s matching pair was clicked), *n-since-last-click* (the number of clicks elapsed since the same tile was clicked last).

2.2 Epilepsy patients and recording procedure

The data analyzed in this project consisted of intracranial field potentials recorded from 20 patients with pharmacologically intractable epilepsy (12-52 years old, nine female, Table A.1) undergoing sEEG monitoring at Boston Children’s Hospital (Boston, US), Brigham and Women’s Hospital (Boston, US) and Xuanwu Hospital (Beijing, China). For each patient, the placement of the depth electrodes was determined exclusively by clinical criteria. All recording sessions were seizure-free. All patients had normal or corrected-to-normal vision. The study protocol was approved by each hospital’s institutional review board. Experiments were run under patients’ or their legal guardians’ informed consent. One patient at Brigham and Women’s Hospital (BWH) was implanted with both sEEG and electrocorticography (ECoG) electrodes, while all other patients had only sEEG electrodes (Ad-tech, USA; ALCIS, France). Intracranial field potentials were recorded with Natus (Pleasanton, CA) and Micromed (Italy). The sampling rate was 2048 Hz at Boston Children’s Hospital, 512 Hz or 1024 Hz at BWH, and 512 Hz at Xuanwu Hospital. Electrode trajectories were determined based on clinical purposes for precisely localizing suspected epileptogenic foci and surgically treating epilepsy [76]. **Ruijie Wu and Yuchen Xiao collected all the data.**

2.3 Electrodes' location

Electrodes were localized in the brain using the iELVis toolbox [77]. Freesurfer [78] was used to segment the preimplant magnetic resonance (MR) images, upon which a post-implant computed-tomography (CT) scan was then rigidly registered to. Electrodes were marked in the CT scan aligned to preimplant MRI using Bioimage Suite [79]. Each electrode was assigned to an anatomical location using the Desikan-Killiany [80] atlas for subdural grids or strips or FreeSurfer's volumetric brain segmentation for depth electrodes. For white matter electrodes, we also reported their closest gray matter locations. Out of 1,750 electrodes in total, we analyzed 676 bipolarly referenced electrodes in the gray matter and 492 in the white matter (Table A.2). 582 electrodes were discarded due to bipolar referencing (one removed from each shank), locations in pathological sites, or containing large artifacts. Electrode locations were mapped onto the MNI305 average brain via affine transformation [81] for display purposes. Figures 2.2 and E.1 show the electrodes' locations in the gray and white matter, respectively. **Yuchen Xiao performed the electrodes' localization and all the brain plots in the Figures.**

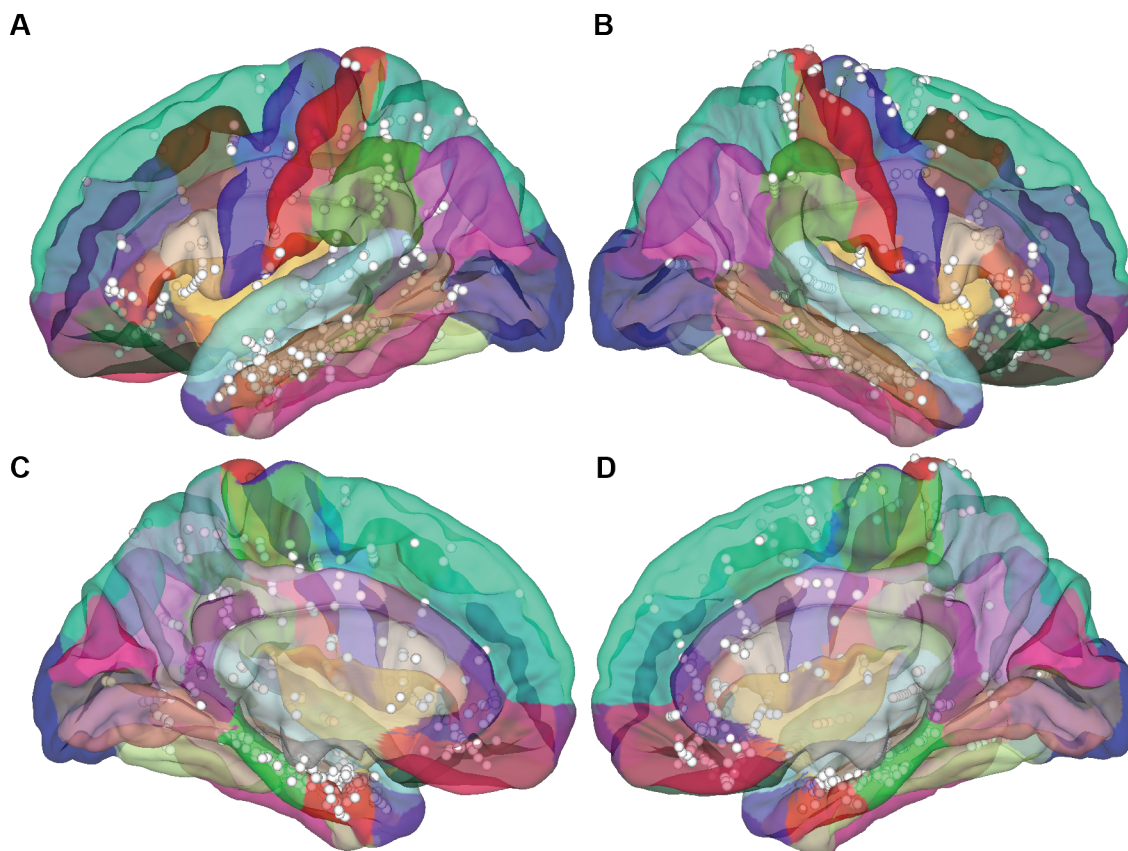


Figure 2.2: Locations of electrodes in the gray matter. Each sphere reflects one of the electrodes that were analyzed ($n=676$), overlaid on the Desikan-Killiany Atlas with different views: **A:** left lateral; **B:** right lateral; **C:** left medial; **D:** right medial.

2.4 Behavioral analyses

Table 2.2 includes the behavioral parameters that we analyzed. In the report, the behavioral parameters (predictors) names are written in italics. We created two computational models to simulate behavior assuming perfect memory and no memory (chance performance). The perfect memory model remembered all revealed tiles without forgetting. The random model simulated random clicking.

We calculated the *reaction time* (RT, time between two clicks in a trial), *n-since-pair* (number of clicks since the matching pair was last seen), *n-since-last-click* (the number of clicks since the same tile was last clicked), and *n-times-seen* (number of times a same image had been seen). See Figure 2.1 for a visual representation of these parameters. We compared these variables for match and mismatch trials at each board size (Figure 3.1, permutation test, 10,000 iterations, $\alpha=0.01$). For this analysis, we excluded *n-since-pair* trials for which the tile’s pair had never been seen. Similarly, for *n-since-last-click* we excluded trials in which the clicked tile was seen for the first time, i.e., it had never been seen before. We defined random matches as a match trial where the 2nd tile had never been seen before; such trials were excluded from both the behavioral and neurophysiological analyses. We used the F-test for linear regression models to assess whether RT, *n-since-pair*, *n-since-last-click*, and *n-times-seen* significantly covary with board size. We created four linear regression models using for each model one of these four behavioral parameters (RT, *n-since-pair*, *n-since-last-click*, and *n-times-seen*) as the predictors and the board size as the response variable. We created separate models for match and mismatch trials, and for the 1st and 2nd tiles. For each subject, we also computed the Pearson correlation [82] between each pair of predictors to analyze how they covary.

Five image categories were included in the game: animal, food, indoor, person, and vehicle. We computed the number of times each tile was clicked before being matched. The larger the number of clicks, the more times a tile was visualized. We grouped the tiles by the image category they displayed, and we tested whether any image category showed a significantly larger number of clicks compared to the other categories (permutation test, 5,000 iterations, $\alpha=0.01$).

2.5 Pre-processing of intracranial field potential data

Bipolar subtraction was applied to each pair of neighboring electrodes on each shank of depth electrodes or surface grid/strip electrodes [83]. A zero-phase digital notch filter (MATLAB function `filtfilt`) was applied to the bipolarly subtracted broadband signals to remove the line frequency at 60 Hz (BCH, BWH) or 50 Hz (Xuanwu) and their harmonics. For each electrode, trials whose amplitudes (voltage range) were larger than 5 standard deviations from the mean amplitude across all trials were considered potential artifacts and discarded from further analyses [84]. For the 1st tile, the time window for artifact rejection was from 400 ms before click until 1,000 ms after the average RT. For the 2nd tile, the time window was [400 ms + average reaction time] before the second click until 1,000 ms after the second click. Across all electrodes, we rejected 1.75% of all trials for the 1st tile and 1.73% for the 2nd tile.

2.6 Time-frequency decomposition

We used the Chronux toolbox [85] to compute the gamma (30-150 Hz), beta (14-30 Hz) and alpha (8-14 Hz) band power from the local field potentials. This toolbox uses the multi-taper method [86] to estimate the time-frequency decomposition. The multi-taper method is typically used to achieve better control over the frequency smoothing: more tapers result in better smoothing [86]. Table 2.1 indicates the number of tapers, window size, and time step used for each frequency band. For the gamma band (30-150 Hz) we used a time-bandwidth product of 5 and 7 leading tapers, a moving window size of 200 ms, and a window and step size of 10 ms [87]. We used a decreasing number of tapers and an increasing time window of analysis for lower frequency bands (Table 2.1). Therefore, the frequency smoothing increased with frequency. For each trial, the power was normalized using z-scored normalization, thus by subtracting the mean band power during the baseline (400 ms before 1st tile) and dividing by the standard deviation of the band power during baseline. Spectrograms considering all frequencies from 1 to 150 Hz were rendered with the Fieldtrip toolbox [88] using the multi-taper method and z-scored normalization again. For lower frequency bands (1-8 Hz), we used a time window of 500 ms and only one taper. We excluded all random matches from analyses.

Table 2.1: Frequency bands and multi-taper parameters. Frequency range for each band and multi-taper method parameters (number of tapers, moving window size and time step) used to analyze each frequency band.

Frequency band	Frequency range	Number of tapers	Moving window size	Time step
Gamma	30-150 Hz	[5 7]	200 ms	10 ms
Beta	14-30 Hz	[3 5]	300 ms	10 ms
Alpha	8-14 Hz	[2 3]	400 ms	10 ms
Delta-Theta	1-8 Hz	1	500 ms	10 ms

2.7 Generalized Linear Model

We used generalized linear models (GLM) [89, 90] to analyze the relationship between the gamma band power and behavioral parameters. Table 2.2 includes the behavioral parameters included as predictors in the models. A visualization of the RT, *n-since-last-click*, *n-since-pair* and *n-times-seen* predictors can be found in Figure 2.1. We used two GLMs, one using neural responses between the 1st and 2nd tile, and the other using neural responses after the 2nd tile. For the first GLM, the time window started when the 1st tile was clicked and ended at a time corresponding to the 90th-percentile of the distribution of RTs for each subject. This criterion showed a reasonable trade-off between minimum overlap with responses after the 2nd tile and maximum amount of information captured. We also refer to this first GLM as *1st tile GLM*, since we used it to analyze neural activities upon the visualization of the 1st tile. For the second GLM, the time window started with the 2nd click and ended one second afterward. We also refer to the second GLM as *2nd tile GLM*, since it analyzed neural activities upon the visualization of the 2nd tile. We defined the area under

the curve (AUC) of the gamma band power over the defined time windows as the response variable to be fit by the GLMs. The AUC was computed using the MATLAB function `trapz`. In all, the model followed:

$$\mathbf{Y} = \beta_0 + \sum_{i=1}^n \beta_i \mathbf{X}_i + \varepsilon \quad (2.1)$$

where \mathbf{Y} represents the AUC of the gamma band power, n indicates the total number of predictors, \mathbf{X}_i represents each predictor and β_i there associated beta coefficient. β_0 represents the intercept and ε the error.

Table 2.2: Behavioral parameters. Description of the behavioral parameters (predictors) analyzed and included in the GLM models. Tile indicates whether the predictor was included in the first GLM (1st tile), in the second GLM (2nd tile) or in both.

Predictor	Description	Tile
match	Whether the trial was a match or mismatch	both
n-since-pair*match	How many clicks ago the tile’s pair was clicked (matched trials only)	1st
n-since-last-click	How many clicks ago the same tile was clicked	both
first-click	Whether a tile was clicked the very first time	both
n-times-seen	Number of times the same image had been previously clicked	both
next-match	Whether the next trial was a match or mismatch	both
reaction-time	Time between the 1st and 2nd tile	both
board-size	Total number of tiles in the current block	both
x-position	x position in pixel	both
y-position	y position in pixel	both
distance	Euclidean distance between the 1st and 2nd tile in pixel	both
animal	Image belonged to animal category	both
food	Image belonged to food category	both
person	Image belonged to person category	both
vehicle	Image belonged to vehicle category	both

We performed multicollinearity analysis to discard the presence of highly correlated predictors that could affect the performance of the model [91, 92]. We calculated the variance inflation factor (VIF) [93] for each predictor to detect the presence of multicollinearities. A VIF of 1 indicated that there were no collinearities with the other predictors. The larger the VIF, the higher the collinearities, and a VIF greater than 5 indicated a very high correlation that could significantly harm the performance of the model [94]. The VIFs of all predictors were smaller than 3 (Figure 3.5).

For *n-since-pair*, we included the interaction term between this predictor and *match* (*n-since-pair*match*) to test the hypothesis that for match trials, the strength of the neural response after the 1st tile was modulated by how recently the tile’s matching pair was seen for the last time. We represented the image category by including four out of the five categories (*animal*, *food*, *vehicle*, *person*). We dropped the *indoor* category to avoid falling into the “dummy variable trap” [95]. For each predictor, we calculated the parameter estimate (beta coefficient) from the least mean squares fit of the model to the data, the t-statistic (beta coefficient divided by its standard error), and the

p-value to test the effect of each predictor on the response. We used the MATLAB function `fitglm` to compute the models and their parameters. A beta coefficient or t-statistic of zero indicates that the predictor has no effect on the response. A predictor was considered significant if the GLM model differed from a constant model ($p < 0.01$) and the p-value for that predictor was smaller than 0.01.

To determine if any brain region contained significantly more electrodes significant for one predictor than expected by chance, we randomly sampled the same number (n) of electrodes as those that were significant for this predictor in the GLM, from the total electrode population (separate for gray and white matters) for 10,000 iterations. Taking the match predictor for gray matter electrodes as an example, from the total 676 gray matter locations, we randomly sampled 32 locations (the number of match-significant gray matter electrodes) for 10,000 times, and calculated the p-value of any location, say insula, as the number of times when n (insula, real) was less than n (insula, sampled). If $p < 0.01$, we considered that brain region had significantly more electrodes than purely expected by chance.

2.7.1 Groups of behavioral parameters

We analyzed different brain mechanisms by linking neural responses with the behavioral parameters (Table 2.2). Depending on the brain process to be studied and the tile to be analyzed (1st or 2nd), we considered five main groups of predictors:

Non-associative memory predictors: *first-click* and *n-since-last-click*, for both the 1st and 2nd tile. Gamma responses modulated by these predictors may encode novelty and familiarity to the current viewing tile (Introduction 1.1.1).

Associative memory predictors: *match* and *n-since-pair*match* for the 1st tile and *next-match* for the 2nd tile. Neural responses modulated by these predictors may encode the recollection of the information necessary to perform a match in the current trial (*match* for the 1st tile), or the subsequent trial (*next-match* for the 2nd tile). *n-since-pair*match* may also encode successful recollection, as well as familiarity with the tile's pair (Introduction 1.1.2).

Visual category-selective predictors: *animal*, *food*, *person* and *vehicle*. For the 1st and 2nd tile. These predictors may be linked with visual selectivity to different image categories (Introduction 1.2).

Feedback predictors: *match* after the 2nd tile. Distinct neural responses for match after the trial's outcome is revealed could encode feedback or reward signals (success: match; failed: mismatch; Introduction 1.3).

Game predictors: *board-size*, *x-position*, *y-position* and *distance*. These predictors encode information related to the position and distance between tiles on the board.

2.8 Equalization of match and mismatch trials

For display purposes, we equalized the number of match and mismatch trials in some of the plots, e.g., Figure 3.8C,D. For all subjects, the number of mismatch trials ($n_{mismatch}$) was larger than the number of match trials (n_{match}). To have as many match as mismatch trials, i.e., equalization, we

computed the mean RT for match trials (RT_{match}), and we sampled the n_{match} mismatch trials that presented the closest RT to RT_{match} .

2.9 Latency study

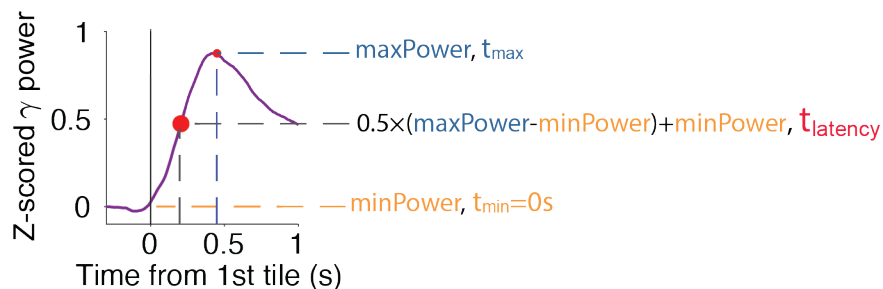


Figure 2.3: Latency estimation example. The line plot (purple) represents the trials’ average gamma power. Max-power (blue) indicates the maximum activation (maximum gamma power). The power at the time of click (0s) is the min-power (yellow). Latency is computed as the time at which the gamma band power achieves 50% of its maximum activation.

To compare the temporal dynamics of different brain regions involved in object recognition, associative memory retrieval and/or non-associative memory retrieval, we computed the latency of each brain region. We defined latency as the time at which the average gamma power over all electrodes’ trials in each region achieved 50% of the maximum gamma power. Figure 2.3 shows a visual representation of how we computed latency.

2.10 Gamma band and lower frequencies interplay

To characterize how different interactions between gamma frequency activities and slower oscillations coordinate WM processes, we computed the time-wise correlation between the gamma band power and the alpha or beta band power. We defined electrodes with gamma and beta/alpha anti-correlation as those with more than 60% of the trials showing negative time-wise correlation. Electrodes with positive correlation presented more than 60% of the trials with positive correlation between gamma and alpha/beta activities. We computed the time-wise correlation for the 1st and 2nd tiles independently. To compute the time-wise correlation, we used the same time windows for analysis as the GLM (Methods 2.7). First, we sampled the gamma and beta or alpha band power every 10 ms from the onset of the click to the end of the window for analysis. Figure 2.4A represents an example of the average gamma and alpha or beta power for one trial. Red dots (gamma power) and blue dots (alpha or beta power) indicate the power at the time points considered for analysis. For better visualization, not all the sampling points are plotted. Next, we computed the time-wise correlation as the Pearson correlation between the gamma and alpha or beta band power samples over time (Figure 2.4B). Figure 2.4B shows a scatter plot of the gamma (Figure 2.4A red dots) and alpha/beta (Figure 2.4A blue dots) power over time. For this example trial, the time-wise

correlation is negative (correlation <0 , Figure 2.4A,B). Hence, alpha/beta power increases when gamma power decreases, and vice versa (Figure 2.4A,B).

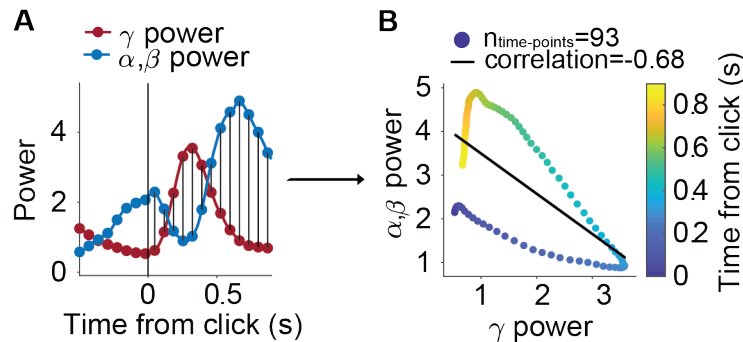


Figure 2.4: Representation of the time-wise correlation between gamma and alpha/beta band power for an example trial. **A.** Line plot represents the z-scored gamma (red) and alpha/beta (blue) band power over time. Red dots (gamma) and blue dots (beta) indicate the power values considered for analysis. For visualization purposes, not all sampling points are shown. **B.** Scatter plot of the red versus blue dots in **A**. Dots are colored by the time from click. Black line indicates the linear regression fit of gamma and alpha/beta power. Both frequency bands were anti-correlated (negative correlation, correlation <0).

2.11 Eye-tracking experiment

Ten non-epileptic subjects (23-35 years old, 9 female) performed the same task while their eye movements were tracked and recorded with the EyeLink 1000 plus system (SR Research, Canada) at a sampling rate of 500 Hz. The task paradigm was the same as the one for epilepsy patients except that before each block began, subjects fixated on a center cross to ensure that the EyeLink eye-tracking system was well-calibrated, otherwise a re-calibration session ensued. The task was presented on a 19-inch CRT monitor (Sony Multiscan G520) and subjects sit about 21 inches away from the monitor screen. The tile size is 1x1 inches (2.7x2.7 DVA) as appeared on the screen. The study protocol was approved by the institutional review board at Boston Children's Hospital and each subject completed the task under informed consent and with compensation. All subjects have normal or corrected-to-normal vision. All subjects completed 16 blocks.

3 Results

3.1 Behavior

The average number of clicks per tile increased with difficulty (board size), as expected (Figure 3.1A). All subjects performed much better than a memoryless model (random clicking, $p < 0.001$, permutation test, 5,000 iterations) and worse than a model assuming perfect memory ($p < 0.001$, Figure 3.1A). The RT is the time difference between the first and second clicks. The RT was longer for mismatch compared to match trials for all board sizes ($p < 0.007$, permutation test, 5,000 iterations, Figure 3.1B).

For a tile in a given trial, we defined *n-since-last-click* as the number of clicks since the last time the same tile was clicked (Figure 2.1). As expected, *n-since-last-click* increased with the board size ($p < 0.001$, linear regression, F-test, Figure 3.1C-D). For the 2nd tile, *n-since-last-click* was larger in mismatch compared to match trials for all board sizes except the 3x3 case ($p < 0.001$, permutation test, 10,000 iterations, Figure 3.1D). This observation also held for the 1st tile only for the 7x7 board size ($p < 0.001$, Figure 3.1C). Since this game consists of a cued-recall task, the 1st tile click guided where to click next (2nd click). If the 1st tile's matching pair was recently seen, participants might have a better memory of the tile's pair location, and thus it is more likely that the 2nd tile clicked is the pair and the trial is matched. Therefore, the 2nd tile *n-since-last-click* can influence whether there would be a match or not. In contrast, the 1st tile is usually clicked in a more exploratory way. This strategy accounts for the differences between the 1st tile (Figure 3.1C) and 2nd tile (Figure 3.1D) for *n-since-last-click*.

For a tile in a given trial, we defined *n-since-pair* as the number of clicks since the last time its matching pair was seen (Figure 2.1). As expected, *n-since-pair* increased with the board size given the increased difficulty ($p < 0.001$, linear regression, F-test, Figure 3.1E-F). Additionally, the more recent the tile's matching pair was seen, the more likely the trial was a match. Thus, *n-since-pair* was larger in mismatch compared to match trials in all cases except the 3x3 board size for the 1st tile ($p < 0.001$, permutation test, 10,000 iterations, Figure 3.1E). For the 2nd tile, *n-since-pair* for any match trial was always one because the matching pair would have been revealed in the previous click by definition.

We also performed correlation analysis to study how the behavioral parameters in Table 2.2 covary. Figure 3.2 shows the pair-wise Pearson correlation across predictors. The *distance* was positively correlated with the *match* predictor. During the initial part of the game, participants tended to click tiles that were next to each other as an exploratory strategy to learn the tile's information. Most of the trials in this exploratory part were mismatched. On the other hand, due to

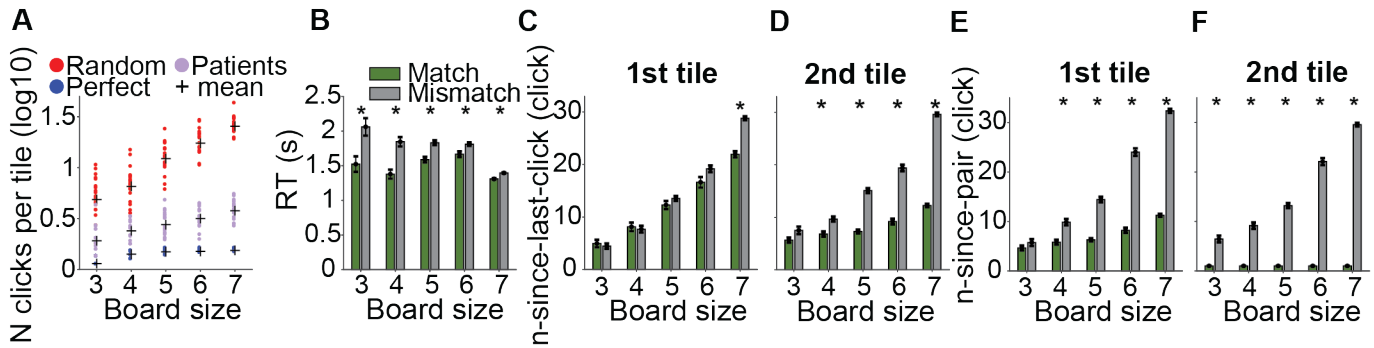


Figure 3.1: Comparison of behavioral parameters for match and mismatch trials across all subjects. **A.** Number of clicks per tile of random simulation model (red, $n=20$), epilepsy patients (purple, $n=20$), and perfect memory simulation model (blue, $n=20$) in log scale when playing the memory matching game (Methods 2.4). **B-F.** Bar plots comparing the reaction time (**B**), n -since-last-click for the 1st tile (**C**) and the 2nd tile (**D**), and n -since-pair for the 1st tile (**E**) and the 2nd tile (**F**), of match and mismatch trials at different board sizes. Asterisks denote significant differences between matched and mismatched trials (permutation test, 5000 iterations, p -value < 0.01). For n -since-last-click, we removed trials in which any tile was clicked the 1st time. For n -since-pair, we removed trials in which the 2nd tile had not been seen. All error bars indicate SEM

the randomized location of the tiles (Methods 2.1), paired tiles, i.e., two tiles containing the same image, were usually not located next to each other. This might explain why distance increased with match trials (Figure3.2).

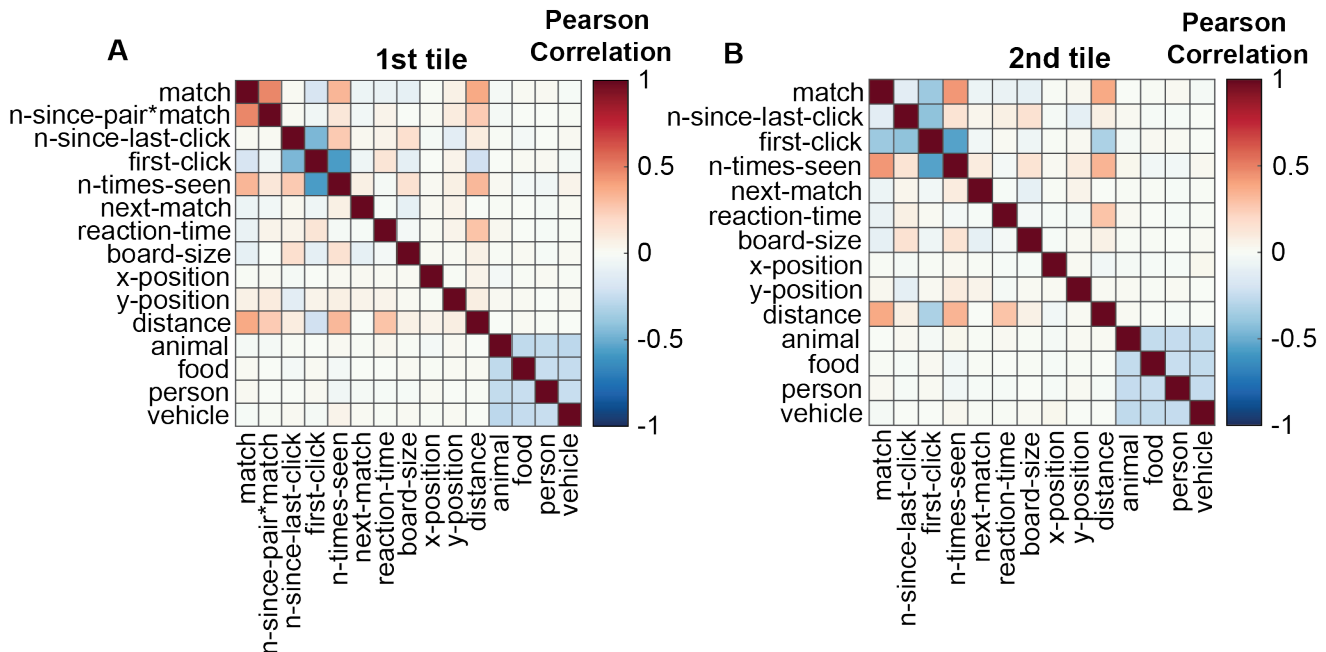


Figure 3.2: Correlation between behavioral parameters. **A, B.** Average across subjects of the Pearson correlation between pairs of predictors for the 1st tile (**A**) and the 2nd (**B**) tile.

Each tile displayed an image belonging to one of five categories: animal, food, indoor, person and vehicle. We compared whether subjects could remember better images belonging to one of these categories. Figure 3.3 shows the average number of clicks per tile before they were matched, grouping tiles by the image category. The larger the number of clicks, the more times the tile had been visualized before match, and thus the more difficult it was to remember. On average, the worst remembered category was vehicle and the best remembered was person (Figure 3.3). However, there was no significant difference across categories. We also performed this comparison for each subject (Table A.3). Three subjects showed a significantly larger number of clicks per tile for tiles containing vehicles compared to other categories such as food, indoor, or person.

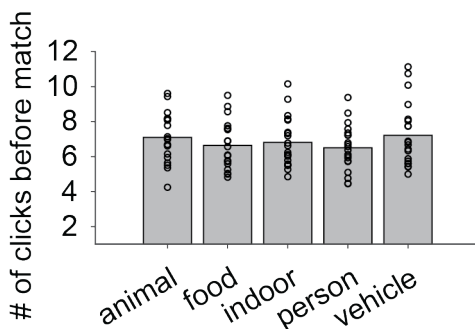


Figure 3.3: Average number of clicks per tile before the exact tile was match, for tiles belonging to each image category. Bar plots indicate the average across subjects of the number of clicks per tile before the exact tile was matched. Tiles are grouped by the image category they display. Dots represent the average for individual subject ($n=20$).

3.2 Eye-tracking experiment

We performed infrared eye-tracking on ten healthy subjects while they played the memory task (Figure 2.1). Figure 3.4 shows the distance in degrees of visual angle (DVA, $^{\circ}$) between the eye location and the center of the tile clicked for match (green) and mismatch (black) trials for the 1st and the 2nd tile. The smaller the distance, the closer the subjects' gaze was to the center of the clicked tile. We found that participants' gaze moved onto target tiles approximately 300 ms before the click. After the click, participants fixed their gaze close to the tile's center for a shorter time for match compared to mismatch trials, for both the 1st and the 2nd tiles (Figure 3.4A,B, compare green and black lines around the clicking time). Hence, subjects tended to move their eyes away faster for match trials. Moreover, 1 s after the 1st click (Figure 3.4A), and before and after the 2nd click, participants had moved their eyes further away for match trials (Figure 3.4A,B, compare green and black lines 1 s after the click). Hence, the correlation between match with faster RT and larger distance (Results 3.1, Figure 3.1A and Figure 3.1B,C) may explain the difference in eye movements. Indeed, no difference in eye movement was detected during the 1st tile when equalizing RT and *distance* (mean RT \pm 200ms; mean distance \pm 3 $^{\circ}$; Figure 3.4G). While for the 2nd tile, subjects tended to move away their gaze earlier for match than mismatch (Figure 3.4H), possibly because there was no need to pay more attention to already matched tiles. When only equalizing

the RT (only taking trials with mean RT \pm 200 ms, Figure 3.4C,D), the eye movements after the 1st click are similar for both match and mismatch trials. However, subjects still looked further away for match trials (Figure 3.4C,D). When equalizing the distance (only taking trials with mean distance \pm 3°, Figure 3.4E,F), there was a smaller difference in distance, but the eye movements were still faster for match trials.

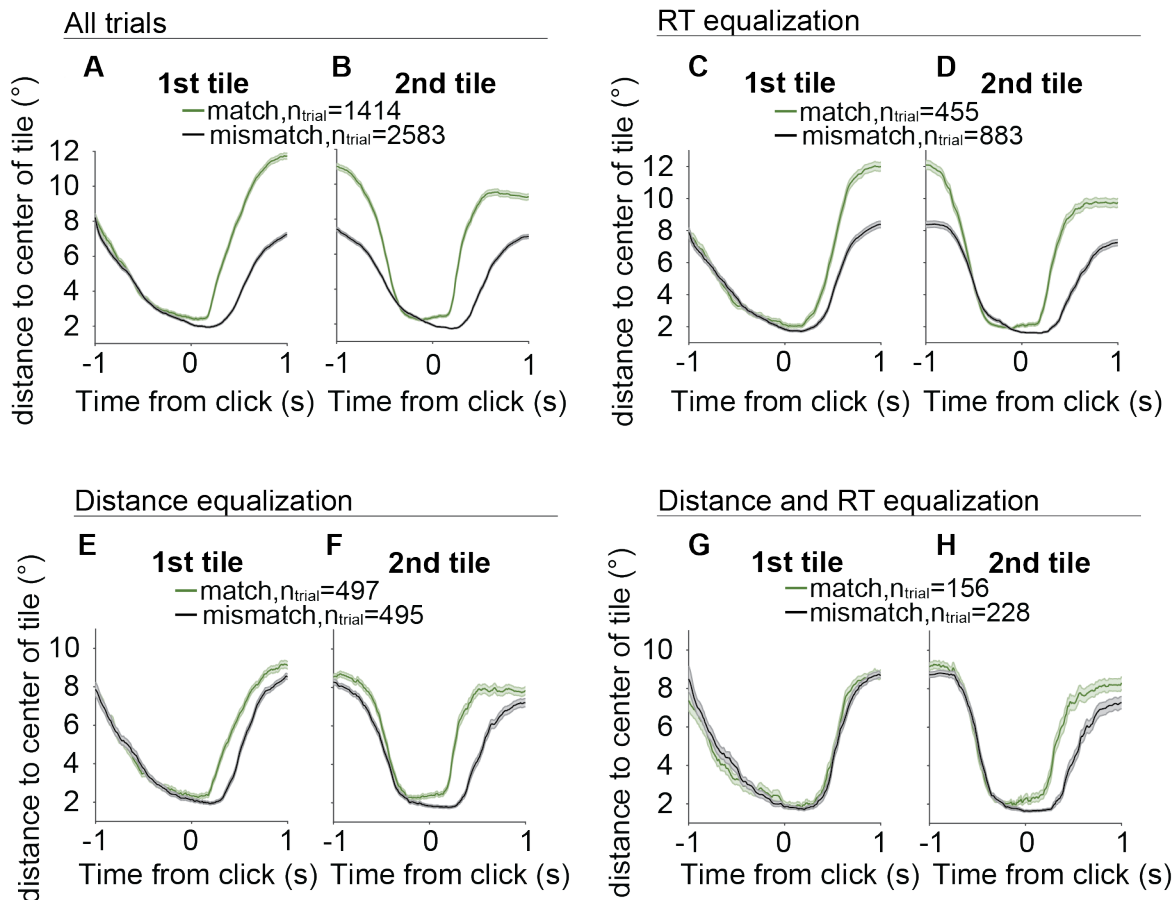


Figure 3.4: Participants' gaze movements during match and mismatch trials. A-H. Line traces (mean \pm SEM) indicate the average distance in DVA between gaze and the center of the tile clicked for match (green) and mismatch (black) trials. **A,B.** Considering all trials for all subjects. **C,D** Reaction time (RT) between the 1st and 2nd tile were equalized (mean RT \pm 200ms). **E,F.** Distance between the 1st and 2nd tile were equalized (mean RT \pm 200ms). **G,H.** Reaction time (RT) and distance between the 1st and 2nd tile were equalized (mean RT \pm 200ms; mean distance \pm 3°). No significant difference in eye-movement was found between match and mismatch during the 1st tile (**G**).

3.3 First tile memory-selective electrodes

We analyzed 676 bipolarly referenced electrodes in the gray matter and 492 in the white matter (Methods 2.3). Although the white matter is presumed to contain mostly myelinated axons, previous works have shown that white matter intracranial field potential signals can demonstrate biologically meaningful information, including activity from both nearby and distant gray matter [96, 97]. We focus on the gray matter electrodes in the main text, and report examples from the white matter electrodes in the Appendices D (Tables) and E (Figures). Electrode locations are shown in Table A.2, Figure 2.2 for the gray matter and Figure E.1 for the white matter. We built two generalized linear models (GLM) to characterize how the neural responses depended on the characteristics of each trial (Methods 2.7). The first model focused on the neural responses between the 1st tile and 2nd tile, and the second model focused on the neural responses between the 2nd tile and the end of the trial. In both cases, we used each trial’s AUC of the gamma band power (30-150 Hz) as the response variable. We considered 14 predictors for the GLM models, including whether a trial was a match or not, RT, *n-since-last-click*, and NSP (Figure 2.1), within others. Table 2.2 lists all the predictors and their definitions. Several predictors were correlated with each other (Figure 3.2). However, the variance inflation factor (VIF) of each predictor was smaller than 3 for all subjects (Figure 3.5); thus, the multi-collinearities between predictors did not harm the performance of our model [98]. Table B.1 for the 1st and Table B.2 for the 2nd tile show the number of electrodes selective for each predictor in the GLM, grouped by brain region. See Table D.1 and Table D.2 for the white matter.

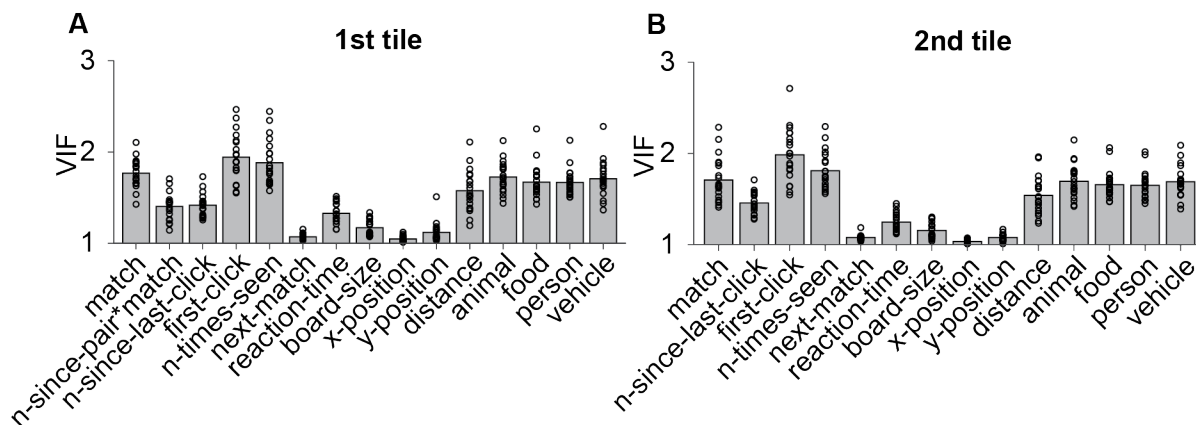


Figure 3.5: Multi-collinearities across predictors.. A, B. Variation Inflation Factor (VIF) of each predictor for the 1st tile (A) and the 2nd (B) tile. Bar plot indicates average VIF across all subjects. Dots represent the VIF of an specific predictor for one subject.

In this section, we present the results obtained from the first GLM model, thus using neural responses after the 1st tile and before the 2nd tile, to study electrodes’ gamma activities that can be involved in STM. Upon the visualization of the 1st tile, neural responses may encode information regarding the novelty or familiarity with the viewing tile (non-associative memory, Introduction 1.1.1), or information about the successful retrieval and familiarity with the tile’s pair (associative memory, Introduction 1.1.2).

3.3.1 Non-associative memory: *first-click* and *n-since-last-click*

When a tile was clicked, subjects could recognize it as a familiar or novel. We refer to this type of memory as non-associative recognition memory (Introduction 1.1.1). If a tile was novel, participants needed to encode the tile’s information in STM for future use. Hence, the ability to detect novelty is a necessary condition for successful encoding. If the tile had been viewed before, it should appear familiar to the subject, and the degree of familiarity may depend on how long ago that same tile was last seen. We used the *first-click* and the *n-since-last-click* predictors to describe novelty and familiarity, and thus the status in STM of the tile clicked. *first-click* refers to whether a tile was seen for the first time, and *n-since-last-click* refers to the number of clicks since the last time seeing the same tile. The smaller the *n-since-last-click*, the more recently the exact tile was seen the last time, as if it is more familiar. As opposed, the larger the *n-since-last-click*, the longer ago the same tile was seen last time, as if it is more unfamiliar, or even considered novel again if the tile had been forgotten. Therefore, we hypothesize that *n-since-last-click* and *first-click* can reflect the status in STM of the viewing tile.

For gamma responses during the 1st tile, the *first-click* predictor was significant ($p < 0.01$, GLM) in 50 electrodes (Figure 3.6G, Table B.3, Table B.1). The lateral orbitofrontal (LOF) cortex and pars opercularis contained significantly more electrodes than expected by chance ($p < 0.01$, bootstrap analysis with 5,000 shuffles, Methods 2.7). White matter results were reported in Table D.3 (33 out of 492, 6.7%). Figure 3.6A-F shows an example electrode in the right LOF gyrus that had *first-click* as a significant predictor. The negative t-statistic ($p < 0.01$, GLM) for *first-click* in the GLM indicates that the AUC of the gamma power dropped for novel tiles (Figure 3.6A, blue line). Hence, when a tile was seen for the first time, there was a drop in gamma power (Figure 3.6B and Figure 3.6D); in contrast, the gamma power increased for non-first-clicks. Such difference can be appreciated from single trials (Figure 3.6C). Figure 3.6D-F shows the trial-averaged spectrograms for *first-clicks*, *n-since-last-click* = 1 (just seen, thus super familiar), and *n-since-last-click* > 1 (less familiar).

The *n-since-last-click* predictor was significant ($p < 0.01$, GLM) in 45 (6.7%) electrodes (Figure 3.7G, Table B.3) during the 1st tile. White matter results (32, 6.5%) were reported in Table D.3. Figure 3.7 and Figure C.1 present two example electrode located in the left pars opercularis where the gamma power levels were predicted by both *n-since-last-click* and *first-click*. The pars opercularis electrode in Figure 3.7 shows a positive t-statistic ($p < 0.01$, GLM) for both the *first-click* and the *n-since-last-click* predictors in the GLM (Figure 3.7A). The positive t-statistic for *n-since-last-click* suggests that the larger the value of this predictor, or the less familiar a tile appeared to be, the higher the gamma power ($p < 0.001$, GLM, Figure 3.7A). Similarly, the positive t-statistic for *first-click* indicates that tiles that were viewed the first-time induced a high gamma response. Indeed, tiles that were clicked in the previous tile (*n-since-last-click*=1, Figure 3.7B red line) did not induce a gamma response, while *first-click* trials induced the highest gamma power (Figure 3.7B blue line), as well as clicks that were seen more than 1 click ago (*n-since-last-click* > 1, Figure 3.7B yellow line). Although RT was a significant predictor for this electrode, the difference in gamma power cannot be entirely due to the difference in RT. After performing RT equalization (see dashed lines indicating equalized RT in Figure 3.7B), the difference in gamma power was still obvious. The modulation of the gamma responses by novelty and familiarity was also evident from single trials (Figure 3.7C) as well as from the spectrograms (Figure 3.7D-F). Such a correlation between

n-since-last-click and gamma power represented most of the data (37 out of 45, 82.2%). Only 8 (17.8%) electrodes showed a negative correlation, indicating higher gamma power towards more familiar items. An example electrode also located in the right parsopercularis is shown in Figure C.1. For this type of electrode, the smaller the *n-since-last-click*, or the more familiar the item, the higher the gamma power. Tiles being clicked the first time were completely unfamiliar and associated with the lowest power (Figure C.1B, blue line).

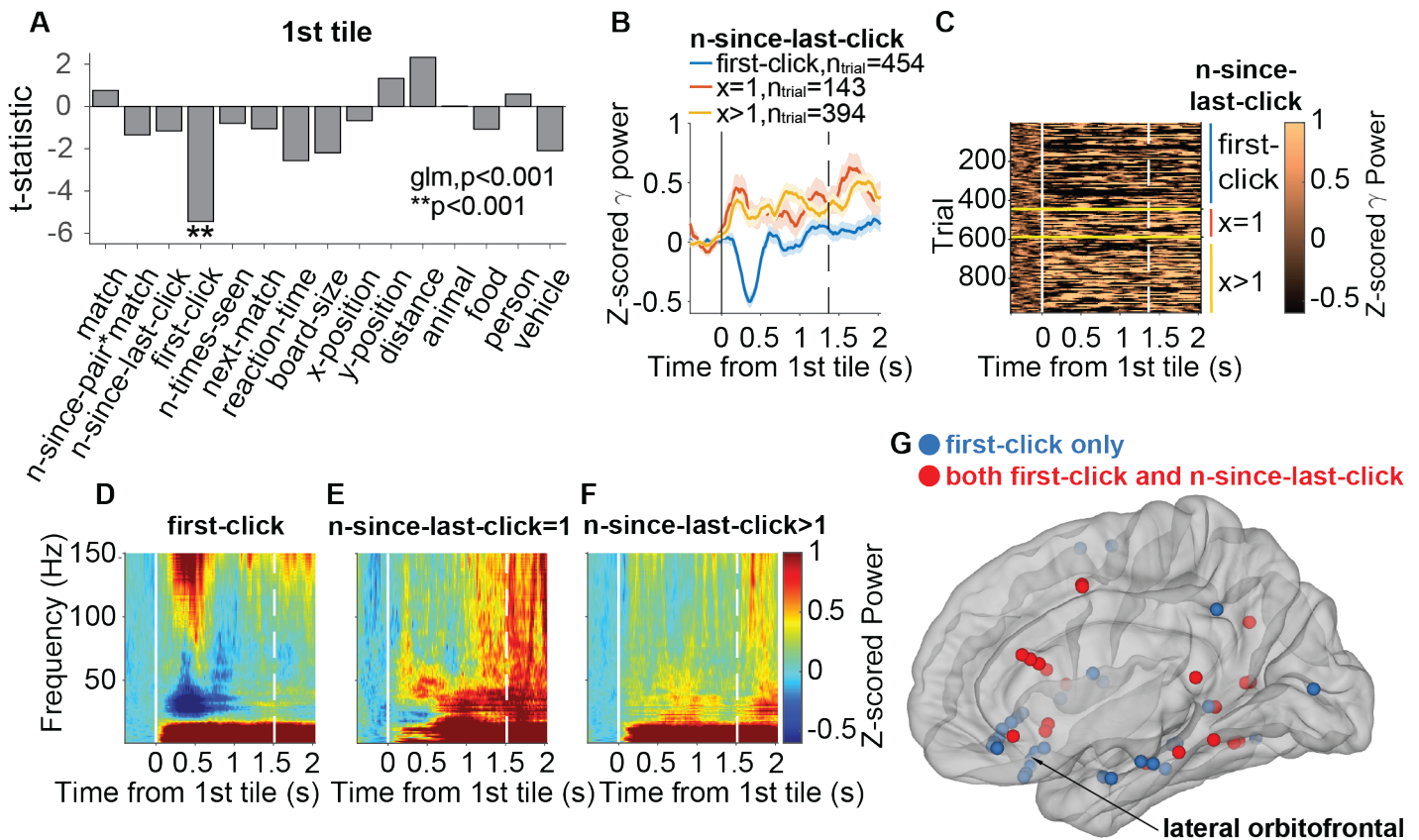


Figure 3.6: An example of a LOF electrode where *first-click* was a significant predictor for gamma activities during the 1st tile. **A.** T-statistic of each predictor in the GLM. Asterisks indicate significant predictors for the gamma power AUC. **B.** Z-scored gamma power aligned to the 1st tile onset for *first-click* (blue line), clicked in the previous tile (red line) or clicked more than one tile ago (yellow line) tiles. Shaded error bars indicate SEM Dashed line indicates the mean RT. **C.** Raster plots showing the z-scored gamma power in individual trials ordered by *first-click* and then from smaller to larger *n-since-last-click*; division indicated by yellow horizontal lines and colored vertical lines. **D-F.** Spectrograms showing the power aligned to the 1st tile onset during *first-click* (**D**), *n-since-last-click*=1 (**E**), and *n-since-last-click*>1 (**F**). **G.** Locations of all *first-click* electrodes during the 1st tile. Blue: *first-click* only; red: both *first-click* and *n-since-last-click*.

The intersect between *first-click* and *n-since-last-click* yielded 20 electrodes (Figure 3.6G, 3.7G and C.1G, red spheres, Table B.3). Among these 20 electrodes, the signs of the t-statistics of *n-since-last-click* and *first-click* predictors were consistent for 18 electrodes (16 positive and 2

negative). Only 2 exhibited the opposite signs. Both the examples in Figure 3.7 and Figure C.1 also had the had both *n-since-last-click* and *first-click* as significant predictors. Figure E.2 shows a white matter electrode located close to the LOF cortex that also presented *n-since-last-click* and *first-click* as significant predictors, both with a positive t-statistic in the GLM. These results indicate that novel tiles show similar responses to tiles viewed many clicks ago. Hence, the latter may have been forgotten and are treated as novel tiles.

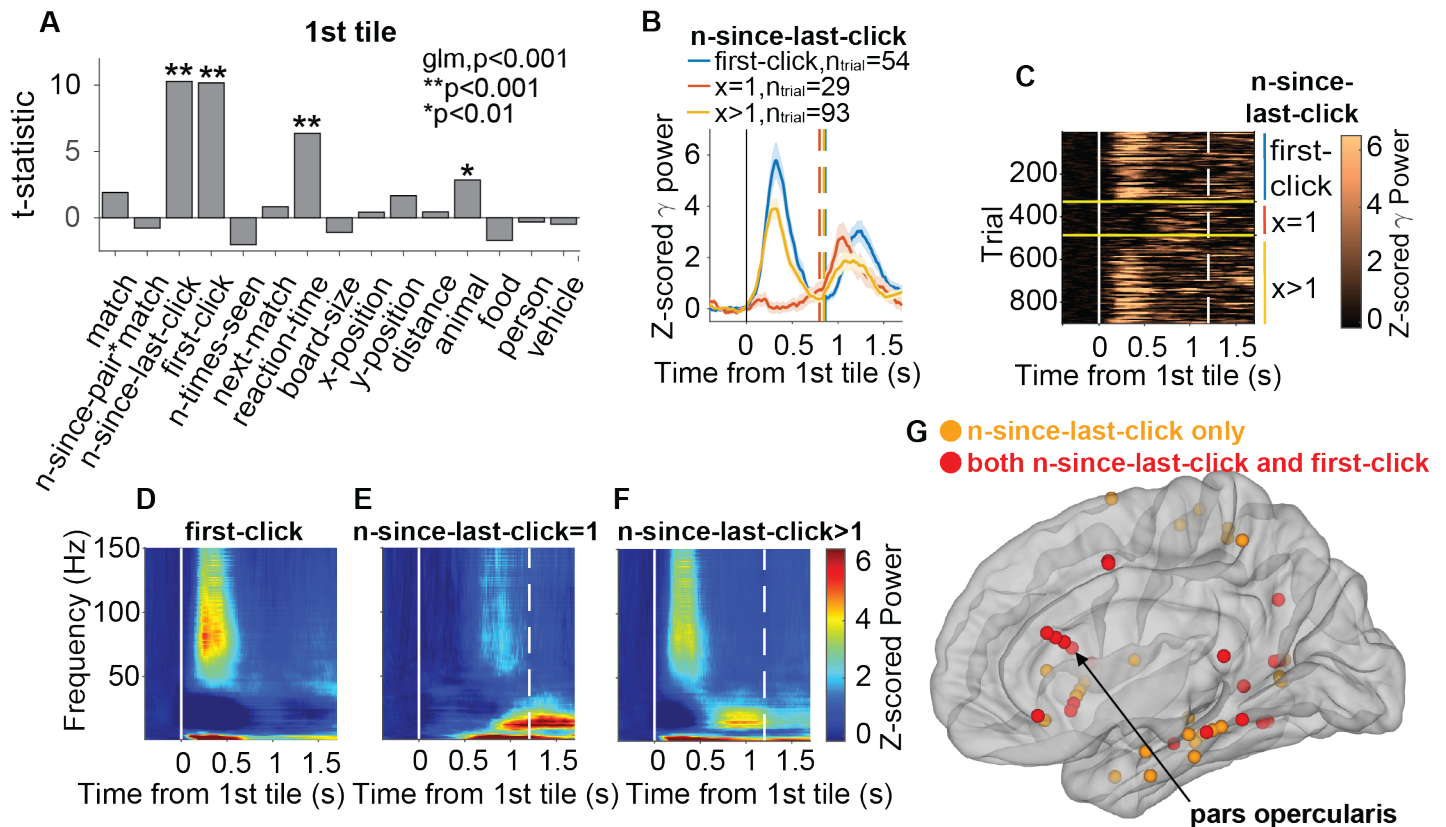


Figure 3.7: An example of a pars opercularis electrode where gamma activities increased for *first-click* and larger *n-since-last-click* tiles. **A.** T-statistic of each predictor in the GLM. Asterisks indicate significant predictors for the gamma power AUC. **B.** Z-scored gamma power aligned to the 1st tile onset for *first-click* (blue line), clicked in the previous tile (red line) or clicked more than one tile ago (yellow line) tiles. Shaded error bars indicate SEM. Dashed line indicates the mean RT. **C.** Raster plots showing the z-scored gamma power in individual trials ordered by *first-click* and then from smaller to larger *n-since-last-click*; division indicated by yellow horizontal lines and colored vertical lines. **D-F.** Spectrograms showing the power aligned to the 1st tile onset during *first-click* (**D**), *n-since-last-click*=1 (**E**), and *n-since-last-click*>1 (**F**). **G.** Locations of all *n-since-last-click* electrodes during the 1st tile. Orange: *n-since-last-click* only; red: both *n-since-last-click* and *first-click*.

3.3.2 Associative memory: *match* and *n-since-pair*match*

Upon the visualization of the 1st tile, participants also had to associate the tile and its pair to cue-recall the tile’s pair position, and so to reactivate the memory of the pair. This mechanism was necessary to successfully perform a match. We refer to this recall memory as associative memory (Introduction 1.1.2). In this section, we analyze electrodes whose neural responses could predict successful (*match*) or failed (*mismatch*) recollection and familiarity with the 1st tile’s pair.

Recollection of the tile’s pair: *match*

We hypothesize that upon the visualization of the 1st tile and before the 2nd tile, differential gamma responses for *match* versus *mismatch* trials could encode successful or failed recollection of the tile’s pair, respectively. The *match* predictor was significant ($p < 0.01$, GLM) for 32 electrodes in the gray matter (4.7% of all gray matter electrodes, Table B.4, Figure 3.8G) and 30 electrodes in the white matter (6% of all white matter electrodes, Table D.4). In the majority of cases (91%), activity was higher during *match* trials (successful recollection of the pair) than during *mismatch* trials (failed recollection). It is important to highlight that the trial’s outcome (*match* or *mismatch*) was only revealed after the 2nd tile was clicked. Hence, increased neural responses for *match* trials after the 1st tile could not be related to feedback signals, but rather to the recollection of the tile’s pair information necessary to perform a *match*.

The locations of all the *match*-selective electrodes after the 1st tile, shown in Figure 3.8G (gray matter), reveal that the majority were located in the LOF cortex and MTL. The LOF cortex had significantly more electrodes than expected by chance ($p < 0.01$, bootstrap analysis with 5,000 shuffles, Methods 2.7). Neural responses from an example electrode located in the right LOF gyrus are shown in Figure 3.8. The only predictor that showed a significant contribution to explaining the neural responses was whether the trial was a *match* or not ($p < 0.001$, Figure 3.8A). Indeed, when aligning the neural responses to the 1st click, there was a large increase in the gamma power in response to *match*, but not to *mismatch* trials (Figure 3.8B). This difference was evident even when examining individual trials (Figure 3.8C versus 3.8D) and was particularly manifested in the low gamma frequency band (Figure 3.8E versus 3.8F). The peak in activity happened at approximately 500 ms after the 1st click (Figure 3.8B). As discussed in Results 3.1, the *match* predictor correlated with several other predictors (Figure 3.1). However, the GLM analysis shows that it is the *match*, but not these other predictors, that accounts for the neural responses (Figure 3.8A). To further establish this point, Figure 3.8H shows the responses of this same electrode, in the same format as Figure 3.8B, after equalizing the *n-since-last-click* distributions for *match* and *mismatch* trials. The same conclusions hold in this case. Furthermore, Figure 3.8I shows a scatter plot of the gamma power AUC for different values of *n-since-last-click* only for *match* trials and Figure 3.8J shows the same plot for this same electrode but only for *mismatch* trials. The variable *n-since-last-click* did not account for the neural responses in either case ($p > 0.18$, linear regression). Similar conclusions hold for the other predictors.

Figure 3.9 shows another example electrode located in the left middle temporal gyrus where *match* was a significant predictor for the gamma band activity between the 1st and 2nd tile (Figure 3.9A-D). Similar to the LOF electrode in Figure 3.8, the gamma power during *match* trials was higher than during *mismatch* trials. However, the pattern of this modulation was different in several

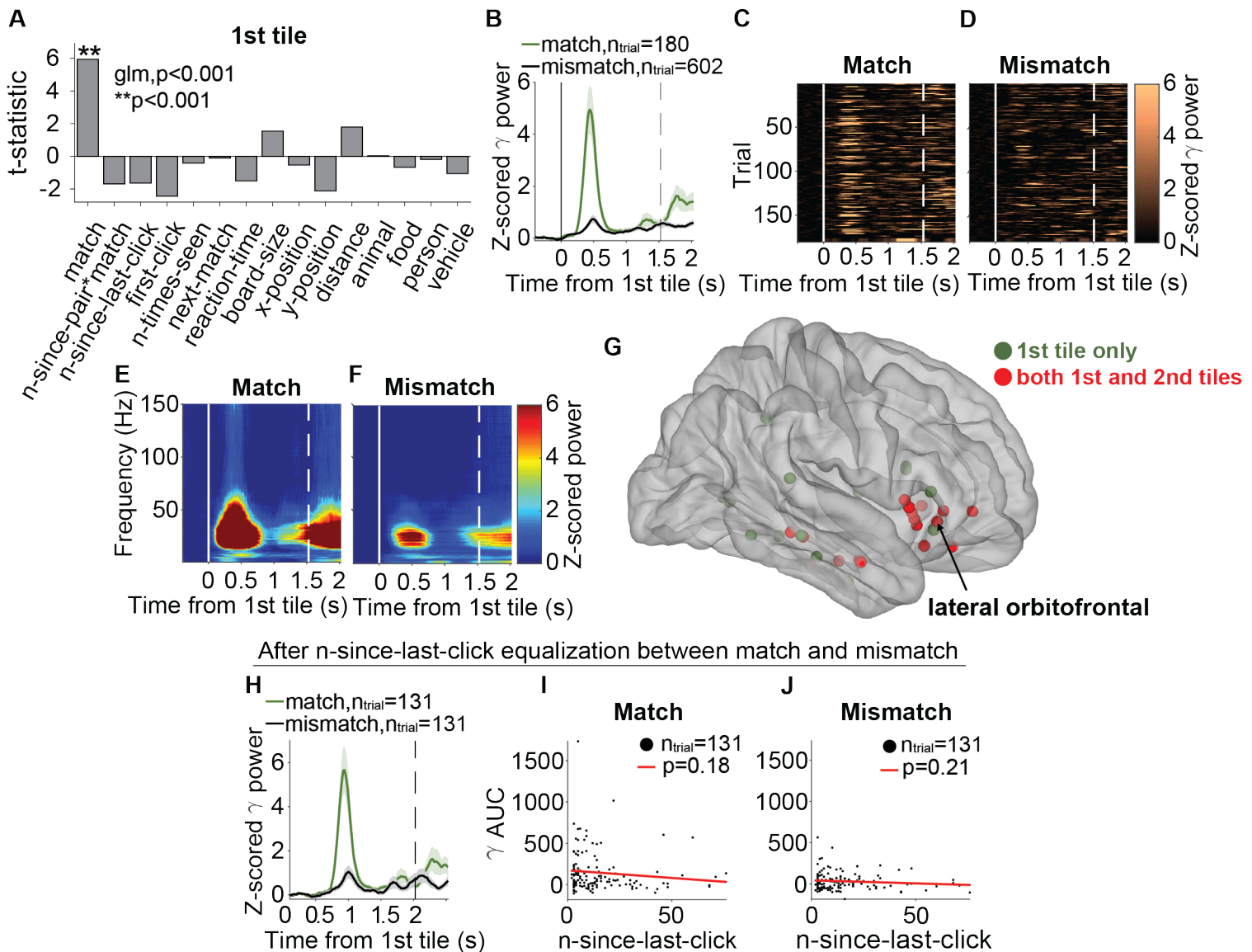


Figure 3.8: An example electrode in the right LOF gyrus where *match* was a significant predictor for gamma activities during the 1st tile. **A.** T-statistic of each predictor in the GLM for the 1st tile. Asterisks indicate significant predictors for the gamma power AUC. **B.** Z-scored gamma power during match (green) and mismatch (black) trials aligned to the 1st tile onset (solid line). Dashed line indicates the mean reaction time. Legend denotes the number of match and mismatch trials. Shaded error bars indicate SEM. **C-D.** Raster plots showing the z-scored gamma power in individual trials. For display purpose, trial number of match and mismatch was equalized (Methods 2.8). **E-F.** Spectrograms showing the band power during match and mismatch trials aligned to the 1st tile onset. **G.** Location of all electrodes where match is a significant predictor during the 1st tile only (green) and during both tiles (red) plotted on one hemisphere. **H-J.** After equalizing *n-since-last-click* values between match and mismatch. **H.** Same as **A.** **I-J:** Scatter plots of AUC gamma power vs. *n-since-last-click* for match (**I**) and mismatch (**J**). Each dot represents data from one trial. Red lines represent linear fits of the data.

ways. First, the power increase was sustained rather than transient (compare Figure 3.9B-D versus Figure 3.8B-D). Second, the frequency modulated by match was higher than the LOF electrode (compare Figure 3.9I-K versus Figure 5E-F). These results suggest that the middle temporal region and LOF cortex might be functionally distinct during associative memory retrieval. Figure 3.10 shows an electrode located in the precuneus where match was also a significant predictor after the 1st tile. This electrode shows a similar pattern of modulation to the LOF electrode 3.8.

In sum, these results indicate that even before the actual trial's outcome, there were distinct neural responses that were predictive of whether a trial would be a match.

Familiarity with the tile's pair: *n-since-pair*match*

We have demonstrated that differential neural responses could predict match or mismatch before the 2nd tile was clicked. Next, we asked whether gamma activity partakes in capturing the tile's pair status in STM. The *n-since-pair* predictor is related to the memory strength or familiarity of a tile's matching pair. The smaller the *n-since-pair*, the more recently the tile's pair had been seen, as if the memory is fresher or more familiar. We considered only match trials for this predictor (*n-since-pair*match*) because there was no successful retrieval of the tile's pair in mismatch trials. *n-since-pair*match* was a significant ($p < 0.01$, GLM) predictor for the gamma power AUC during the 1st tile in 15 (2.2%) electrodes (Table B.4, Figure 3.9E). See Table D.4 for white matter results (9, 1.8%). Figure 3.9 shows an *n-since-pair*match* electrode in the left middle temporal gyrus. The gamma power progressively decreased as the matching pair became more distant in memory (Figure 3.9F-H,I-L) and thus *n-since-pair* exhibited a negative t-statistic (Figure 3.9A). Moreover, we can see that under no successful memory retrieval (mismatch), there was a decrease in the gamma power compared to successful memory retrieval (match) for different *n-since-pair* values (Figure 3.9L versus 3.9I-K). Figure 3.10 shows an example of an electrode located in the precuneus that also presented *n-since-pair*match* as a significant predictor. As for the middle temporal electrode 3.9, the more recently the paired tile was last seen, the higher the gamma responses. The middle temporal (Figure 3.9) and precuneus (Figure 3.10) electrodes showed different patterns of frequency modulation. The precuneus electrode showed a transient activity increase in the low gamma and beta frequency band (Figure 3.9I-K). On the other hand, the middle temporal electrode showed a sustained increase of gamma activities that did not expand to the beta band (Figure 3.9I-K).

We hypothesize that *n-since-pair*match* electrodes with negative t-statistics are more sensitive to recently viewed pairs and make them readily available for retrieval. We then asked whether any electrode showed the reverse phenomenon, that is, higher gamma activity toward a tile whose pair was seen a long time ago; thus, *n-since-pair*match* would have a positive t-statistic. Indeed, three electrodes (20%) had this property (see Figure C.2 for an example of an electrode in the LOF cortex). Since we did not consider *n-since-pair*mismatch* in the GLM, we added a linear regression analysis using *n-since-pair* as the independent variable and the gamma-band power AUC as the dependent variable, for match and mismatch trials separately (Figure 3.9G-H, Table B.5). All except for one *n-since-pair*match* electrodes could significantly predict the gamma power of match trials from *n-since-pair* values ($p < 0.01$, linear regression). In contrast, none of these electrodes could predict gamma power AUC from *n-since-pair* using mismatch trials ($p > 0.06$, linear regres-

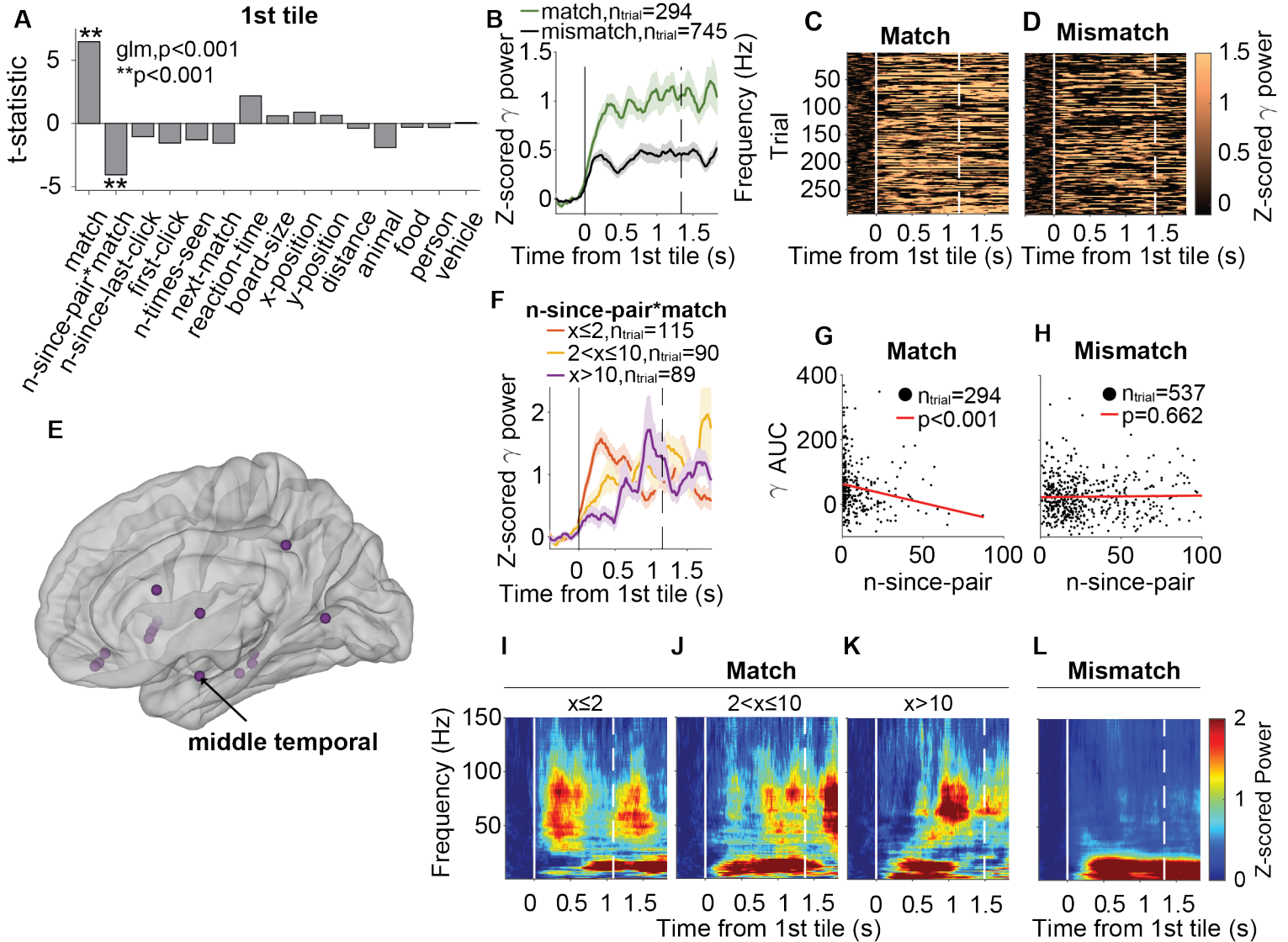


Figure 3.9: An example electrode located in the left middle temporal gyrus where *match* and *n-since-pair*match* were significant predictors **A.** T-statistic of each predictor in the GLM for the 1st tile. Asterisks indicate significant predictors for the gamma power AUC. **B.** Z-scored gamma power during match (green) and mismatch (black) trials aligned to the 1st tile onset (solid line). **C-D.** Raster plots showing the z-scored gamma power in individual trials. For display purpose, trial number of match and mismatch was equalized (Methods). **F.** Z-scored gamma power grouped by different *n-since-pair* ranges for match trials aligned to the 1st tile onset (solid line). Dashed line indicate the mean reaction time. Shaded error bars indicate SEM. **G-H.** Scatter plots of AUC gamma power vs. *n-since-pair* for match (**G**) and mismatch (**H**). Each dot represents data from one trial. Red lines represent linear fits of the data. **I-K.** Spectrograms showing the band power aligned to the 1st tile for different *n-since-pair* ($x=n-since-pair$) values for match trials. **L.** Spectrogram showing the band power aligned to the 1st tile for mismatch trials. **E.** Locations of all *n-since-pair*match* electrodes plotted on one hemisphere.

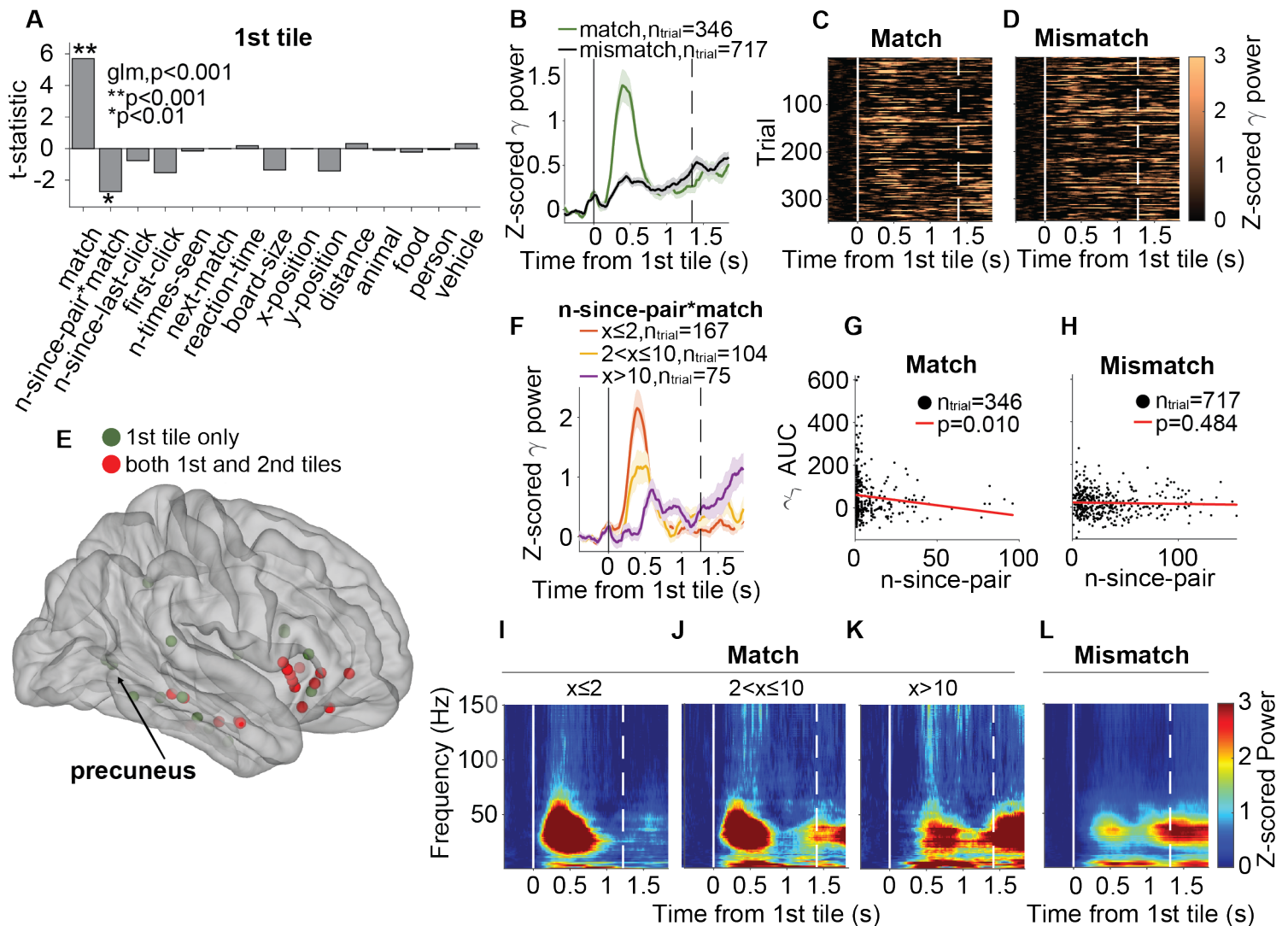


Figure 3.10: An example electrode located in the precunes where *match* and *n-since-pair*match* were significant predictors. **A.** T-statistic of each predictor in the GLM for the 1st tile. Asterisks indicate significant predictors for the gamma power AUC. **B.** Z-scored gamma power during match (green) and mismatch (black) trials aligned to the 1st tile onset (solid line). **C-D.** Raster plots showing the z-scored gamma power in individual trials. For display purpose, trial number of match and mismatch was equalized (Methods). **F.** Z-scored gamma power grouped by different *n-since-pair* ranges for match trials aligned to the 1st tile onset (solid line). Dashed line indicate the mean reaction time. Shaded error bars indicate SEM. **G-H.** Scatter plots of AUC gamma power vs. *n-since-pair* for match (**G**) and mismatch (**H**). Each dot represents data from one trial. Red lines represent linear fits of the data. **I-K.** Spectrograms showing the band power aligned to the 1st tile for different *n-since-pair* ($x=n$ -since-pair) values for match trials. **L.** Spectrogram showing the band power aligned to the 1st tile for mismatch trials. **E.** Locations of all *n-since-pair*match* electrodes plotted on one hemisphere.

sion). Therefore, the ability to code the memory strength and/or familiarity of the associative pair only existed in the context of successful retrieval. Moreover, 11 of these electrodes (73.3%) also had match as a significant predictor (Table B.4, both Figure 3.9 and 3.10 are examples), meaning that they encoded both successful retrieval and the memory strength or familiarity to the tile’s pair. These results support the continuous strength model of familiarity and recollection rather than the dual-process model (Introduction 1.1.3). Figure E.4 and Figure E.5 show two examples of white matter electrodes located close to the pars opercularis and LOF cortex, respectively, whose gamma activities were also modulated by the *n-since-pair* and *match* predictors.

3.4 Second tile memory-selective electrodes

Next, we examined neural activities after the 2nd tile, when participants already knew the trial’s outcome (match or mismatch). We used a separate GLM using the same 14 predictors as for the 1st tile, except for *n-since-pair*match* (Table 2.2), to describe the AUC of the gamma power during 1 s after the 2nd tile click.

3.4.1 Non-associative memory: *first-click* and *n-since-last-click*

First, we asked whether novelty and familiarity were also encoded in the neural responses upon the 2nd visualization. Similar to the 1st tile, *first-click* and *n-since-last-click* could represent the degree of novelty or familiarity with the 2nd tile. For the 2nd tile, *first-click* was a significant predictor in 24 electrodes in the gray matter (Figure 3.11H, Table B.6) and 12 in the white matter (Table D.5). *N-since-last-click* was a significant predictor in 9 electrodes for the 2nd tile in the gray matter (Figure 3.11G, Table B.6) and 24 in the white matter (Table D.5). Among all the nine *n-since-last-click* electrodes during the 2nd tile, seven electrodes also had *first-click* as a significant predictor (Figure 3.11G,H, red spheres). During the 2nd tile, two images (same if match, different if mismatch) were present at the same time on the board. If the trial was a match, the consecutive visualization of the same image might make appear the 2nd tile as more familiar, regardless of when it was clicked last time. Moreover, for match trials, the information about the 2nd tile no longer needs to be encoded in working memory. Therefore, after the 2nd tile, we do not expect to find signals related to the tile’s information maintenance in STM for match trials. These facts might explain the drastic reduction in the number of *n-since-last-click* and *first-click* electrodes compared to the 1st tile. In all, it is more difficult to interpret novelty or familiarity after the 2nd tile. The LOF cortex contained four *n-since-last-click* electrodes for the 2nd tile, which were significantly more than chance ($p < 0.01$, 5,000 random sampling, Methods 2.7). Figure 3.11 shows an example electrode in the LOF region. Similar to the pars opercularis responses in Figure 3.7, this electrode exhibited the highest gamma power towards novel and less familiar tiles. The pars opercularis electrode in Figure 3.7 was also capable of distinguishing first-clicks versus else, while the *first-click* predictor was not significant for the LOF electrode (*first-click* $p > 0.01$, GLM, Figure 3.11A). However, it showed almost the same responses to first clicks and unfamiliar images (Figure 3.11B, blue line; Figure 3.11D, F versus Figure 3.11E). This difference was also observed at the single trial level (Figure 3.11C).

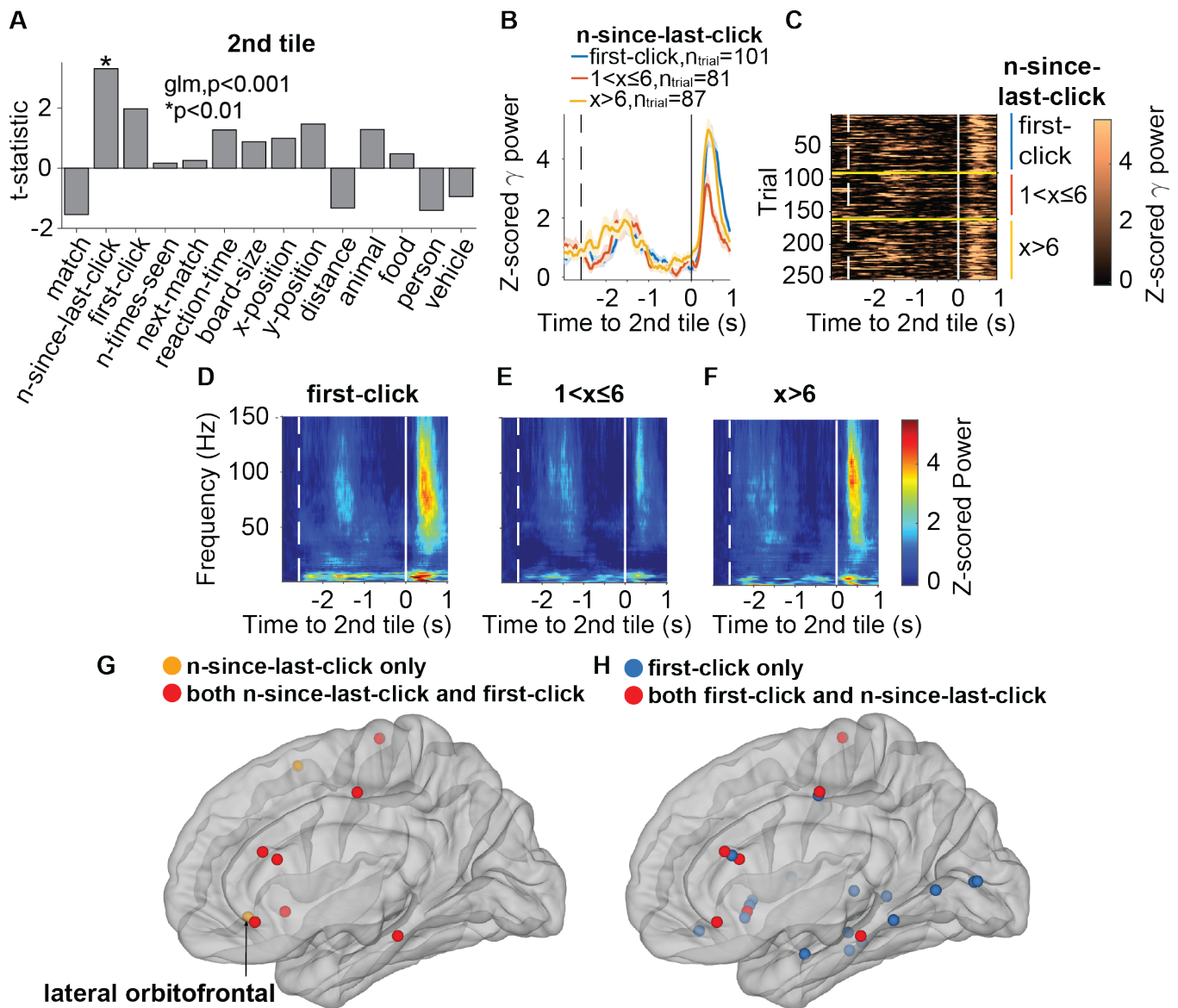


Figure 3.11: An example of a LOF electrode where *n-since-last-click* was a significant predictor for gamma activities after the 2nd tile. **A.** T-statistic of each predictor in the GLM. Asterisks indicate significant predictors for the gamma power AUC. **B.** Z-scored gamma power aligned to the 2nd tile click for *first-click* (blue line), *n-since-last-click* ≤ 6 (orange line) and *n-since-last-click* > 6 . *n-since-last-click* threshold (6) was selected to maximize the number of trials in each group. Shaded error bars indicate SEM. Dashed line indicates the mean RT. **C.** Raster plots showing the z-scored gamma power in individual trials ordered by *first-click* and then from smaller to larger *n-since-last-click*; division indicated by yellow horizontal lines and colored vertical lines. **D-F.** Spectrograms showing the power aligned to the 1st tile onset during *first-click* **D**, *n-since-last-click* ≤ 6 **E**, and *n-since-last-click* > 6 **F**. **G.** Locations of all *n-since-last-click* electrodes after the 2nd tile. Orange: *n-since-last-click* only; red: both *n-since-last-click* and *first-click*. **H.** Locations of all *first-click* electrodes after the 2nd tile. Blue: *first-click* only; red: both *n-since-last-click* and *first-click*.

3.4.2 Associative memory: *next-match*

Inspired by the observation that distinct gamma power levels for match versus mismatch could predict successful retrieval before the 2nd tile was clicked (Results 3.3.2), we used the *next-match* predictor to ask whether gamma responses during the current trial can predict the outcome of the subsequent trial. This predictor was significant ($p < 0.01$, GLM) for 10 electrodes during the 2nd tile (Table B.8). Results of white matter were reported in Table D.7. Figure 3.12 shows an example electrode located in the left precuneus where the gamma responses after the 2nd tile predicted whether the next trial was a match or not. There were higher gamma activities after the 2nd tile if the subsequent trial was a match (Figure 3.12B). Figure 3.12D-E presents the z-scored gamma band power in individual trials and divides the match trials by whether the current trial contained the same image as in the next trial (above the yellow line) or not (below the yellow line). There were stronger gamma activities if the current and the next trial contained the same image, which supports the hypothesis that the visualization of the 2nd tile prompted the retrieval of the associative information necessary to match the subsequent trial.

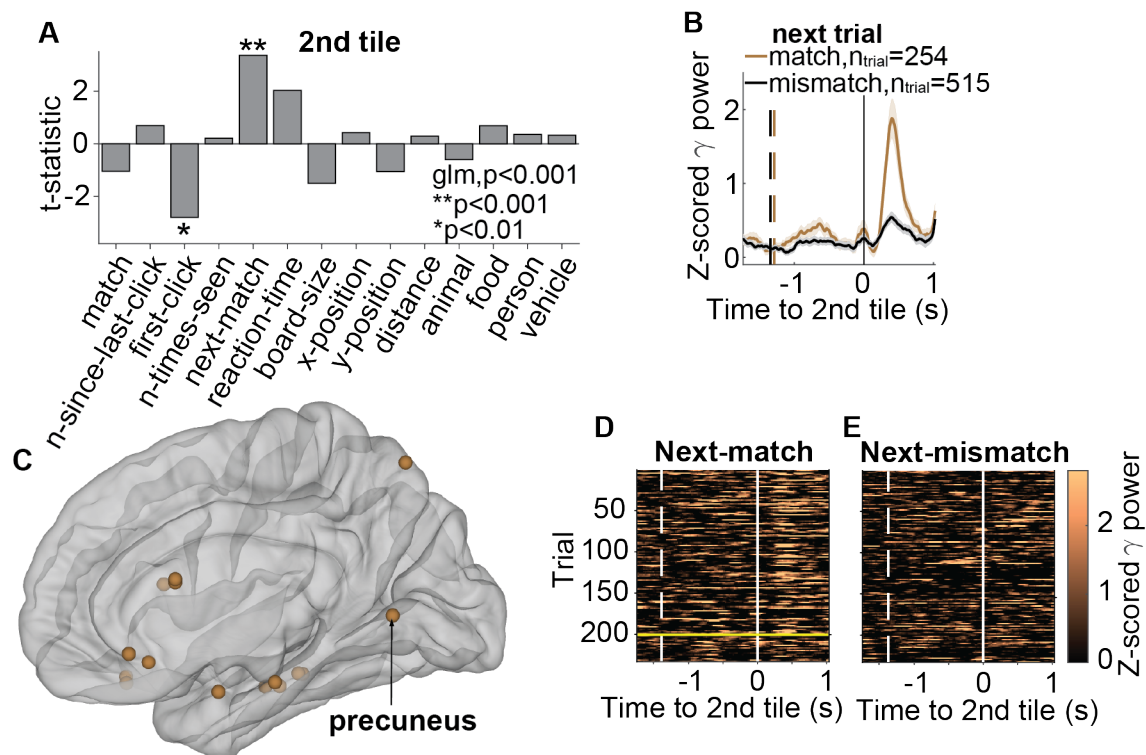


Figure 3.12: Example *next-match* electrode during the 2nd tile, located in the left precuneus.

A. T-statistic of each predictor in the GLM. Asterisks indicate significant predictors for the gamma power AUC. **B.** Z-scored gamma power during the current mismatch trials aligned to the 2nd tile onset grouped by whether the next trial was a match (brown) or mismatch (black). Shaded error bars indicate SEM. **B.** Locations of all *next-match* electrodes during the 1st and 2nd tile plotted on one hemisphere. **D-E.** Raster plots showing the z-scored gamma power in individual trials. Trials above the yellow line contained the same image as in the next trial.

3.5 Feedback: *match* after the second tile

Next, we asked whether the differences between match and mismatch trials were also manifested after participants had clicked the 2nd tile, i.e., after the participant became explicitly aware of whether the trial was a match or not. After the 2nd tile, the *match* predictor was statistically significant ($p < 0.01$, GLM) for 112 electrodes in the gray matter (16.6% of all gray matter electrodes, Table B.7, Figure 3.13G) and 66 electrodes in the white matter (13.4% of all white matter electrodes, Table D.6). The locations of all these electrodes, shown in Figure 3.13G (gray matter), reveal that the majority were located in the LOF cortex and the insula. The proportion of significant electrodes in both regions was higher than expected by chance ($p < 0.01$, bootstrap analysis with 5,000 random shuffles, Methods 2.7).

Figure 3.13 shows an example electrode located in the insula where *match* was a significant predictor for the gamma band activity after the 2nd tile ($p < 0.001$, GLM, Figure 3.13A). The neural signals during match trials were larger than during mismatch trials (Figure 3.13B). It is to be noted that the frequency increase for match trials was circumscribed to the lower gamma frequency band, and also to the beta band (Figure 3.13E). In the raster plots, we show the average beta band power for single trials, but not gamma-band power (Figure 3.13C-D). We can see that the increase in beta power for match versus mismatch trials happens even at the single trial level (Figure 3.13C versus 3.13D). For these electrodes, the GLM after the 1st tile was not significant ($p > 0.01$). Therefore, increased gamma activities for match were exclusive of positive feedback (successful match) after the 2nd tile was revealed. The increase in gamma activities for match trials happened approximately 500 ms after the 1st click (Figure 3.13B). Figure C.3 shows another electrode located in the insula that also presented match as a significant predictor after the 2nd tile. This electrode showed the same pattern of modulation as the insula electrode in Figure 3.13. However, the insula electrode in Figure C.3 showed a small increase in gamma activities before the 2nd tile was revealed (Figure C.3B), which could be related to reward anticipation. However, the GLM for the 1st tile was not significant ($p > 0.01$). It is to be noted that these insula electrodes (Figure 3.13 and Figure C.3) were recorded from different subjects. The same pattern of modulation was found for other insular electrodes in other subjects.

Figure C.4 shows another example electrode in the LOF cortex that also presented match as a significant predictor after the 2nd tile. This electrode showed a different pattern of modulation, characterized by a drop of gamma activities for mismatch trials after the 2nd tile was revealed (Figure C.4B, E versus F). See Figure C.2 for an analysis of gamma activities after the 1st tile for this electrode.

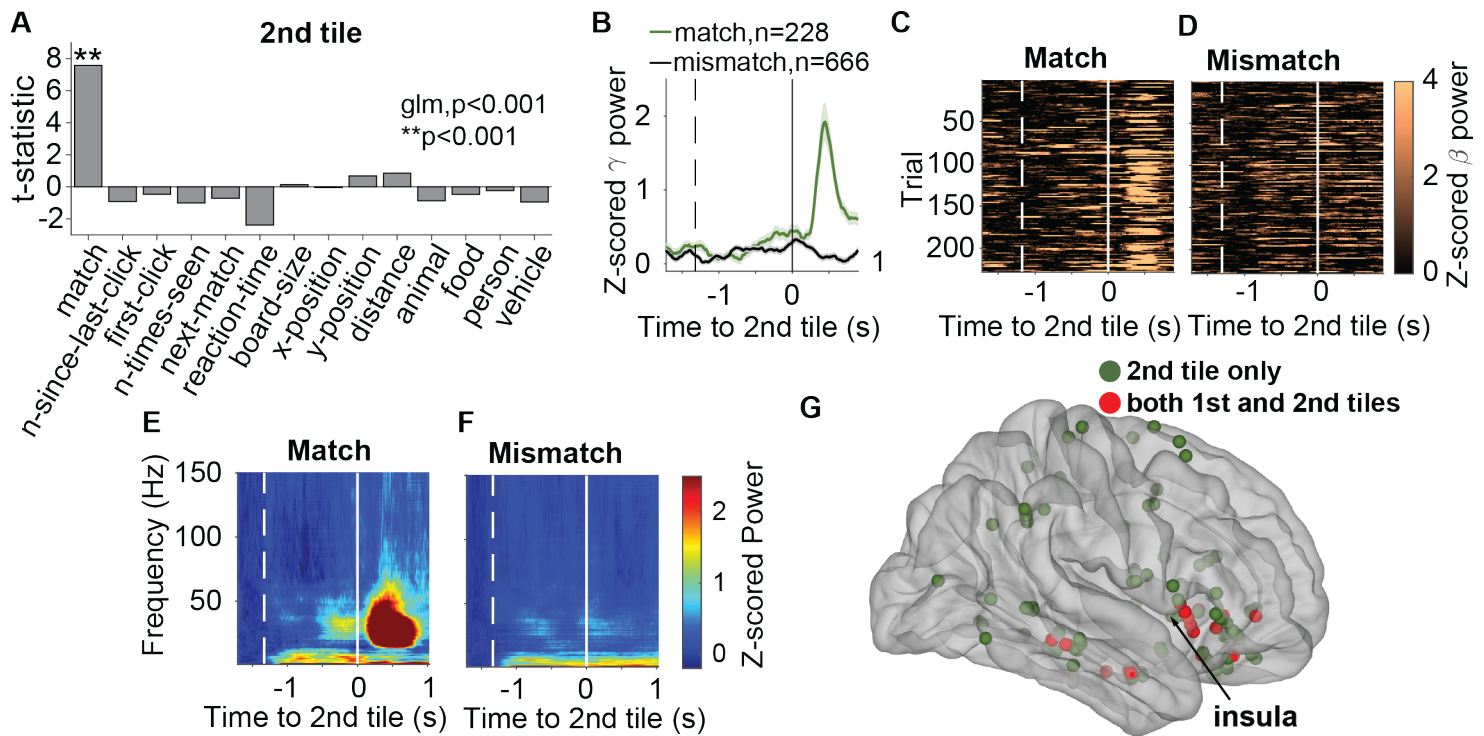


Figure 3.13: An example electrode in the insula where *match* was a significant predictor for gamma activities after the 2nd tile. **A.** T-statistic of each predictor in the GLM for the 2nd tile. **B.** Z-scored gamma power during match and mismatch trials aligned to the 2nd tile onset (solid line). Dashed line indicates the mean onset of the 1st tile. **C-D.** Raster plots showing the z-scored gamma power in individual trials. Number of match and mismatch trials was equalized (Methods 2.8). **E-F.** Spectrograms showing the band power during matched and mismatched trials aligned to the 2nd tile onset. **G.** Location of all electrodes where *match* is a significant predictor during the 2nd tile only (green) or during both tiles (red).

There were 17 electrodes in the gray matter and 15 electrodes in the white matter that presented *match* as a significant predictor both for the 1st and 2nd tiles. These electrodes represented 53.1% and 50% of the electrodes that were significant according to the 1st tile and 15.2%, and 22.8% of the electrodes that were significant according to the 2nd tile. These electrodes were located in the LOF cortex and medial temporal lobe (Figure 3.13G). The LOF electrodes in Figure 3.8 and the medial temporal electrode in Figure 3.9 are examples of such electrodes. After the 2nd tile, the middle temporal electrode (Figure 3.9 for the 1st tile and Figure 3.14 for the 2nd tile) revealed a continuous enhancement after the 1st tile (Figure 3.9B) that was sustained and enhanced after the onset of the 2nd tile (Figure 3.14B,C,E). On the other hand, mismatch trials did not induce gamma activities after the 1st or the 2nd tile (Figure 3.14B,D,F). See Figure C.5 for the analysis after the 2nd tile of the LOF cortex in Figure 3.8. See Figure E.6 for a white matter electrode located close to the LOF cortex that presented *match* as a significant predictor after the 2nd tile.

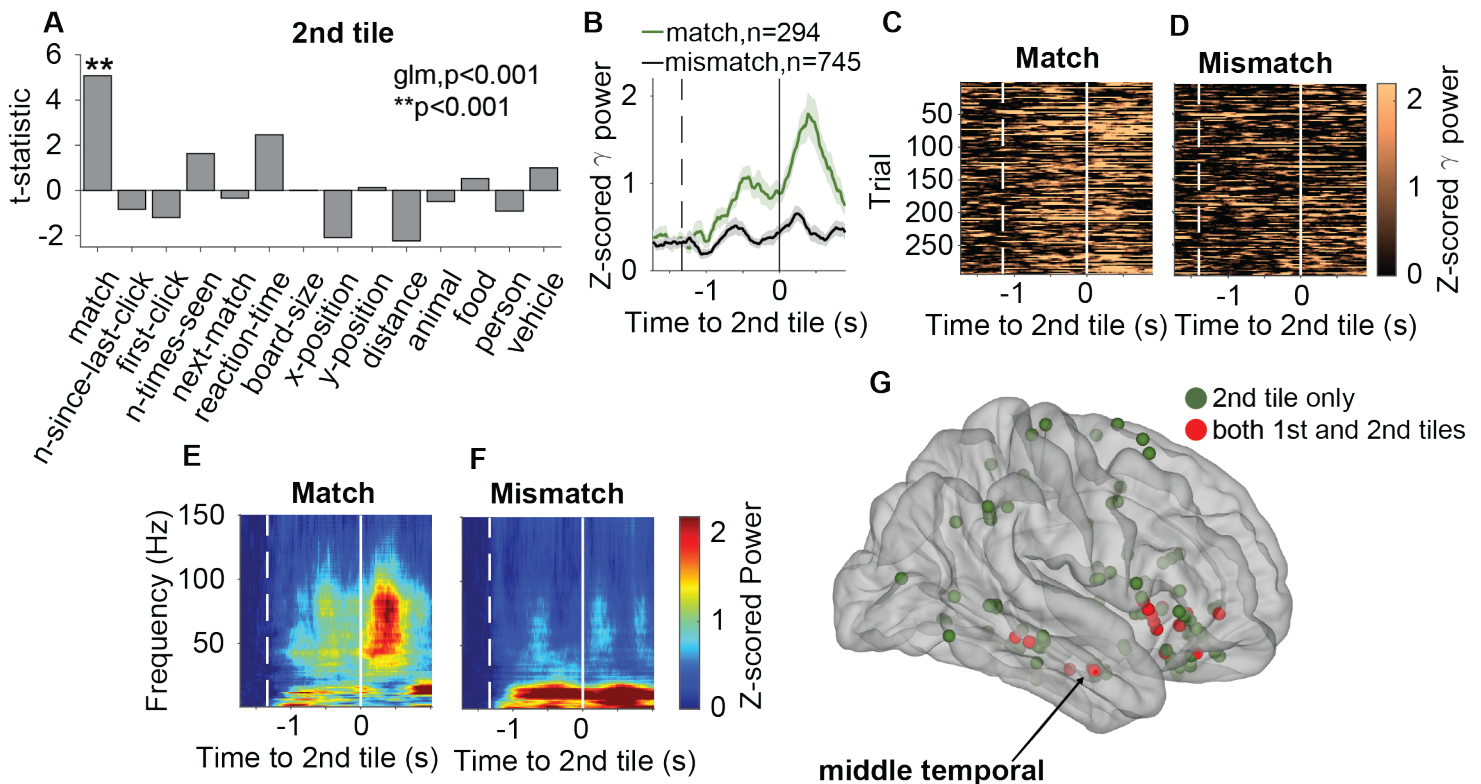


Figure 3.14: An example electrode in the middle temporal cortex where *match* was a significant predictor for gamma activities for both the 1st the 2nd tiles. See Figure 3.9 for the 1st tile. **A.** T-statistic of each predictor in the GLM for the 2nd tile. **B.** Z-scored gamma power during matched and mismatched trials aligned to the 2nd tile onset (solid line). Dashed line indicates the mean onset of the 1st tile. **C-D.** Raster plots showing the z-scored gamma power in individual trials. Number of match and mismatch trials was equalized (Methods). **E-F.** Spectrograms showing the band power during matched and mismatched trials aligned to the 2nd tile onset. **G.** Location of all electrodes where *match* is a significant predictor during the 2nd tile only (green) or during both tiles (red).

3.6 Visual selective electrodes

Next, we asked whether neural responses could encode information related to the tile’s content. Each of the tiles’ image belonged to one of 5 different categories: person, animal, food, vehicle or indoor scenes. We considered visual selective (VS) electrodes those that presented one or more of the image-category predictors (*animal*, *food*, *person*, *vehicle*) as significant predictors. There were 44 electrodes in the gray matter (6.5%, Table B.9, Figure 3.15A) and 29 electrodes in the white matter (6.1%, Table D.8) for which one of the image categories was significant after the 1st tile. After the 2nd tile, there were 37 VS electrodes in the gray matter (5.5%, Table B.10, Figure 3.15B) and 27 in the white matter (5.5%, Table D.9). The fusiform cortex contained significantly more VS electrodes than expected by chance ($p < 0.01$, 5,000 random sampling, Methods 2.7).

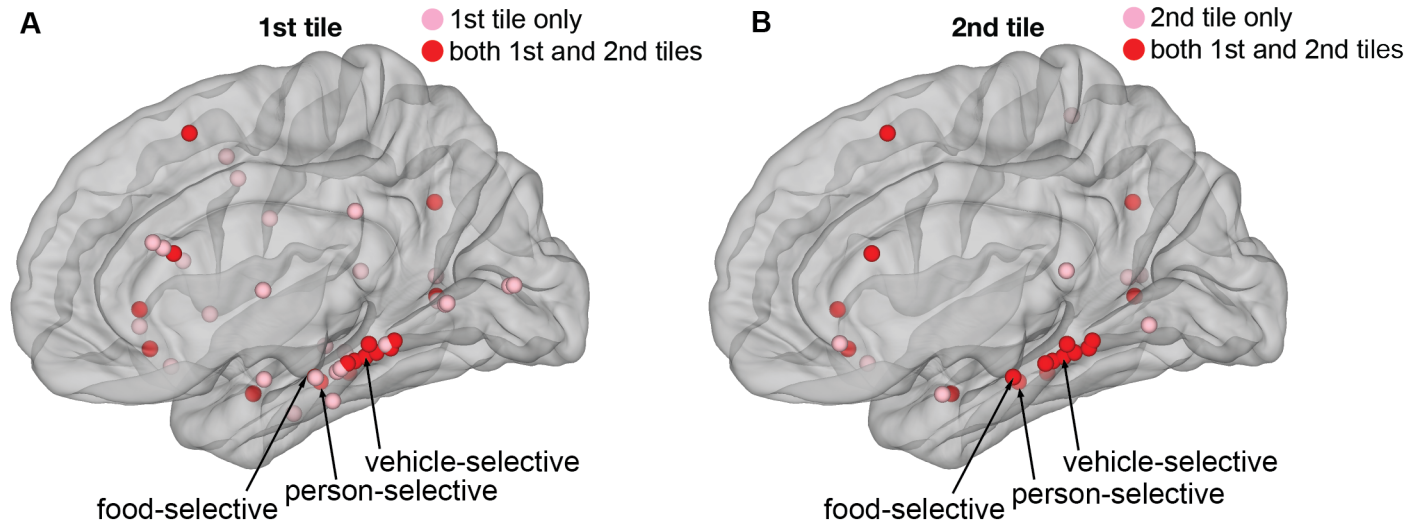


Figure 3.15: Visual selective electrodes' location. Location of all electrodes where one or more image categories were significant for the 1st tile (A) and 2nd tile (B) GLM. Pink: only selective during the indicated tile. Red: selective for both tiles. *person-selective* indicates the location of the electrode in Figure 3.16A-D. *food-selective* indicates the location of the electrode in Figure 3.16E-H. *vehicle-selective* indicates the location of electrode in Figure 3.16I-L.

Figure 3.16 shows two examples of VS electrodes located in the fusiform, whose preferred categories were *person* (Figure 3.16A-D) and *food* (Figure 3.16E-H). Figure 3.16I-L shows an example parahippocampal electrode selective for *vehicle* (Figure 3.16I-L). These electrodes exhibited the highest gamma response towards their preferred category for both the 1st (Figure 3.16A,E,I) and the 2nd (Figure 3.16B,F,J) tiles. The spectrograms show that the increased activity happened mostly in the gamma power (3.16 C vs. D, G vs. H, K vs. L). It is interesting to note that for the person-selective electrode (Figure 3.16A-D), the animal category (Figure 3.16A-B green line), also presented slightly higher gamma responses compared to the other categories. This could be explained by the fact that person and animal are alive or animated objects, unlike the other categories. The food-selective electrode (3.16E-H), also presented increased gamma responses for indoor categories (3.16E-F yellow line). This result might be explained by the fact that some indoor images contained food items. See Figure E.7 for an example of a white matter electrode selective to person and animal, located close to the fusiform.

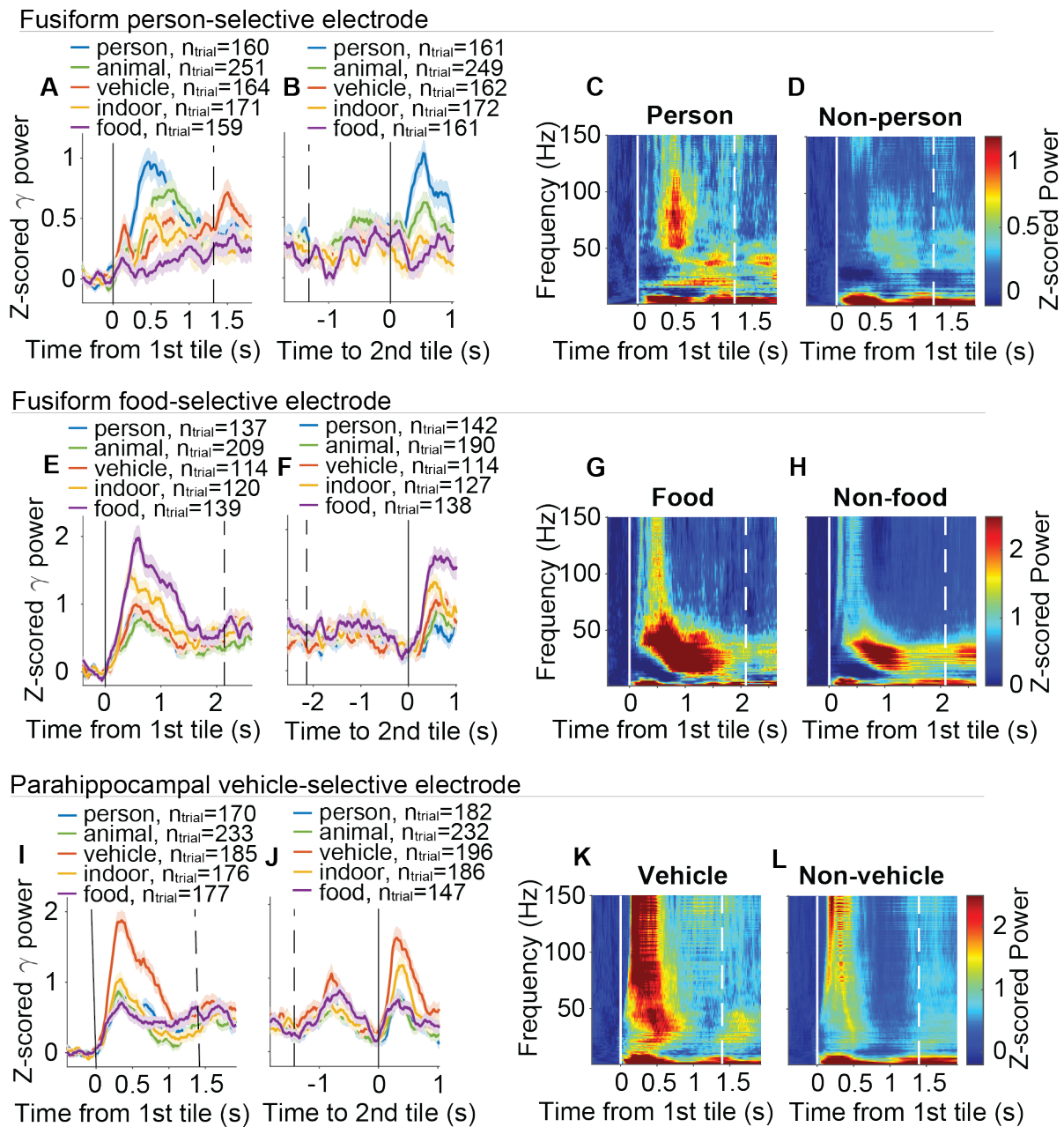


Figure 3.16: Examples of visual selective electrodes. A-D. Example of a person-selective electrode in the fusiform. E-H. Example of a food-selective electrode in the fusiform. I-J. Example of a parahippocampal vehicle-selective electrode. A-B, E-F, I-J Z-scored gamma power for tiles containing a person (blue), animal (green), vehicle (red), indoor (yellow), food (purple) image category. A, E, I. Aligned to the 1st tile. B, F, J. Aligned to the 2nd tile. C-D, G-H, K-L Spectrograms aligned to the 1st tile showing the band power for the preferred (C, G, K) and non-preferred (D, H, L) image category for each electrode. Figure 3.15 shows the location in the brain of these electrodes.

3.7 Visual selective vs. memory selective electrodes

In this section, we compare three types of electrodes. First, VS electrodes, which we defined as electrodes selective for one or more image categories (Results 3.6). Second, non-associative memory selective (NAMS) electrodes, which presented *first-click* and/or *n-since-last-click* as significant predictors and thus encoded novelty and familiarity to the current viewing tile (Results 3.3.1). Third, associative memory selective electrodes (AMS), whose neural responses encoded information about the retrieval of the tile’s pair (3.3.2) and thus presented *match* and/or *n-since-pair*match* as significant predictors. Due to the consecutive visualization of two tiles after the 2nd tile was clicked, it is more difficult to analyze NAMS electrodes when using the neural responses after the 2nd tile. Moreover, since this game consists of a cue-recall visual task upon the 1st tile visualization, AMS electrodes are better studied when considering neural responses after the 1st tile. Therefore, in this section we focus on the electrodes that were VS (Results 3.16), AMS (Results 3.3.2) or NAMS (Results 3.3.1) after the 1st tile.

First, we analyzed whether these three populations were independent or not. Table 3.1 compares the proportion of VS, AMS or NAMS electrodes belonging to each of the other categories. For instance, 43.18% of the VS electrodes also contained information about familiarity and novelty to the current tile (NAMS), while only 13.64% contained information about the tile’s pair. Similarly, 25.33% of NAMS electrodes also contained information about the image category (VS), while only 13.64% of NAMS electrodes also encoded information about the tile’s pair (AMS). Both VS and NAMS electrodes encoded information regarding the current viewing tile, while AMS electrodes contained information about the tile’s pair. Therefore, it is to be expected that there is a higher overlap between VS and NAMS, than between VS or NAMS and AMS electrodes. Figure 3.17 shows an example of an electrode located in the fusiform that presented *first-click*, *n-since-last-click* and *vehicle* as significant predictors for the 1st tile GLM (Figure 3.17A), all of them positively correlated with the gamma power AUC. Hence, this electrode showed increased gamma responses towards novel or unfamiliar items (Figure 3.17B). Moreover, it also showed increased gamma responses for tiles displaying vehicles (Figure 3.17C).

Table 3.1: Percentage of VS, NAMS and AMS electrodes that are also VS, AMS and NAMS. Each row indicates the percentage of electrodes in the indicated population that are also VS (column 1), NAMS (column 2) and/or AMS (column 3). n indicates the total number of electrodes in each population.

	% Visual Selective	% Non-Associative MS	% Associative MS
Visual Selective (n=44)	100	43.18	13.64
Non-Associative MS (n=75)	25.33	100	16
Associative MS (n=36)	16.67	33.33	100

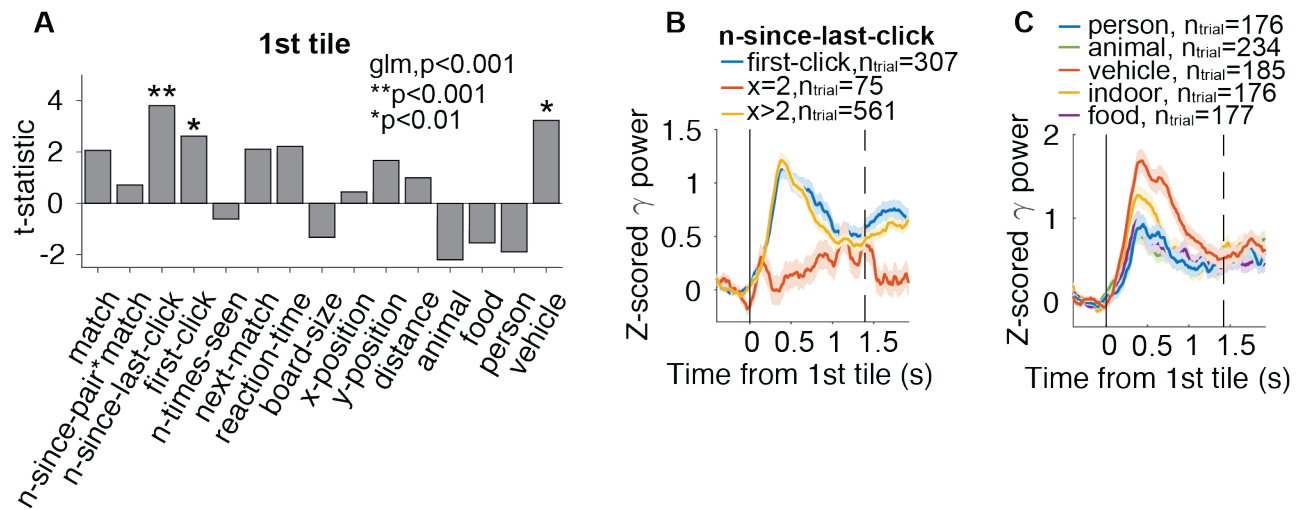


Figure 3.17: Example of a VS and NAMS electrode located in the fusiform. **A.** T-statistic of each predictor in the GLM. Asterisks indicate significant predictors for the gamma power AUC. **B.** Z-scored gamma power aligned to the 1st tile onset for first-click (blue line), clicked in the previous trial (red line) or clicked more than one trial ago (yellow line) tiles. **C.** Z-scored gamma power for tiles containing a person (blue), animal (green), vehicle (red), indoor (yellow), food (purple) image category. Shaded error bars indicate SEM. Dashed line indicates the mean RT.

For AMS electrodes, 16.67% and 33.3% of electrodes were also VS or NAMS, respectively. The higher overlap of AMS electrodes with NAMS than with VS might be explained by the fact that both AMS and NAMS were involved in working memory processes. Overall, there was a large number of VS, NAMS and AMS electrodes that only belonged to their population, and thus only encoded the object category, novelty or familiarity to the viewing tile, or retrieval of the tile’s pair, respectively. Table B.11 shows the percentage of VS, NAMS and AMS electrodes for each brain region.

3.7.1 Latency of visual selective and memory selective electrodes

We next estimated the response latency of VS, NAMS and AMS brain regions. We defined latency as the time at which the average gamma power over trials achieved 50% of the maximum gamma power (Methods 2.9, Figure 2.3). Figure 3.18 shows the average gamma power of all brain regions that contained two or more VS, AMS, or NAMS electrodes. Brain regions are ordered from smaller to larger latency and red dots indicate their estimated latency.

The fusiform, LOF, and pars opercularis cortex contained significantly more VS, match significant, and first-click significant electrodes than expected by chance after the 1st tile, respectively (Results 3.6, Results 3.3). Therefore, we compared the latency of these brain regions to analyze the dynamics of visual recognition, non-associative memory and associative memory. Figure 3.19A-B compares the latency of the fusiform (only VS electrodes) and pars opercularis (only NAMS electrodes) regions. Since the pars opercularis electrodes’ neural responses were modulated by familiarity and novelty, we divided the trials into first-clicks (3.19A) and non-first-click (3.19B). The

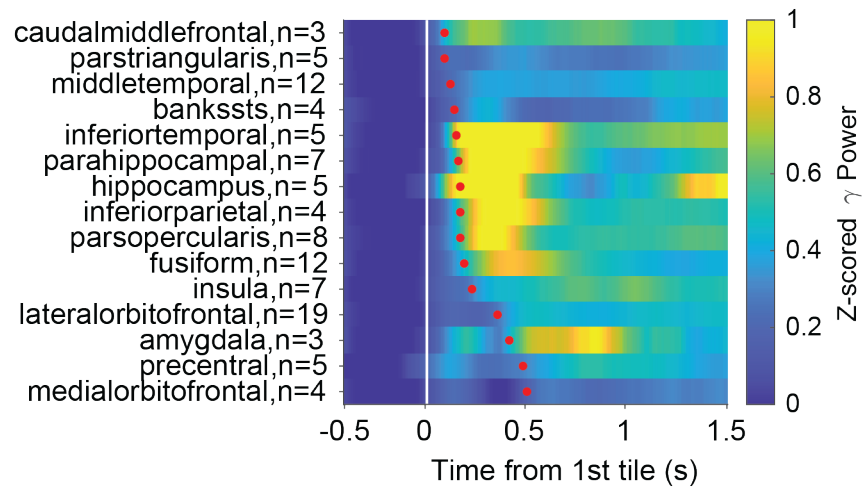


Figure 3.18: Comparison of the latency between VS, NAMS and AMS brain regions.. Raster plot showing the average z-scored gamma power in brain regions that contained more than two VS, AMS or NAMS electrodes. Alignment to the 1st tile. Red dot indicates the latency of each brain region. n indicates the number of electrodes.

line plots show the average gamma power over all trials of all the selected electrodes in each brain region. For the pars opercularis region (example electrode in Figure 3.7), the gamma power was higher for first-click than non-first-click trials, as expected (Figure 3.19A versus B orange line). However, this difference was less noticeable for the fusiform VS electrodes (Figure 3.19A versus B purple line). For both first-clicks and non-first-clicks, the latency of the fusiform (0.22s and 0.21s, respectively) and pars opercularis (0.21s and 0.19s, respectively) was very similar. Thus, it is not clear that object recognition in the fusiform happened before novelty recognition in the pars opercularis cortex.

Figure 3.19C-D compares the latency of the fusiform (only VS electrodes) and LOF cortex (only AMS electrodes, example Figure 3.8). We can see that match trials, but not mismatch trials, induced an increase in gamma power in the LOF cortex (Figure 3.19C versus D green line). However, the VS electrodes' response did not depend on whether the trial would be matched or not (Figure 3.19C versus D purple line). In this case, the average differential latencies of fusiform VS electrodes and LOF AMS electrodes was 100 ms. In all, comparing the activity of fusiform VS, LOF AMS and pars opercularis NAMS electrodes, we found that object and novelty recognition in the fusiform and pars opercularis cortex happened at a similar time. In contrast, AMS activity in the LOF happened later.

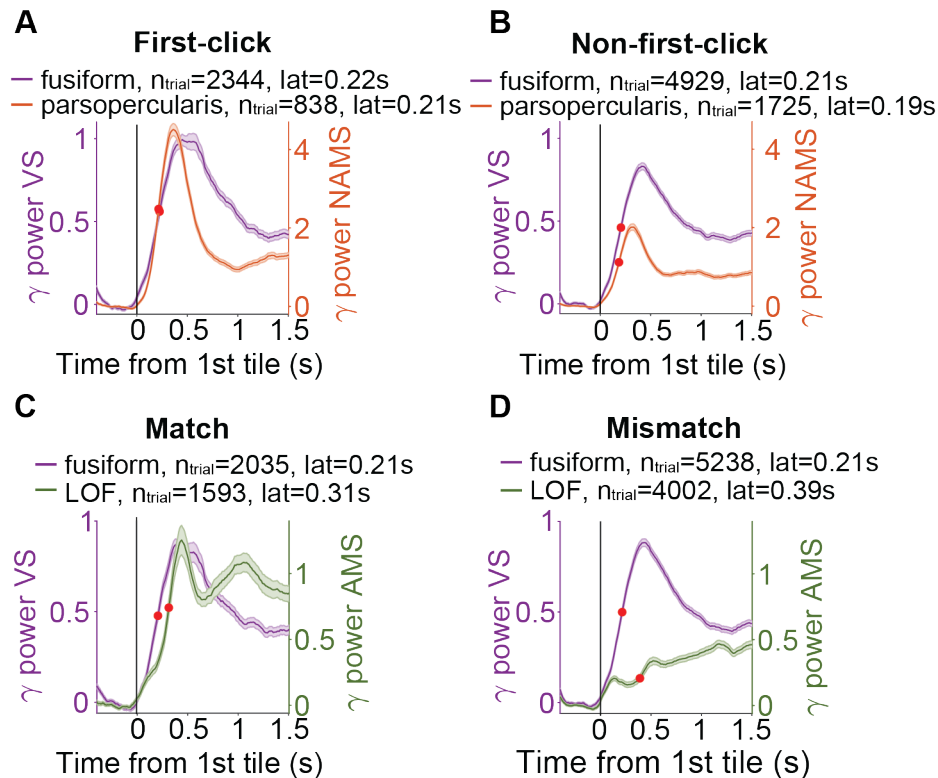


Figure 3.19: Comparison of the latency between VS fusiform, NAMS pars opercularis and AMS LOF electrodes. **A.** Average z-scored gamma power of all first-click (**A**) and non-first-click (**B**) trials for VS electrodes in the fusiform gyrus (purple line) and NAMS electrodes in the pars opercularis (orange line). Red dot indicates the latency. **C,D.** Average z-scored gamma power of all match (**C**) and mismatch (**D**) trials of VS electrodes in the fusiform gyrus (purple line) and AMS electrodes in the lateral orbitofrontal (LOF) cortex (orange line). Red dot indicates the latency.

3.8 Gamma band and lower frequencies interplay

Research has shown that different modes of WM could be reflected by an interplay between gamma and slower frequency activities (Introduction 1.4). In this section, we analyze how different patterns of frequency modulation, related to interactions between gamma activities and slower oscillations, can characterize different STM processes. For this analysis, we considered 1st tile VS, AMS and NAMS electrodes, as well as electrodes that presented *match* as a significant predictor after the 2nd tile (2nd tile match-significant). Our analysis reveal that different locations showed distinct patterns of frequency modulation. For instance, both the LOF electrode in Figure 3.8 and the middle temporal electrode in Figure 3.9 presented increased gamma responses for match versus mismatch after the 1st tile. However, the pattern of this modulation was different in several ways. First, the power increase in the middle temporal cortex was rather sustained, while the power increase in the LOF was transient (compare Figure 3.8B-D versus Figure 3.9B-D). Second, the frequency modulated by match for the LOF electrodes extended from the low gamma to the beta band (Figure

3.8C-D), while the middle temporal electrode showed an increase in higher frequencies (Figure 3.9I-K).

We computed the time-wise correlation between the gamma band power and the alpha or beta band power for every trial (Figure 2.4, Methods 2.10). We defined electrodes with gamma and beta/alpha anti-correlation as those where more than 60% of the trials showed a negative correlation. Table 3.2 shows the percentage of VS, AMS, and NAMS and 2nd tile match-selective electrodes with positive or negative time-wise correlation between gamma and slower frequencies. For the gamma-beta correlation, there was a larger percentage of positive-correlated (more than 58% for all populations) than anti-correlated (less than 10% for all populations). A positive gamma-beta correlation indicates that gamma band activity extended to the beta band activity. In contrast, the gamma-alpha interplay showed a larger percentage of anti-correlation than positive correlation. Gamma-alpha anti-correlation indicates a push-pull relationship: turning up gamma activities would turn down alpha activities, and vice-versa. Similar results were found when considering neural responses after the 2nd tile (Table B.12). Table B.13 (1st tile) and Table B.14 (2nd tile) show the same analysis when grouping electrodes by brain region.

Table 3.2: Proportion VS, AMS and NAMS electrodes showing gamma and slower frequency interactions for the 1st tile Columns indicate percentage of electrodes showing positive or negative time-wise correlation between the gamma and beta or alpha band power, using the 1st tile alignment. n indicated the total number of electrodes.

	Gamma - Beta		Gamma-Alpha	
	Anti-corr. (-)	Positive corr. (+)	Anti-corr. (-)	Positive corr. (+)
VS 1st tile (n = 44)	9.09% (4)	65.91% (29)	13.64% (6)	15.91% (7)
NAMS 1st tile (n = 75)	4% (3)	58.67% (44)	12% (9)	8% (6)
AMS 1st tile (n = 36)	2.78% (1)	77.78% (28)	8.33% (3)	5.54% (2)
Match-selective 2nd tile (n = 112)	2.68% (3)	60.71% (68)	15.18% (17)	8.04% (9)

Figure 3.20 shows two examples of electrodes that exhibited gamma-alpha anti-correlation. The LOF electrode in Figure 3.20A-C presented more than 60% of the trials with gamma-alpha anti-correlation for both tiles. No interactions were found between gamma and beta power (Figure 3.20A). Figure 3.20B-C compares the gamma and alpha power during the 1st and 2nd tiles. In both cases, revealing a tile induced a peak of gamma-band power that was coupled to a drop of alpha band power (Figure 3.20B-C). This LOF electrode presented *n-since-pair*match* as a significant predictor after the 1st tile (Figure C.2) and *match* as a significant predictor after the 2nd tile (Figure C.4). The gamma-alpha anti-correlation can also be observed from the trial-averaged spectrograms (Figure C.4E-F). Most noticeably, mismatch trials induced a sharp gamma decrease that was coupled with an alpha increase (C.4F), while match trials showed increased gamma activities and decreased alpha activities (C.4E). Figure 3.20D-F shows another example electrode in the pars opercularis where gamma and alpha power were anti-correlated for both tiles. This electrode was sensitive to novelty and familiarity to the current viewing tile (Figure 3.7, Results 3.3.1). Trial-averaged spectrograms (Figure Figure 3.7D-F) and power line plots (Figure 3.20E-F) show

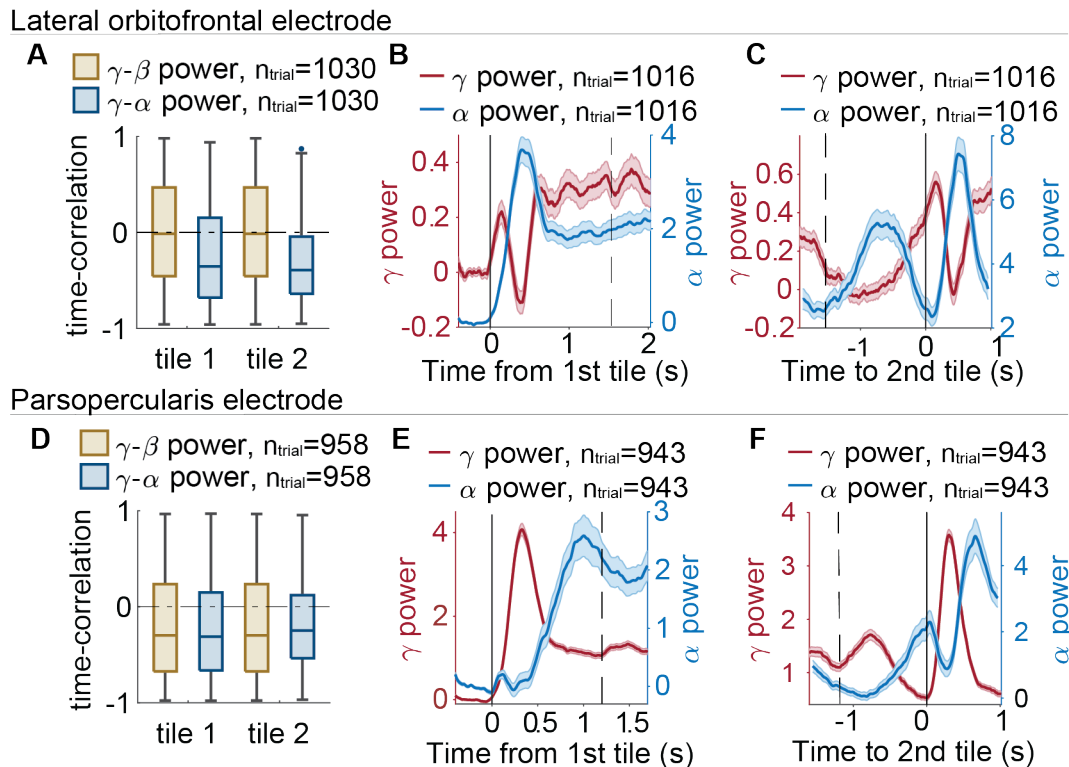


Figure 3.20: Example of a LOF and pars opercularis electrode that showed gamma-alpha anti-correlation. **A-C.** LOF electrode in Figure C.4 for the 2nd tile and C.2 for the 1st tile. **D-F.** Pars opercularis electrode in Figure 3.7. **A,B.** Box and whisker plots of individual trials' gamma-beta (yellow) and gamma-alpha (blue) power time-wise correlation for the 1st tile and 2nd tile. The center line of the box indicates the median value (0.5 quantile), while the box contains the 0.25 to 0.75 quantiles. **B-C,E-F.** Average z-scored gamma power (red) and alpha power (blue), aligned to the 1st tile (**B,E**), and aligned to the 2nd tile **C,F**. Shaded error bars indicate SEM.

that when gamma power decreased, alpha power increased. In all, Figure 3.20 presents two examples of electrodes with gamma-alpha anti-correlation that were located in distinct brain regions and were involved in different STM mechanisms.

Figure 3.21 shows two examples of electrodes in the insula and LOF cortex that exhibited a positive correlation between the gamma and beta band power. The line plots indicate that the increase in gamma power was coupled with an increase in beta power (Figure 3.21B-C,E-F). Both electrodes presented more than 60% of trials with positive gamma-beta correlation (Figure 3.21A,D), while this was not the case for the gamma-alpha correlation. This result indicates that the increase in gamma power extended to the beta band power, but not to the alpha band power, as can also be observed from the spectrograms (Figure 3.8E-F for the LOF electrode and Figure C.3E-F for the insula electrode). Both electrodes presented *match* as a significant predictor after the 2nd tile (Figure C.5 for the LOF electrode and Figure C.3 for the insula electrode). The increase in gamma-beta band power happened for *match* but not *mismatch* trials (Figure 3.8E versus F and Figure C.3E versus F). The LOF electrode was also selective for *match* trials after the 1st tile (Figure 3.8). In

contrast, the 1st tile GLM for the insula electrode was not significant, i.e., none of the included predictors could explain the neural responses. Indeed, we can see that there is a sharp gamma-beta increase after the 2nd tile click for the insula electrode (Figure 3.21F), while no increased activities were found after the 1st tile (Figure 3.21E). Thus, despite both the LOF and insula electrodes presenting similar responses after the 2nd tile, their distinct responses after the 1st tile might indicate that they were involved in different mechanisms. It is to be highlighted that all 2nd tile match-significant electrodes located in the insula ($n=12$) exhibited a positive gamma-beta correlation, but not gamma-beta anti-correlation or gamma-alpha anti- or positive-correlation (Table B.14). Hence, the pattern of modulation found in the insula examples (Figure 3.21D-F and C.3, see also Figure 3.13) may be a characteristic pattern of the insula. On the other hand, the LOF presented electrodes with gamma-alpha anti-correlation (Figure 3.20A-C), gamma-beta positive correlation (Figure 3.21A-C) and gamma-alpha positive-correlation (Table B.14).

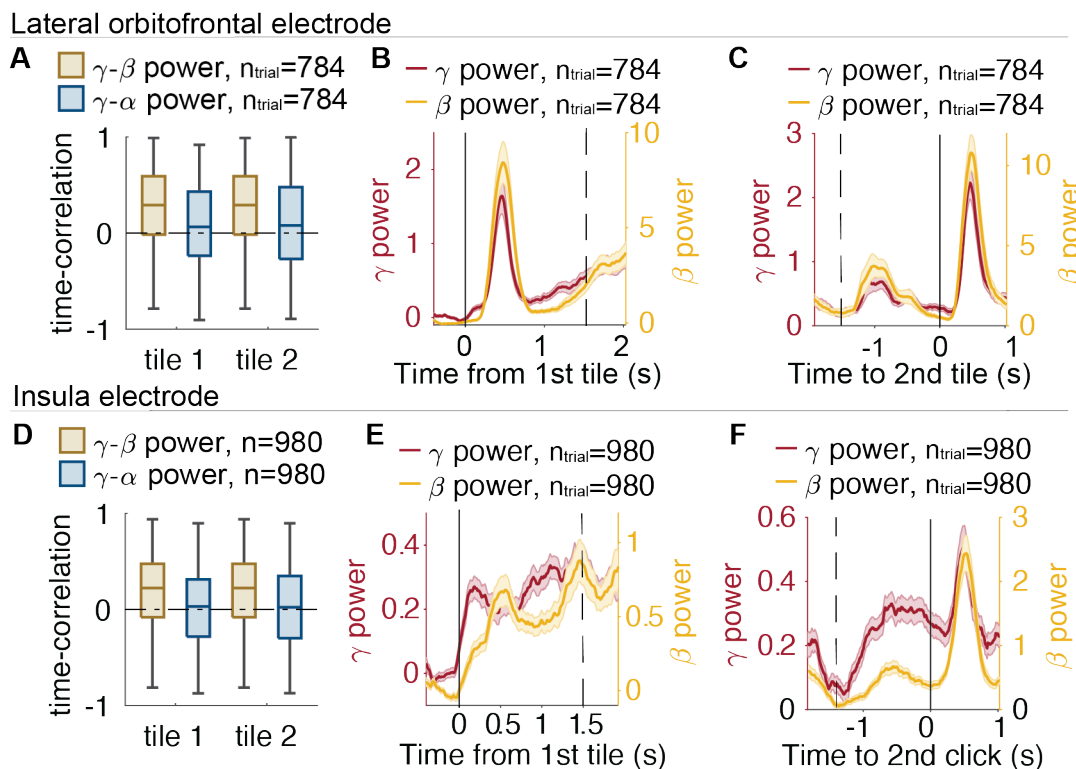


Figure 3.21: Example of a LOF and insula electrode that showed gamma-alpha anti-correlation.. A-C. LOF electrode in Figure 3.8. D-F. Insula electrode in figure C.3. A,B. Box and whisker plots of individual trials' gamma-beta (yellow) and gamma-alpha (blue) power time-wise correlation for the 1st tile and 2nd tile. The center line of the box indicates the median value (0.5 quantile), while the box contains the 0.25 to 0.75 quantiles. B-C,E-FJ-M. Average z-scored gamma power (red) and beta power (yellow), aligned to the 1st tile (B,E), and aligned to the 2nd tile C,F. Shaded error bars indicate SEM.

3.9 Other predictors: *distance*

The estimation of the distance between tiles is a necessary mechanism to compute the correct movement trajectory from the 1st to the 2nd tile. We found 14 electrodes for which distance was a significant predictor. Figure 3.22 shows an example of an electrode located in the IT cortex that presented distance as a significant predictor. The larger the Euclidean distance between tiles (Figure 3.22B) the larger the gamma response. The distance between tiles and the RT are slightly correlated predictors (Figure 3.2). We could consider that the more distant the tiles are, the longer it takes to move from one to the other, thus the larger the RT. However, from the scatter plots we can see that the AUC of the gamma power increased with distance ($p < 0.001$, Figure 3.22C) but not with RT ($p = 0.802$, Figure 3.22D). Moreover, the increase in gamma activities happened from the visualization of the 1st tile. We hypothesize that this electrode could be involved in the computation of the distance between the 1st tile and the to-be-clicked 2nd tile, to e.g. guide movement, or could be involved in movement itself.

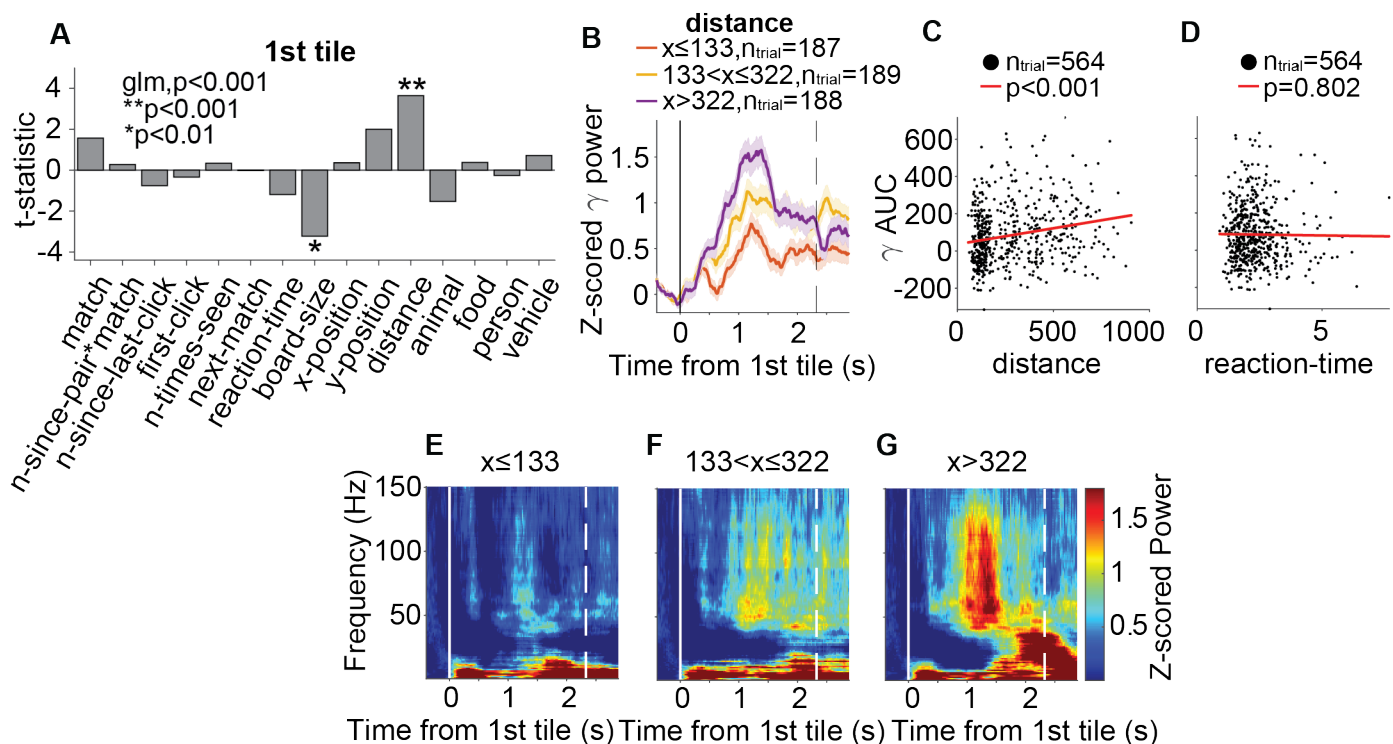


Figure 3.22: Example of an IT electrode selective for *distance*. **A.** T-statistic of each predictor in the GLM for the 2nd tile. **B.** Z-scored gamma power for different distance values. **C** Scatter plot of AUC gamma power vs. distance. **D** Scatter plot of AUC gamma power vs. RT. Each dot represents data from one trial. Red lines represent linear fits of the data. **E-F.** Spectrograms showing the power aligned to the 1st tile for different values of distance.

4 Discussion

We studied neural mechanisms involved in STM by recording intracranial field potentials from 676 bipolarly-referenced electrodes in the gray matter (Figure 2.2, Table A.2) and 491 in the white matter (Figure E.1, Table A.2) from 20 pharmacologically-intractable epilepsy patients implanted with sEEG electrodes (one patient also had ECoG electrodes). During intracranial EEG monitoring, patients played the memory matching game (Figure 2.1), where they were instructed to find pairs of images from image matrices of different sizes. We used generalized linear models to assess the relative contribution of different predictors (Table 2.2) to the gamma activities. These predictors were related to different STM processes, including the recognition of the viewing tile (*first-click*, *n-since-last-click*; non-associative recognition memory) as well as the retrieval of the tile's pair (*match*, *n-since-pair*match*; associative memory). These predictors also included the visual category of the objects on the tiles (*animal*, *food*, *person*, *vehicle*), which allowed us to study the existence of brain locations selective to different categories. We also studied whether neural responses could encode for both object category and memory retrieval. Finally, we compared different patterns of frequency modulation related to WM processes.

Behavior

Subjects performed significantly better than a memoryless model and worse than a perfect memory model (Figure 3.1A). We observed distinct behaviors for match and mismatch trials. RTs were significantly faster in match than mismatch trials (Figure 3.1B), as expected from previous studies [19, 99, 100]. We used the variable *n-since-last-click* to estimate the degree of familiarity with a viewing tile and *n-since-pair* the degree of familiarity with a tile's matching pair. The larger the number of tiles seen since the last time a tile was viewed, the larger the number of items (tiles information) kept in STM, and thus the larger the memory load [99]. Therefore, *n-since-last-click* also reflected the relative memory load from the last time seeing a tile, and *n-since-pair* also reflected the relative memory load from the most recent view of a tile's pair until the current viewing of a tile. Since memory load was higher in more difficult blocks that contained more tiles, both *n-since-last-click* and *n-since-pair* increased as board size incremented (Figure 3.1C-F). The level of familiarity with the to-be-clicked 2nd tile in a trial, indexed by the recency since last seeing itself (*n-since-last-click*), influenced the trial result (match or mismatch) more strongly than that with the 1st tile (Figure 3.1C,D versus 3.1C,D). In addition, we found that the difference in eye movements between match and mismatch (Figure 3.4) was explained by the larger distances between the 1st and 2nd tiles and faster RTs for match compared to mismatch trials (Figure 3.2C,D).

Non-associative memory

First, we asked whether the neural responses could differentiate if the currently viewing tile, i.e., the clicked tile, was novel or familiar. This process is necessary to: (1) rapidly recognize the tile in order to proceed with recalling its associated pair; (2) if it was novel, support the initial encoding and maintenance of the tile's information in STM [2, 8, 101]. We found electrodes that were selective to novel tiles (*first-click*) information, as well as those that could encode the degree of familiarity (*n-since-last-click*). We consider that the longer ago a tile had been seen (large *n-since-last-click*), the higher the memory load or the more likely the tile was forgotten, and thus the less familiar. Hence, we could expect that novel tiles trigger similar responses to unfamiliar tiles since, in both cases, the tile's information has to be encoded (if considered novel) or maintained in STM. We found several electrodes' locations that contained information about both novelty and familiarity, and for which novel and very unfamiliar items triggered similar neural responses (Figure C.1, 3.7). Most of those electrodes showed increased gamma responses for novel or unfamiliar items (Figure 3.7). In contrast, only a few showed increased gamma responses towards familiar items (Figure C.1). Rutishauser et al. [13] also described two similar populations of neurons that showed (1) increased firing rate for novel stimuli (referred as to novelty-detectors), or (2) increased firing rate for familiar stimuli (referred as to familiarity-detectors). The the pars opercularis and LOF cortex were significantly rich in novelty-selective electrodes (Figure 3.6G and 3.7G, bootstrap analysis, Methods 2.7). Though it did not reach statistical significance, the medial temporal lobe (MTL) also contained a good number of electrodes that were selective for novelty, the gradient of familiarity, or both. These results are consistent with previous works that reported the role of the prefrontal cortex [102, 103, 104], and the MTL [2, 14, 101], in processing novelty and familiarity.

Similar to the first tile, some electrodes' neural responses after the 2nd tile were also modulated by novelty (*first-click*, Figure 3.11H) or familiarity (*n-since-last-click*, Figure 3.11G) to the 2nd tile. The number of such electrodes was much fewer than for the 1st tile. If the trial was a match, the consecutive visualization of the same image might reduce the detection of novelty or familiarity after the 2nd tile. Moreover, the 2nd tile no longer needed to be encoded in WM for match trials since this information was no longer necessary. Hence, it was more difficult to study novelty, familiarity, and encoding signals when considering neural responses after the 2nd tile.

Associative memory

Upon the visualization of the 1st tile, differential gamma responses could also predict successful (match) or failed (mismatch) associative memory retrieval of the tile's pair location. Hence, these neural responses predicted whether the trial would be match before participants clicked the 2nd tile, and thus before the trial's outcome was revealed. For those electrodes, we found that match trials usually manifested higher gamma responses than mismatch (Figure 3.8, 3.9 and 3.10). Match signals could be related to a process of correct association of the 1st tile and its pair, as well as recollection of the tile's pair position. Bootstrap sampling showed that the LOF cortex is a critical region (Figure 3.8G, example in Figure 3.8) for associative memory, providing an important update to the existing literature that mostly emphasizes the role of the hippocampus and its surrounding structures in the MTL [2, 13, 18, 21, 23]. We also found some electrodes in the MTL that could predict successful memory retrieval (example Figure 3.9), though the number of MTL did not reach

statistical significance.

Neural responses predictive of successful associative retrieval may also encode the degree of familiarity with the tile's pair [102]. We considered that the longer ago the tile's pair had been seen, the worse the memory of the pair, and thus the less familiar it was. In contrast, if the 1st tile's pair had been recently seen, its location was more fresh in memory, and it was more likely that the trial would be matched (Figure 3.1D,E). We used *n-since-pair* to index the degree of familiarity with a cue's pair when only the cue (1st tile) was shown. *N-since-pair*match* electrodes only showed modulation of the gamma activities when match but not mismatch trials were considered (Table B.5). Hence, they also signaled successful memory retrieval since they only encoded the grade of familiarity to the tile's pair when the pair was known (see examples Figure 3.9, Figure 3.10). Moreover, 73% of *n-since-pair*match* electrodes also had *match* as a significant predictor (see examples Figure 3.9, Figure 3.10). These findings support the continuous strength model that states that brain activity involved in retrieval can track both recollection and familiarity, and so they are consistent with results from several studies that addressed this topic using long-term memory paradigms [14, 31].

We found that differential responses for match and mismatch could present distinct patterns of modulation across recording sites. The gamma responses could be transient (Figure 3.8B-D) or sustained (Figure 3.9B-D), and may vary in time and frequency (compare Figure 3.8E-F with Figure 3.9I-L), suggesting possibly different operations during associative memory retrieval. For example, transient activities may signal fast events like suddenly knowing or being confident about the trial outcome (match or mismatch) and sustained responses may correspond to active retrieval processes. Sustained activities could also be due to averaging across temporally distinct activities [64]; however, it has been reported that single neurons in the hippocampus could show sustained firing rate increase for successful associative retrieval [18].

We also studied associative memory signals upon the visualization of the 2nd tile. The 2nd tile visualization could prompt the retrieval of its pair, but both tiles could only be matched in the following trial. Only a few electrodes could predict whether the subsequent trial would be matched or not (*next-match* predictor, Figure 3.12C). The task was designed so that the associative recall of the matching pair happened after the 1st tile; thus, a small number of electrodes involved in associative memory after the 2nd tile was expected. It is to be highlighted the example electrode in the precuneus, which showed associative memory signals both for the 1st tile (Figure 3.10; significant for both *match* and *n-since-pair*match*) and the 2nd tile (Figure 3.12, significant for *next-match*). We could not test the significance of the precuneus in associative memory retrieval since we only had recordings from 3 electrodes, all from the same subject. However, the role of the precuneus in memory retrieval has been extensively studied in the literature [105, 106, 107, 108, 109, 110].

Distinct neural responses for match and mismatch after the 2nd tile

Many electrodes (16.6% in the gray matter and 13.4% in the white matter) showed distinct gamma responses for match versus mismatch after the 2nd tile. Most of these electrodes did not show differential gamma responses for *match* after the 1st tile. After the 2nd tile, the trial's outcome was already known; thus, the role of these locations might may not be related to associative memory

retrieval. Many factors could explain distinct neural responses for match and mismatch after the 2nd tile: (1) a feedback response (match: reward; mismatch: failure); (2) the consecutive visualization of the same image for match trials, which could potentiate or suppress a visual response; (3) a “clearing” mechanism of the tiles information for match trials, since this information is no longer needed, or the “encoding” of the 2nd tile if the trial is mismatch; (4) different eye-movements for match and mismatch (Figure 3.4H).

The LOF cortex and the insula presented a significantly large number of electrodes selective for *match* after the 2nd tile. Based on the literature, we hypothesize that the insula may encode feedback signals: match trials elicited neural responses encoding a positive reward since the desired outcome of the trials was achieved [57, 111]. The majority (66.7%) of the insula electrodes selective for *match* for the 2nd tile did not present any significant predictor for the 1st tile GLM. We could consider that neural responses were contingent on feedback signals after the outcome of the trial was revealed (see examples Figure 3.13 and Figure C.3). The other insula electrodes (33.3%) were selective for *match* after the 1st tile. Several studies have pointed out a higher activation of the insula not only after reward but also during reward anticipation [57, 58]. Hence, match signals after the 1st tile might reflect anticipation of the reward, i.e., the tile’s pair is known and so the match is expected.

Visual category selectivity

The matching card memory game was a highly dynamic task that was not designed to study VS responses. Still, we found neural responses that encoded the content a tile displayed (Figure 3.16). VS electrodes showed increased gamma responses towards their preferred image category, such as images of vehicles (Figure 3.16), people (Figure 3.16) or food (Figure 3.16). We found that some person-selective electrodes also presented slightly increased gamma activities for animal images compared to the other categories (Figure 3.16A-B, Figure E.7A-B). This result may indicate: (1) these locations encoded information about animated objects; or (2) they averaged information from two distinct object-category sites or neurons in proximity, one selective for person and the other for animal.

The fusiform gyrus contained more VS electrodes than expected by chance ($p < 0.01$ bootstrap analysis, Methods 2.7, 36% of total fusiform electrodes). The FG is a key structure within the high-level visual cortex that has been extensively studied for its role in high-level visual computations such as object recognition and face perception [39, 40, 41]. Most fusiform electrodes showed selectivity for images containing people, and thus faces (Figure 3.16A-D, Figure E.7). We hypothesize that these electrodes may be located in or close to the FFA [39, 40, 41]. Other fusiform electrodes also showed selectivity for animal, vehicle or food (Figure 3.16 and Figure 3.17). Though it did not show statistical significance, the parahippocampal cortex also contained a large number of VS electrodes for different object categories (Table B.11) such as vehicles (Figure 3.16A-D). Consistent with the literature, we found that the parahippocampal and the fusiform areas are not dedicated to representing only spatial arrangements or human faces (FFA) or buildings and scenes (PPA) but, rather, are part of a more extended representation of all objects [39, 41]. Other locations also showed visual-selective properties, supporting the idea that object recognition may happen in widely distributed areas in the brain [15].

Visual selectivity versus non-associative and associative memory selectivity

We systematically compared three populations of electrodes: VS, non-associative recognition memory selective (NAMS), and associative memory selective (AMS) electrodes. The former encoded information about one or more “preferred” image categories, and thus the tile’s content. NAMS electrodes signaled the novelty or familiarity with the tile clicked, while AMS electrodes could predict the successful recollection and familiarity with the tile’s pair. We found neural responses that were both VS and NAMS (Figure 3.17, Table 3.1), thus conveying information about the category of the tile’s image, as well as the familiarity with the tile. There were more electrodes that presented both VS and AMS properties, than electrodes VS and AMS, or NAMS and AMS. The larger overlap between the VS and AMS populations might be explained by the fact that VS and NAMS responses conveyed information about the current viewing tiles, while AMS encoded information about the tiles’ pair. We found a large number of electrodes that only showed VS, AMS or NAMS neural responses. This result suggests that the representation of the familiarity gradient may not be item-specific, i.e., specific to the tile’s content. That is, different object categories with the same level of familiarity may induce the same responses, consistent with the notion that single memory cells are rarely sharply tuned to particular sensory features [2, 22, 112].

Our results point to the role of the fusiform gyrus, pars opercularis and LOF as significant VS, NAMS and AMS regions. We defined latency as the time at which the average gamma power achieved 50% of its maximum latency. The fusiform gyrus (only VS electrodes) and pars opercularis (only NAMS electrodes) exhibited a similar latency (Figure 3.19A,B), and thus it is not clear whether the recognition of the viewing tile and the recognition of the specific image on the tile happened at distinct times in these regions (Figure 3.19A,B). Our analysis was limited to only a few brain regions. However, the dynamics of object recognition and familiarity might be coordinated and started at other brain locations that were not included here. For instance, previous literature has reported that VS activity happens before NAMS activity in the MTL [15]. The activity of the LOF AMS electrodes happened later than the fusiform VS and the pars opercularis NAMS locations. This result suggests that the information about the 1st tile is processed before recollecting information about its pair, as expected. Again, a more exhaustive study across brain regions is necessary to understand the dynamics of VS, AMS, and NAMS neural responses.

Gamma and slower oscillations interplay

We found that the interplay between gamma and slower frequency bands could orchestrate different WM processes. For the VS, AMS, and NAMS electrodes, as well as for those that presented match as a significant predictor after the 2nd tile, we computed the time-wise correlation between gamma and beta/alpha band power for every individual trial. We found electrodes that showed more than 60% of trials with gamma-alpha anti-correlated for both the 1st and 2nd tile alignments. The AMS LOF electrode and NAMS pars opercularis electrode (Figure 3.20) are examples of gamma-alpha anti-correlation. We hypothesize that upon the 1st tile visualization, the turning up of gamma activities allowed the access to the STM content about the tile (pars opercularis, Figure 3.7) or its pair (LOF, Figure C.2). After the memory was retrieved, the turn-up of beta activities suppressed gamma activities to clear out the memory and so as to free STM space [64, 69, 70].

We also found electrodes that showed more than 60% of trials with a positive correlation be-

tween gamma and beta activities for both the 1st and 2nd tile alignments (Figure 3.21, Table 3.2). For those electrodes, the low gamma band activities extended to the beta band (Figure 3.8, Figure C.3). Noticeably, this behavior was characteristic of electrodes in the insula (100%) that were selective for match after the 2nd tile (Figure 3.13 and C.3). Some brain region presented electrodes with both gamma-alpha/beta positive and negative correlation. Thus, it is unclear whether these different modulation patterns are specific to brain locations. It has been proposed that beta in deep-layer cortex interacts with gamma in superficial layer cortex [70]. Therefore, one possible hypothesis is that gamma-beta positive correlation happens at deeper layers in the cortex, e.g., the insula. In contrast, high gamma and slower oscillations anti-correlation is a specific mechanism in the superficial cortex. This is a question for future studies.

Limitations

One of the main limitations of iEEG is the limited accessibility to this type of recordings [60, 113]. First, the recordings must be performed in a clinical setting, and only a few hospitals and clinicians are trained to do so. Second, participants have a clinical condition that brought them to the operating room. We analyzed data from 20 patients, which is a larger number than most iEEG studies on humans. Nevertheless, it is still a limited number and it would be interesting to include more patients in future studies. Third, the electrodes' location is decided for clinical purposes and electrodes cannot be moved once implanted. Hence, some brain regions are much less frequently studied. These brain regions could also play an important role in STM, object recognition, or feedback signals, but we may not have covered them in the present study. Fourth, there is no global coverage of the brain since the distribution of the electrodes is sparse. Thus, we cannot guarantee that we are recording the main regions of interest. Finally, iEEG records the average activity of a large and diverse population of neurons and it is difficult to interpret the information carried in different frequency bands. The gamma band has been interpreted as a proxy of neural activity [60, 61, 62]. Other frequency bands (beta, alpha, theta) have also been found to carry important information, though their underlying neural mechanisms are not clearly understood [60].

Implications and future directions

Our findings suggest that non-associative and associative STM processes are neurally distinct, i.e., happen at different locations. Thus, they can be functionally dissociable. This finding could justify that some memory disorders may be related to the loss of one type of memory, but not the other. For instance, a patient may maintain the ability to store and recognize information previously encountered, but could lose the ability to make links between two pieces of information, as has also been studied in mice [114]. We also found multiple different electrode locations that contributed to each subtype of STM. Hence, we could consider that non-associative and associative memory processes depend on the dynamic interactions between these different brain locations [115]. These interactions could also imply that if one type of memory is lost, the other could be affected. For instance, recognizing an item (non-associative memory) could trigger the neural mechanisms necessary to recollect the information about its pair in another location. The distributed location in the brain of some electrodes involved in non-associative (Figure 3.6G), associative (Figure 3.8G) and object recognition (Figure 3.15) supports the idea that there is redundancy in the brain, i.e., distinct

neural circuits or brain locations can enable the same functions [116]. Brain redundancy may have key implications when studying brain disorders [116]. In all, a better understanding of the STM mechanisms in the human brain is necessary to understand memory-related disorders and develop novel neural intervention techniques to treat them. Moreover, findings from STM in humans can be used to improve biologically-inspired artificial intelligence models.

To further establish and elaborate our findings, it would be necessary to increase the number of participants and electrode locations analyzed. It is also worth noting that the mechanisms of non-associative and associative retrieval might be fundamentally different between long-term memory and STM [23], an important question to be addressed by future studies. Finally, future studies could benefit from the use of micro-electrodes recordings [113] that can identify the activity of single neurons.

5 Conclusion

In this project, we took advantage of the high spatiotemporal resolution of human iEEG to study the mechanisms underlying non-associative and associative STM, object recognition, and feedback responses. Participants played a highly dynamic memory game where subjects had to keep track of the tile's information in STM, thus allowing us to study how neural activities can track STM processes. We investigated both non-associative and associative aspects of memory by carefully dissociating neural responses towards the tile (the cue) and the tile's pair. Gamma activities were selective to novelty and represented different degrees of familiarity with the viewing tile. Moreover, gamma responses could also predict the successful retrieval and familiarity with a tile's pair. We also analyzed electrodes selective for different object categories, even if our task was not designed for this purpose. We found that most neural responses encoding information about a viewing tile did not encode information about its pair, and vice versa. Finally, we found different patterns of frequency modulation involved in STM processes. To our knowledge, it is the first time that human neural responses involved in both subtypes of STM processes and object recognition have been studied under the same experimental paradigm. Our results may have implications for understanding memory disorders related to both associative and non-associative recognition memory.

Bibliography

- [1] Elizabeth L Johnson and Robert T Knight. Intracranial recordings and human memory. *Current opinion in neurobiology*, 31:18–25, 2015.
- [2] Ueli Rutishauser, Leila Reddy, Florian Mormann, and Johannes Sarnthein. The architecture of human memory: insights from human single-neuron recordings. *Journal of Neuroscience*, 41(5):883–890, 2021.
- [3] Youssef Ezzyat, Paul A Wanda, Deborah F Levy, Allison Kadel, Ada Aka, Isaac Pedisich, Michael R Sperling, Ashwini D Sharan, Bradley C Lega, Alexis Burks, et al. Closed-loop stimulation of temporal cortex rescues functional networks and improves memory. *Nature communications*, 9(1):1–8, 2018.
- [4] Lisa H Evans and Edward L Wilding. Recollection and familiarity make independent contributions to memory judgments. *Journal of Neuroscience*, 32(21):7253–7257, 2012.
- [5] Sander M Daselaar, Mathias S Fleck, and R Cabeza. Triple dissociation in the medial temporal lobes: recollection, familiarity, and novelty. *Journal of neurophysiology*, 96(4):1902–1911, 2006.
- [6] C.E. Stern and M.E. Hasselmo. Recognition memory. In Larry R. Squire, editor, *Encyclopedia of Neuroscience*, pages 49–54. Academic Press, Oxford, 2009.
- [7] Daniela Montaldi, Tom J Spencer, Neil Roberts, and Andrew R Mayes. The neural system that mediates familiarity memory. *Hippocampus*, 16(5):504–520, 2006.
- [8] Jinsick Park, Hojong Lee, Taekyung Kim, Ga Young Park, Eun Mi Lee, Seunghee Baek, Jeonghun Ku, In Young Kim, Sun I Kim, Dong Pyo Jang, et al. Role of low-and high-frequency oscillations in the human hippocampus for encoding environmental novelty during a spatial navigation task. *Hippocampus*, 24(11):1341–1352, 2014.
- [9] Ueli Rutishauser, Ian B Ross, Adam N Mamelak, and Erin M Schuman. Human memory strength is predicted by theta-frequency phase-locking of single neurons. *Nature*, 464(7290):903–907, 2010.
- [10] Michael A Yassa and Craig EL Stark. Multiple signals of recognition memory in the medial temporal lobe. *Hippocampus*, 18(9):945–954, 2008.
- [11] Itzhak Fried, Katherine A MacDonald, and Charles L Wilson. Single neuron activity in human hippocampus and amygdala during recognition of faces and objects. *Neuron*, 18(5):753–765, 1997.
- [12] Ryan J Murray, Tobias Brosch, and David Sander. The functional profile of the human amygdala in affective processing: insights from intracranial recordings. *Cortex*, 60:10–33, 2014.
- [13] Ueli Rutishauser, Adam N Mamelak, and Erin M Schuman. Single-trial learning of novel stimuli by individual neurons of the human hippocampus-amygdala complex. *Neuron*, 49(6):805–813, 2006.
- [14] Ueli Rutishauser, Erin M Schuman, and Adam N Mamelak. Activity of human hippocampal and amygdala neurons during retrieval of declarative memories. *Proceedings of the National Academy of Sciences*, 105(1):329–334, 2008.
- [15] Ueli Rutishauser, Shengxuan Ye, Matthieu Koroma, Oana Tudusciuc, Ian B Ross, Jeffrey M Chung, and Adam N Mamelak. Representation of retrieval confidence by single neurons in the human medial temporal lobe. *Nature neuroscience*, 18(7):1041–1050, 2015.

- [16] Indre V Viskontas, Barbara J Knowlton, Peter N Steinmetz, and Itzhak Fried. Differences in mnemonic processing by neurons in the human hippocampus and parahippocampal regions. *Journal of cognitive neuroscience*, 18(10):1654–1662, 2006.
- [17] Tino Zaehle, Eva M Bauch, Hermann Hinrichs, Friedhelm C Schmitt, Jürgen Voges, Hans-Jochen Heinze, and Nico Bunzeck. Nucleus accumbens activity dissociates different forms of salience: evidence from human intracranial recordings. *Journal of Neuroscience*, 33(20):8764–8771, 2013.
- [18] Bernhard P Staresina, Thomas P Reber, Johannes Niediek, Jan Boström, Christian E Elger, and Florian Mormann. Recollection in the human hippocampal-entorhinal cell circuitry. *Nature communications*, 10(1):1–11, 2019.
- [19] Charan Ranganath, Michael X Cohen, Cathrine Dam, and Mark D’Esposito. Inferior temporal, prefrontal, and hippocampal contributions to visual working memory maintenance and associative memory retrieval. *Journal of Neuroscience*, 24(16):3917–3925, 2004.
- [20] Matias J Ison, Rodrigo Quiñ Quiroga, and Itzhak Fried. Rapid encoding of new memories by individual neurons in the human brain. *Neuron*, 87(1):220–230, 2015.
- [21] Kuniyoshi Sakai and Yasushi Miyashita. Neural organization for the long-term memory of paired associates. *Nature*, 354(6349):152–155, 1991.
- [22] Yong-Di Zhou, Allen Ardestani, and Joaquín M Fuster. Distributed and associative working memory. *Cerebral Cortex*, 17(suppl_1):i77–i87, 2007.
- [23] Heiko C Bergmann, Mark Rijpkema, Guillén Fernández, and Roy PC Kessels. Distinct neural correlates of associative working memory and long-term memory encoding in the medial temporal lobe. *Neuroimage*, 63(2):989–997, 2012.
- [24] Silvia A Bunge, B Burrows, and AD Wagner. Prefrontal and hippocampal contributions to visual associative recognition: interactions between cognitive control and episodic retrieval. *Brain and cognition*, 56(2):141–152, 2004.
- [25] Andrew Mayes, Daniela Montaldi, and Ellen Migo. Associative memory and the medial temporal lobes. *Trends in cognitive sciences*, 11(3):126–135, 2007.
- [26] Katrin Göthe and Klaus Oberauer. The integration of familiarity and recollection information in short-term recognition: Modeling speed-accuracy trade-off functions. *Psychological research*, 72(3):289–303, 2008.
- [27] Mark W Schurgin. Visual memory, the long and the short of it: A review of visual working memory and long-term memory. *Attention, Perception, & Psychophysics*, 80(5):1035–1056, 2018.
- [28] Andrew P Yonelinas. Components of episodic memory: the contribution of recollection and familiarity. *Philosophical Transactions of the Royal Society of London. Series B: Biological Sciences*, 356(1413):1363–1374, 2001.
- [29] Maxwell B Merkow, John F Burke, and Michael J Kahana. The human hippocampus contributes to both the recollection and familiarity components of recognition memory. *Proceedings of the National Academy of Sciences*, 112(46):14378–14383, 2015.
- [30] Peter E Wais, Larry R Squire, and John T Wixted. In search of recollection and familiarity signals in the hippocampus. *Journal of cognitive neuroscience*, 22(1):109–123, 2010.
- [31] Peter E Wais, John T Wixted, Ramona O Hopkins, and Larry R Squire. The hippocampus supports both the recollection and the familiarity components of recognition memory. *Neuron*, 49(3):459–466, 2006.
- [32] John T Wixted and Larry R Squire. The medial temporal lobe and the attributes of memory. *Trends in cognitive sciences*, 15(5):210–217, 2011.
- [33] John P Aggleton and Malcolm W Brown. Episodic memory, amnesia, and the hippocampal–anterior thalamic axis. *Behavioral and brain sciences*, 22(3):425–444, 1999.

- [34] Andrew P Yonelinas. The hippocampus supports high-resolution binding in the service of perception, working memory and long-term memory. *Behavioural brain research*, 254:34–44, 2013.
- [35] Jared F Danker, Grace M Hwang, Lynne Gauthier, Aaron Geller, Michael J Kahana, and Robert Sekuler. Characterizing the erp old–new effect in a short-term memory task. *Psychophysiology*, 45(5):784–793, 2008.
- [36] Klaus Oberauer. Binding and inhibition in working memory: individual and age differences in short-term recognition. *Journal of experimental psychology: General*, 134(3):368, 2005.
- [37] Nelson Cowan. Chapter 20 what are the differences between long-term, short-term, and working memory? In Wayne S. Sossin, Jean-Claude Lacaille, Vincent F. Castellucci, and Sylvie Belleville, editors, *Essence of Memory*, volume 169 of *Progress in Brain Research*, pages 323–338. Elsevier, 2008.
- [38] Geoffrey K Aguirre, Eric Zarahn, and Mark D’esposito. Neural components of topographical representation. *Proceedings of the National Academy of Sciences*, 95(3):839–846, 1998.
- [39] James V Haxby, M Ida Gobbini, Maura L Furey, Alomit Ishai, Jennifer L Schouten, and Pietro Pietrini. Distributed and overlapping representations of faces and objects in ventral temporal cortex. *Science*, 293(5539):2425–2430, 2001.
- [40] Rafael Malach, Ifat Levy, and Uri Hasson. The topography of high-order human object areas. *Trends in cognitive sciences*, 6(4):176–184, 2002.
- [41] Mona Spiridon and Nancy Kanwisher. How distributed is visual category information in human occipito-temporal cortex? an fmri study. *Neuron*, 35(6):1157–1165, 2002.
- [42] Paul E Downing, Yuhong Jiang, Miles Shuman, and Nancy Kanwisher. A cortical area selective for visual processing of the human body. *Science*, 293(5539):2470–2473, 2001.
- [43] Rebecca F. Schwarzlose, Jascha D. Swisher, Sabin Dang, and Nancy Kanwisher. The distribution of category and location information across object-selective regions in human visual cortex. *Proceedings of the National Academy of Sciences*, 105(11):4447–4452, 2008.
- [44] Truett Allison, Aina Puce, Dennis D Spencer, and Gregory McCarthy. Electrophysiological studies of human face perception. i: Potentials generated in occipitotemporal cortex by face and non-face stimuli. *Cerebral cortex*, 9(5):415–430, 1999.
- [45] Chou P Hung, Gabriel Kreiman, Tomaso Poggio, and James J DiCarlo. Fast readout of object identity from macaque inferior temporal cortex. *Science*, 310(5749):863–866, 2005.
- [46] Hesheng Liu, Yigal Agam, Joseph R Madsen, and Gabriel Kreiman. Timing, timing, timing: fast decoding of object information from intracranial field potentials in human visual cortex. *Neuron*, 62(2):281–290, 2009.
- [47] Eran Privman, Yuval Nir, Uri Kramer, Svetlana Kipervasser, Fani Andelman, Miri Y Neufeld, Roy Mukamel, Yehezkel Yeshurun, Itzhak Fried, and Rafael Malach. Enhanced category tuning revealed by intracranial electroencephalograms in high-order human visual areas. *Journal of Neuroscience*, 27(23):6234–6242, 2007.
- [48] Gabriel Kreiman, Christof Koch, and Itzhak Fried. Category-specific visual responses of single neurons in the human medial temporal lobe. *Nature neuroscience*, 3(9):946–953, 2000.
- [49] R Quian Quiroga, Leila Reddy, Gabriel Kreiman, Christof Koch, and Itzhak Fried. Invariant visual representation by single neurons in the human brain. *Nature*, 435(7045):1102–1107, 2005.
- [50] Ignacio Saez, Jack Lin, Arjen Stolk, Edward Chang, Josef Parvizi, Gerwin Schalk, Robert T Knight, and Ming Hsu. Encoding of multiple reward-related computations in transient and sustained high-frequency activity in human ofc. *Current Biology*, 28(18):2889–2899, 2018.
- [51] Wolfram Schultz, Léon Tremblay, and Jeffrey R Hollerman. Reward processing in primate orbitofrontal cortex and basal ganglia. *Cerebral cortex*, 10(3):272–283, 2000.
- [52] Benjamin Y Hayden and Michael L Platt. Neurons in anterior cingulate cortex multiplex information about reward and action. *Journal of Neuroscience*, 30(9):3339–3346, 2010.

- [53] Mauricio R Delgado. Reward-related responses in the human striatum. *Annals of the New York Academy of Sciences*, 1104(1):70–88, 2007.
- [54] Yutaka Komura, Ryoji Tamura, Teruko Uwano, Hisao Nishijo, Kimitaka Kaga, and Taketoshi Ono. Retrospective and prospective coding for predicted reward in the sensory thalamus. *Nature*, 412(6846):546–549, 2001.
- [55] Rebecca Elliott, Karl J Friston, and Raymond J Dolan. Dissociable neural responses in human reward systems. *Journal of neuroscience*, 20(16):6159–6165, 2000.
- [56] Mauricio R Delgado, Leigh E Nystrom, Catherine Fissell, DC Noll, and Julie A Fiez. Tracking the hemodynamic responses to reward and punishment in the striatum. *Journal of neurophysiology*, 84(6):3072–3077, 2000.
- [57] Peter Kirsch, Anne Schienle, Rudolf Stark, Gebhard Sammer, Carlo Blecker, Bertram Walter, Ulrich Ott, Jessica Burkart, and Dieter Vaitl. Anticipation of reward in a nonaversive differential conditioning paradigm and the brain reward system: an event-related fmri study. *Neuroimage*, 20(2):1086–1095, 2003.
- [58] Brian Knutson, Charles M Adams, Grace W Fong, and Daniel Hommer. Anticipation of increasing monetary reward selectively recruits nucleus accumbens. *Journal of Neuroscience*, 21(16):RC159–RC159, 2001.
- [59] Jeffrey P Mullin, Michael Shriver, Soha Alomar, Imad Najm, Juan Bulacio, Patrick Chauvel, and Jorge Gonzalez-Martinez. Is seeg safe? a systematic review and meta-analysis of stereo-electroencephalography-related complications. *Epilepsia*, 57(3):386–401, 2016.
- [60] Josef Parvizi and Sabine Kastner. Promises and limitations of human intracranial electroencephalography. *Nature neuroscience*, 21(4):474–483, 2018.
- [61] Ole Jensen, Jochen Kaiser, and Jean-Philippe Lachaux. Human gamma-frequency oscillations associated with attention and memory. *Trends in neurosciences*, 30(7):317–324, 2007.
- [62] Peter J Uhlhaas, Gordon Pipa, Sergio Neuenschwander, Michael Wibral, and Wolf Singer. A new look at gamma? high- γ (60 hz) γ -band activity in cortical networks: function, mechanisms and impairment. *Progress in biophysics and molecular biology*, 105(1-2):14–28, 2011.
- [63] György Buzsáki, Costas A Anastassiou, and Christof Koch. The origin of extracellular fields and currents—eeg, ecog, lfp and spikes. *Nature reviews neuroscience*, 13(6):407–420, 2012.
- [64] Mikael Lundqvist, Jonas Rose, Pawel Herman, Scott L Brincat, Timothy J Buschman, and Earl K Miller. Gamma and beta bursts underlie working memory. *Neuron*, 90(1):152–164, 2016.
- [65] Jessica A Cardin, Marie Carlén, Konstantinos Meletis, Ulf Knoblich, Feng Zhang, Karl Deisseroth, Li-Huei Tsai, and Christopher I Moore. Driving fast-spiking cells induces gamma rhythm and controls sensory responses. *Nature*, 459(7247):663–667, 2009.
- [66] Nathan E Crone, Anna Korzeniewska, and Piotr J Franaszczuk. Cortical gamma responses: searching high and low. *International Journal of Psychophysiology*, 79(1):9–15, 2011.
- [67] Nima Mesgarani, Connie Cheung, Keith Johnson, and Edward F Chang. Phonetic feature encoding in human superior temporal gyrus. *Science*, 343(6174):1006–1010, 2014.
- [68] Jean-Philippe Lachaux, Nikolai Axmacher, Florian Mormann, Eric Halgren, and Nathan E Crone. High-frequency neural activity and human cognition: past, present and possible future of intracranial eeg research. *Progress in neurobiology*, 98(3):279–301, 2012.
- [69] Mikael Lundqvist, Pawel Herman, Melissa R Warden, Scott L Brincat, and Earl K Miller. Gamma and beta bursts during working memory readout suggest roles in its volitional control. *Nature communications*, 9(1):1–12, 2018.
- [70] Earl K Miller, Mikael Lundqvist, and André M Bastos. Working memory 2.0. *Neuron*, 100(2):463–475, 2018.
- [71] Saskia Haegens, Verónica Nácher, Rogelio Luna, Ranulfo Romo, and Ole Jensen. α -oscillations in the monkey sensorimotor network influence discrimination performance by rhythmical inhibition of neuronal spiking. *Proceedings of the National Academy of Sciences*, 108(48):19377–19382, 2011.

- [72] Eelke Spaak, Mathilde Bonnefond, Alexander Maier, David A Leopold, and Ole Jensen. Layer-specific entrainment of gamma-band neural activity by the alpha rhythm in monkey visual cortex. *Current biology*, 22(24):2313–2318, 2012.
- [73] Tsung-Yi Lin, Michael Maire, Serge Belongie, James Hays, Pietro Perona, Deva Ramanan, Piotr Dollár, and C Lawrence Zitnick. Microsoft coco: Common objects in context. In *European conference on computer vision*, pages 740–755. Springer, 2014.
- [74] David H Brainard and Spatial Vision. The psychophysics toolbox. *Spatial vision*, 10(4):433–436, 1997.
- [75] Denis G Pelli and Spatial Vision. The videotoolbox software for visual psychophysics: Transforming numbers into movies. *Spatial vision*, 10:437–442, 1997.
- [76] Itzhak Fried, Ueli Rutishauser, Moran Cerf, and Gabriel Kreiman. *Single neuron studies of the human brain: probing cognition*. MIT Press, 2014.
- [77] David M Groppe, Stephan Bickel, Andrew R Dykstra, Xiuyuan Wang, Pierre Mégevand, Manuel R Mercier, Fred A Lado, Ashesh D Mehta, and Christopher J Honey. ielvis: An open source matlab toolbox for localizing and visualizing human intracranial electrode data. *Journal of neuroscience methods*, 281:40–48, 2017.
- [78] Anders M Dale, Bruce Fischl, and Martin I Sereno. Cortical surface-based analysis: I. segmentation and surface reconstruction. *Neuroimage*, 9(2):179–194, 1999.
- [79] Alark Joshi, Dustin Scheinost, Hirohito Okuda, Dominique Belhachemi, Isabella Murphy, Lawrence H Staib, and Xenophon Papademetris. Unified framework for development, deployment and robust testing of neuroimaging algorithms. *Neuroinformatics*, 9(1):69–84, 2011.
- [80] Rahul S Desikan, Florent Ségonne, Bruce Fischl, Brian T Quinn, Bradford C Dickerson, Deborah Blacker, Randy L Buckner, Anders M Dale, R Paul Maguire, Bradley T Hyman, et al. An automated labeling system for subdividing the human cerebral cortex on mri scans into gyral based regions of interest. *Neuroimage*, 31(3):968–980, 2006.
- [81] Jianxiao Wu, Gia H Ngo, Douglas Greve, Jingwei Li, Tong He, Bruce Fischl, Simon B Eickhoff, and BT Thomas Yeo. Accurate nonlinear mapping between mni volumetric and freesurfer surface coordinate systems. *Human brain mapping*, 39(9):3793–3808, 2018.
- [82] Jacob Benesty, Jingdong Chen, Yiteng Huang, and Israel Cohen. Pearson correlation coefficient. In *Noise reduction in speech processing*, pages 1–4. Springer, 2009.
- [83] Jiarui Wang, Annabelle Tao, William S Anderson, Joseph R Madsen, and Gabriel Kreiman. Mesoscopic physiological interactions in the human brain reveal small-world properties. *Cell reports*, 36(8):109585, 2021.
- [84] Arjun K Bansal, Jedediah M Singer, William S Anderson, Alexandra Golby, Joseph R Madsen, and Gabriel Kreiman. Temporal stability of visually selective responses in intracranial field potentials recorded from human occipital and temporal lobes. *Journal of neurophysiology*, 108(11):3073–3086, 2012.
- [85] Hemant Bokil, Peter Andrews, Jayant E Kulkarni, Samar Mehta, and Partha P Mitra. Chronux: a platform for analyzing neural signals. *Journal of neuroscience methods*, 192(1):146–151, 2010.
- [86] Behtash Babadi and Emery N Brown. A review of multitaper spectral analysis. *IEEE Transactions on Biomedical Engineering*, 61(5):1555–1564, 2014.
- [87] Yuchen Xiao, Chien-Chen Chou, Garth Rees Cosgrove, Nathan E Crone, Scellig Stone, Joseph R Madsen, Ian Reucroft, Yen-Cheng Shih, Daniel Weisholtz, Hsiang-Yu Yu, et al. Task-specific neural processes underlying conflict resolution during cognitive control. *bioRxiv*, 2022.
- [88] Robert Oostenveld, Pascal Fries, Eric Maris, and Jan-Mathijs Schoffelen. Fieldtrip: open source software for advanced analysis of meg, eeg, and invasive electrophysiological data. *Computational intelligence and neuroscience*, 2011, 2011.

- [89] Keith J Worsley and Karl J Friston. Analysis of fmri time-series revisited—again. *Neuroimage*, 2(3):173–181, 1995.
- [90] Keith J Worsley and Karl J Friston. Analysis of fmri time-series revisited—again. *Neuroimage*, 2(3):173–181, 1995.
- [91] Roy E Welsch and Edwin Kuh. Linear regression diagnostics. Technical report, National Bureau of Economic Research, 1977.
- [92] Carsten F Dormann, Jane Elith, Sven Bacher, Carsten Buchmann, Gudrun Carl, Gabriel Carré, Jaime R García Marquéz, Bernd Gruber, Bruno Lafourcade, Pedro J Leitão, et al. Collinearity: a review of methods to deal with it and a simulation study evaluating their performance. *Ecography*, 36(1):27–46, 2013.
- [93] Christopher Glen Thompson, Rae Seon Kim, Ariel M Aloe, and Betsy Jane Becker. Extracting the variance inflation factor and other multicollinearity diagnostics from typical regression results. *Basic and Applied Social Psychology*, 39(2):81–90, 2017.
- [94] Robert M O’Brien. A caution regarding rules of thumb for variance inflation factors. *Quality & quantity*, 41(5):673–690, 2007.
- [95] Manoranjan Pal and Premananda Bharati. The regression models with dummy explanatory variables. In *Applications of regression techniques*, pages 135–153. Springer, 2019.
- [96] Manuel R Mercier, Stephan Bickel, Pierre Megevand, David M Groppe, Charles E Schroeder, Ashesh D Mehta, and Fred A Lado. Evaluation of cortical local field potential diffusion in stereotactic electro-encephalography recordings: a glimpse on white matter signal. *Neuroimage*, 147:219–232, 2017.
- [97] Gregory McCarthy, Anna C Nobre, Shlomo Bentin, and Dennis D Spencer. Language-related field potentials in the anterior-medial temporal lobe: I. intracranial distribution and neural generators. *Journal of neuroscience*, 15(2):1080–1089, 1995.
- [98] Robert M O’Brien. A caution regarding rules of thumb for variance inflation factors. *Quality & quantity*, 41(5):673–690, 2007.
- [99] Jan Kamiński, Shannon Sullivan, Jeffrey M Chung, Ian B Ross, Adam N Mamelak, and Ueli Rutishauser. Persistently active neurons in human medial frontal and medial temporal lobe support working memory. *Nature neuroscience*, 20(4):590–601, 2017.
- [100] Saul Sternberg. In defence of high-speed memory scanning. *The Quarterly Journal of Experimental Psychology*, 69(10):2020–2075, 2016.
- [101] Robert T Knight. Contribution of human hippocampal region to novelty detection. *Nature*, 383(6597):256–259, 1996.
- [102] E Düzel, R Habib, S Guderian, and HJ Heinze. Four types of novelty–familiarity responses in associative recognition memory of humans. *European Journal of Neuroscience*, 19(5):1408–1416, 2004.
- [103] Mark M Kishiyama, Andrew P Yonelinas, and Robert T Knight. Novelty enhancements in memory are dependent on lateral prefrontal cortex. *Journal of Neuroscience*, 29(25):8114–8118, 2009.
- [104] Robert T Knight. Decreased response to novel stimuli after prefrontal lesions in man. *Electroencephalography and Clinical Neurophysiology/Evoked Potentials Section*, 59(1):9–20, 1984.
- [105] Denise Dörfel, Annett Werner, Michael Schaefer, Rüdiger Von Kummer, and Anke Karl. Distinct brain networks in recognition memory share a defined region in the precuneus. *European Journal of Neuroscience*, 30(10):1947–1959, 2009.
- [106] Melissa Hebscher, Jed A Meltzer, and Asaf Gilboa. A causal role for the precuneus in network-wide theta and gamma oscillatory activity during complex memory retrieval. *Elife*, 8, 2019.

- [107] Giuliana Mazzone, Andrew Clark, Adriana De Bartolo, Chiara Guerrini, Zacharia Nahouli, Davide Duzzi, Matteo De Marco, William McGeown, and Annalena Venneri. Brain activation in highly superior autobiographical memory: the role of the precuneus in the autobiographical memory retrieval network. *Cortex*, 120:588–602, 2019.
- [108] Melissa Hebscher, Brian Levine, and Asaf Gilboa. The precuneus and hippocampus contribute to individual differences in the unfolding of spatial representations during episodic autobiographical memory. *Neuropsychologia*, 110:123–133, 2018.
- [109] Maxime Freton, Cédric Lemogne, Loretxu Bergouignan, Pauline Delaveau, Stéphane Lehericy, and Philippe Fossati. The eye of the self: precuneus volume and visual perspective during autobiographical memory retrieval. *Brain Structure and Function*, 219(3):959–968, 2014.
- [110] Sonia Bonni, Domenica Veniero, Chiara Mastropasqua, Viviana Ponzio, Carlo Caltagirone, Marco Bozzali, and Giacomo Koch. Tms evidence for a selective role of the precuneus in source memory retrieval. *Behavioural Brain Research*, 282:70–75, 2015.
- [111] Marco K Wittmann, Elsa Fouragnan, Davide Folloni, Miriam C Klein-Flügge, Bolton KH Chau, Mehdi Khamassi, and Matthew FS Rushworth. Global reward state affects learning and activity in raphe nucleus and anterior insula in monkeys. *Nature communications*, 11(1):1–17, 2020.
- [112] Joaquin M Fuster and John P Jervey. Neuronal firing in the inferotemporal cortex of the monkey in a visual memory task. *Journal of Neuroscience*, 2(3):361–375, 1982.
- [113] J Ph Lachaux, D Rudrauf, and P Kahane. Intracranial eeg and human brain mapping. *Journal of Physiology-Paris*, 97(4-6):613–628, 2003.
- [114] David IG Wilson, Sakurako Watanabe, Helen Milner, and James A Ainge. Lateral entorhinal cortex is necessary for associative but not nonassociative recognition memory. *Hippocampus*, 23(12):1280–1290, 2013.
- [115] Gareth RI Barker and Elizabeth Clea Warburton. Multi-level analyses of associative recognition memory: the whole is greater than the sum of its parts. *Current Opinion in Behavioral Sciences*, 32:80–87, 2020.
- [116] Beatriz EP Mizusaki and Cian O’Donnell. Neural circuit function redundancy in brain disorders. *Current opinion in neurobiology*, 70:74–80, 2021.

Appendices

A Methods and behavior tables

Table A.1: Epileptic subjects. Patients' sex, gender, age and hospital where recordings were performed.

Subject No.	Hospital	Gender	Age
1	Xuanwu	female	22
2	Xuanwu	male	32
3	Xuanwu	male	19
4	Xuanwu	male	33
5	Xuanwu	male	35
6	Xuanwu	male	21
7	Xuanwu	male	26
8	Xuanwu	male	23
9	Xuanwu	female	47
10	Xuanwu	female	21
11	Xuanwu	female	26
12	BWH	female	32
13	BWH	female	31
14	BWH	female	26
15	BWH	male	22
16	BWH	female	52
17	BWH	male	44
18	BCH	male	18
19	BCH	female	12
20	BCH	male	15

Table A.2: Electrodes' location. Number of electrodes analyzed in each brain region in the gray and white matter. Left and Right indicate whether electrodes were located in the left or right hemisphere, respectively. Total indicates the total number of electrodes in both right and left hemispheres.

Gray matter				White matter (closest gray matter)			
Region	Left	Right	Total	Region	Left	Right	Total
amygdala	21	24	45	bankssts	5	2	7
bankssts		7	7	caudalanteriorcingulate	1	0	1
caudalanteriorcingulate	1	3	4	caudalmiddlefrontal	1	7	8
caudalmiddlefrontal	1	5	6	cuneus	1	1	2
entorhinal	5		5	entorhinal	2	2	4
fusiform	15	10	25	fusiform	21	14	35
hippocampus	36	31	67	inferiorparietal	7	3	10
inferiorparietal	11	8	19	inferiortemporal	31	16	47
inferiortemporal	14	9	23	insula	11	12	23
insula	13	15	28	isthmuscingulate	1	0	1
isthmuscingulate	6		6	lateraloccipital	2	3	5
lateraloccipital	3	2	5	lateralorbitofrontal	23	30	53
lateralorbitofrontal	19	32	51	lingual	2	2	4
lingual	3	2	5	medialorbitofrontal	6	8	14
medialorbitofrontal	4	7	11	middletemporal	31	21	52
middletemporal	53	38	91	paracentral	3	3	6
paracentral	4		4	parahippocampal	6	5	11
parahippocampal	10	13	23	parsopercularis	5	3	8
parsopercularis	11	5	16	parsorbitalis	4	7	11
parsorbitalis	2	3	5	parstriangularis	10	10	20
parstriangularis	13	19	32	pericalcarine	4	0	4
pericalcarine		1	1	postcentral	6	0	6
postcentral	8	12	20	posteriorcingulate	10	1	11
posteriorcingulate	4	3	7	precentral	11	15	26
precentral	8	21	29	precuneus	12	3	15
precuneus	3		3	rostralanteriorcingulate	3	3	6
rostralanteriorcingulate	7	7	14	rostralmiddlefrontal	2	7	9
rostralmiddlefrontal	1	4	5	superiorfrontal	10	18	28
superiorfrontal	13	19	32	superiorparietal	10	7	17
superiorparietal	8	12	20	superiortemporal	21	13	34
superiortemporal	26	21	47	supramarginal	4	4	8
supramarginal	10	4	14	transversetemporal	6	0	6
transversetemporal	6		6	Total	272	220	492
Total	339	337	676				

Table A.3: Comparison for each subject of the number of clicks before a tile was matched. Tiles were grouped by image category. Columns represent the comparison between two categories of the number of times a tile had to be clicked to perform a match. The letter indicates the most difficult image category to match, i.e., its tiles were clicked more times before being matched. ***: $p < 0.001$, **: $p < 0.01$. X indicates the predictor with the biggest t-statistic. Abbreviations: A: animal; F: food; I: indoor; P: person; V: vehicle.

Subject	Animal- Food	Animal - Indoor	Animal - Person	Animal - Vehicle	Food - Indoor	Food - Person	Food - Vehicle	Indoor - Person	Indoor - Vehicle	Person - Vehicle
XW01	A	A	A	A	I	P	V	P	I	P
XW02	A	A	A	A	F	F	F	I	I	P
XW03	A	A	A	A	I	F	V	I	I	V
XW04	A	A	A	V	F	F	V **	I	V ***	V ***
XW06	A	A	A	V	I	F	V	I	V	V
XW07	A	A	A	A	I	P	F	P	I	P
XW08	A	A	A	A	I	F	V	I	V	V
XW11	A	I	P	V	I	P	V	I	I	V
XW12	A	A	A	V	I	F	V	I	V	V
XW13	A	A	A	V	F	P	V	P	V	V
XW15	F	I	A	A	I	F	F	I	I	P
BWH5	A	A	A	A	I	F	V	I	V	V
BWH52	F	I	P	V	F	F	F	I	V	V
BWH6	A	I	A	V	I	F	V	I **	V	V **
BWH7	A	A	A	A	I	F	V	I	V	V
BWH8	F	I	A	A	I	F	F	I	I	P
BWH9	F	I	P	V	I	F	V	I	V	V
BCH3	A	I	A	A	I	F	V	I	I	V
BCH4	A **	A **	A	A	F	P	V	P	V	V
BCH5	F	A	P	V	F	P	V	P	V **	V

B Gray matter tables

Table B.1: Number of gray matter electrodes that presented each predictor as significant for the 1st tile GLM. Abbreviations: NSP, n-since-pair*match; NSLC, n-since-last-click; NTS, n-times-seen; RT: reaction-time.

Region	# Ch	match	NSP	NSLC	first_click	NTS	next_match	RT	board-size	x-pos.	y-pos.	distance	animal	food	person	vehicle
amygdala	45	0	0	0	2	0	0	2	2	0	1	0	0	0	2	0
hippocampus	66	2	0	1	0	1	0	1	1	0	0	0	0	2	0	0
bankssts	7	1	0	2	1	0	0	0	0	0	0	0	2	2	2	0
caudalanteriorcingulate	3	0	0	0	0	0	0	0	0	0	0	0	0	0	0	0
caudalmiddlefrontal	6	0	0	0	1	0	0	1	0	0	0	0	1	0	2	0
entorhinal	5	1	0	1	0	0	0	0	0	0	0	0	0	0	0	0
fusiform	25	1	0	4	5	0	1	2	2	0	1	1	4	2	3	4
inferioparietal	19	0	0	4	3	0	0	1	3	1	1	2	0	0	2	0
inferiotemporal	23	3	0	3	2	0	0	1	1	2	0	0	0	1	0	0
insula	28	4	3	4	1	0	0	0	1	0	0	0	1	0	0	0
isthmuscingulate	6	0	0	0	0	0	0	0	0	0	0	0	0	0	0	0
lateraloccipital	5	0	0	0	1	0	0	1	0	1	0	0	2	0	2	0
lateralorbitofrontal	51	7	3	4	12	2	1	3	6	1	2	2	1	0	1	0
lingual	5	0	0	0	0	0	0	0	0	0	0	0	1	1	1	0
medialorbitofrontal	11	0	1	0	2	0	1	0	1	0	0	1	0	0	1	0
middletemporal	91	5	3	4	4	2	2	4	0	1	1	2	1	0	3	0
paracentral	4	0	0	0	0	0	0	0	0	0	0	0	0	0	0	0
parahippocampal	23	1	1	3	1	1	0	0	0	1	0	0	2	1	1	2
parsopercularis	16	3	1	4	5	0	2	3	1	0	0	0	2	0	1	1
parsorbitalis	5	0	0	0	0	0	0	0	0	0	0	0	0	0	0	0
parstriangularis	32	0	0	1	3	0	0	0	2	0	0	2	2	1	1	0
pericalcarine	1	0	0	0	0	0	0	0	0	0	0	0	0	0	0	0
postcentral	20	0	0	2	0	0	0	2	0	1	1	0	0	0	0	0
posteriorcingulate	7	0	0	0	0	0	0	0	0	0	0	0	0	0	1	0
precentral	29	1	1	2	4	0	0	1	1	0	0	0	0	0	1	0
precuneus	3	1	1	0	0	0	0	0	0	0	0	0	0	0	0	0
rostralanteriorcingulate	14	1	0	0	0	0	0	0	0	0	0	0	0	0	0	0
rostralmiddlefrontal	5	0	0	1	1	0	0	1	0	0	0	0	0	0	1	0
superiorfrontal	32	0	0	1	0	0	0	3	0	0	1	1	0	0	0	0
superiorparietal	20	0	0	2	0	0	0	4	1	1	0	1	0	0	0	0
superiortemporal	46	0	0	1	1	0	0	0	0	0	0	0	0	0	0	0
supramarginal	14	1	1	1	1	1	0	2	0	0	0	2	0	0	0	0
transversestemporal	6	0	0	0	0	0	0	0	0	0	0	0	0	0	0	0
Total	676	32	15	45	50	7	7	32	22	8	9	14	19	10	25	7

Table B.2: Number of gray matter electrodes that presented each predictor as significant for the 2nd tile GLM. Abbreviations: NSLC, n-since-last-click; NTS, n-times-seen; RT: reaction-time.

Region	Ch	match	NSLC	first_click	NTS	next_match	RT	board_size	x_pos.	y_pos.	distance	animal	food	person	vehicle
amygdala	45	3	0	1	0	1	2	1	0	0	0	0	0	0	1
hippocampus	66	6	0	1	3	0	4	2	1	4	0	0	0	0	1
bankssts	7	3	0	1	0	0	3	3	0	0	0	0	1	0	0
caudalanteriorcingulate	3	0	0	0	0	0	0	0	0	0	0	0	0	0	0
caudalmiddlefrontal	6	2	0	0	0	0	0	0	1	0	0	0	0	0	0
entorhinal	5	1	0	0	0	0	0	0	0	1	1	1	0	0	0
fusiform	25	0	1	2	0	1	2	0	0	1	0	5	2	3	1
inferioparietal	19	4	0	0	0	0	2	3	0	1	0	2	0	3	0
inferiortemporal	23	5	0	0	0	1	5	0	0	0	0	0	0	1	1
insula	28	12	0	2	2	0	4	0	0	0	0	0	0	0	0
isthmuscingulate	6	0	0	0	0	0	0	0	0	0	0	0	0	0	0
lateraloccipital	5	1	0	2	0	0	2	0	0	0	0	0	0	0	0
lateralorbitofrontal	51	21	4	4	2	3	5	6	0	2	0	0	2	2	2
lingual	5	1	0	1	0	0	0	0	0	1	0	0	1	0	0
medialorbitofrontal	11	3	0	0	0	0	1	2	0	0	0	0	0	1	0
middletemporal	91	14	0	0	0	0	1	2	0	4	0	0	0	0	0
paracentral	4	0	0	0	0	0	0	0	0	0	0	0	0	0	0
parahippocampal	23	2	0	1	0	0	0	1	0	0	0	2	1	2	2
parsopercularis	16	6	1	2	1	2	6	4	1	0	2	1	0	0	0
parsorbitalis	5	0	0	0	0	0	0	0	0	0	0	0	0	0	0
parstriangularis	32	8	0	0	0	0	4	2	0	0	1	0	0	0	1
pericalcarine	1	0	0	0	0	0	0	0	0	0	0	0	0	0	0
postcentral	20	2	1	2	0	0	0	0	1	0	0	0	0	0	0
posteriorcingulate	7	1	0	0	1	0	0	0	0	0	0	0	0	0	0
precentral	29	7	1	2	2	0	0	0	1	0	2	1	0	0	0
precuneus	3	0	0	1	0	1	0	0	0	0	0	0	0	0	0
rostralanteriorcingulate	14	1	0	0	0	0	0	0	0	0	0	0	0	0	0
rostralmiddlefrontal	5	1	1	1	0	0	1	0	0	0	0	0	0	0	0
superiorfrontal	32	2	0	0	0	0	2	0	0	0	0	0	0	0	0
superiorparietal	14	3	0	0	0	0	3	3	3	0	0	0	0	0	2
superiorparietal	6	0	0	0	0	0	0	0	0	0	1	0	0	0	0
superiortemporal	46	0	0	1	0	0	0	1	1	2	0	0	0	0	0
supramarginal	14	3	0	0	1	1	0	0	0	0	0	0	0	1	1
transversestemporal	6	0	0	0	0	0	0	0	0	0	0	0	0	0	0
Total	676	112	9	24	12	10	47	30	9	16	7	12	7	13	12

Table B.3: First-tile GLM results of gray matter electrodes that presented n-since-last-click and/or first-click as significant predictors. Columns 4-19 represent each predictor in the GLM. ***: $p < 0.001$, **: $p < 0.01$, empty: $p > 0.01$ (not-significant). X indicates the predictor with the biggest t-statistic. Abbreviations: NSP, n-since-pair*match; NSLC, n-since-last-click; NTS, n-times-seen; RT: reaction-time.

Brain region	Subject	Ch	match	NSP	NSLC	first_click	NTS	next_match	RT	board_size	x_pos.	y_pos.	distance	animal	food	person	vehicle
fusiform	XW03	150			**	**			***					*** X			
fusiform	XW07	151			*** X	**											**
fusiform	XW11	143			***	*** X											
inferioparietal	XW03	144			*** X	***		***							**		
inferioparietal	BCH3	22			*** X	***				***		**					
inferioparietal	BCH3	25			*** X	***					**				**		
inferiortemporal	BCH3	26	**		***	*** X											
inferiortemporal	BCH3	134			*** X	**											
lateralorbitofrontal	BWH8	22			*** X	***	**	**	**			**					
lateralorbitofrontal	BCH3	23	**		**	** X				**							
lateralorbitofrontal	BCH3	78	***	***	***	*** X				**							
middletemporal	BCH3	32			**	** X											
parsopectularis	XW11	15			*** X	***		***						**			
parsopectularis	XW11	16			***	*** X		***							***		
parsopectularis	XW15	24			**	*** X	**							**			**
parsopectularis	BCH3	44			**	*** X											
precentral	BWH8	3			**	*** X		***									
precentral	BWH8	81			***	*** X			***								
rostralmiddlefrontal	XW11	131			***	*** X		***							**		
superiortemporal	XW02	43			**	*** X											
Amygdala	XW08	42				** X											
Amygdala	BWH8	92				**										*** X	
bankssts	BCH3	50				*** X											
caudalmiddlefrontal	BWH5	5				*** X											
fusiform	XW01	40				**		**		**							*** X
fusiform	BWH9	32				** X											
insula	XW03	5				** X											
lateraloccipital	BCH5	6				***		*** X		**	**		**	**	**		
lateralorbitofrontal	XW03	7				*** X		***		**		**	**				
lateralorbitofrontal	BWH7	20				** X	**										
lateralorbitofrontal	BCH3	21				***				*** X							
lateralorbitofrontal	BCH3	22		**		*** X				***							
lateralorbitofrontal	BCH3	41				*** X				**							
lateralorbitofrontal	BCH3	18				*** X	**										
lateralorbitofrontal	BCH3	19				*** X											
lateralorbitofrontal	BCH3	108				*** X											
lateralorbitofrontal	BCH4	110				** X											
medialorbitofrontal	BCH3	148				** X				**							
medialorbitofrontal	BCH3	27				*** X											
middletemporal	BCH3	30				*** X											
middletemporal	BCH3	11	*** X	**		**									**		
middletemporal	BCH3	13				*** X											
parahippocampal	XW12	14				** X											
parsopectularis	BCH3	38				*** X											
parstriangularis	BCH3	42				**		**		**			** X	**	**		
parstriangularis	BCH3	32				***							*** X				
parstriangularis	BCH3	6				*** X							**				
precentral	BCH3	41				*** X											
precentral	BWH5	42				*** X											
supramarginal	XW02	27	*** X	***		**	***	***	***				**				
Hippocampus	XW07	13			**		** X							**			
bankssts	BWH9	152			**									**		*** X	
bankssts	BWH9	38			**									**	**	*** X	
entorhinal	XW07	27	**		** X												
fusiform	XW02	28			** X												
inferioparietal	BCH3	29			*** X												
inferiortemporal	XW08	34	**		**	**		*** X		**							
insula	BCH3	73	***	***	*** X												
insula	BCH3	45	***	***	*** X												
insula	BCH3	48	***	***	*** X												
insula	BCH3	24			***					*** X							
lateralorbitofrontal	BWH8	8			**	**		***								*** X	
middletemporal	XW15	9		**	** X		**										
middletemporal	BWH7	8			** X												
middletemporal	BWH9	59			**	**		**					** X				
parahippocampal	XW07	39			***	**											*** X
parahippocampal	XW07	49			***	**						***					*** X
parahippocampal	XW13	6			** X	**											
parstriangularis	XW13	111			*** X	**											
postcentral	BWH5	112			**	**		** X		**		**					
postcentral	BWH5	37			*** X	**		**		**		**					
superiorfrontal	BWH5				***	**		*** X		**							
superiorparietal	XW03				**	**		**		**	*** X						
superiorparietal	XW03				**	**		** X		**							
supramarginal	XW02				**	**		*** X		**			***				

Table B.4: First-tile GLM results of gray matter electrodes that presented match and/or n-since-pair*match as significant predictors. Columns 4-19 represent each predictor in the GLM. ***: $p < 0.001$, **: $p < 0.01$, empty: $p > 0.01$ (not-significant). X indicates the predictor with the biggest t-statistic. Abbreviations: NSP, n-since-pair*match; NSLC, n-since-last-click; NTS, n-times-seen; RT: reaction-time.

Region	Subject	Ch	match	NSP	NSLC	first.click	NTS	next.match	RT	board-size	x-pos.	y-pos.	distance	animal	food	person	vehicle
insula	BCH3	27	***	***	*** X												
insula	BCH3	28	***	***	*** X												
insula	BCH3	29	***	***	*** X												
lateralorbitofrontal	BCH3	26	***	***	***	*** X				**							
middletemporal	XW02	52	*** X	***													
middletemporal	BCH3	110	*** X	**		**										**	
parahippocampal	XW13	7	*** X	**													
parsopercularis	XW07	83	*** X	**													
precentral	BCH4	106	*** X	**												**	
precuneus	XW01	77	*** X	**													
supramarginal	XW02	32	*** X	***		**	***		***				**				
Hippocampus	XW02	47	** X														
Hippocampus	BWH9	28	*** X														
bankssts	XW04	36	** X											**			
entorhinal	XW07	27	**		** X												
fusiform	XW07	10	**														** X
inferiortemporal	XW08	18	*** X														
inferiortemporal	XW08	38	**		**				*** X		**						
inferiortemporal	BCH3	143	**		***	*** X											
insula	BCH4	55	** X														
lateralorbitofrontal	XW04	39	** X											**			
lateralorbitofrontal	XW04	42	** X														
lateralorbitofrontal	XW04	43	*** X														
lateralorbitofrontal	XW04	45	*** X								**						
lateralorbitofrontal	XW13	46	*** X														
lateralorbitofrontal	BCH3	25	**		**	** X				**							
middletemporal	XW11	37	**				**									**	** X
middletemporal	BWH6	45	***						**			**	*** X				
middletemporal	BCH3	109	** X						**								
parsopercularis	XW07	82	*** X				**		**								
parsopercularis	XW13	57	*** X							**							
rostralanteriorcingulate	XW12	34	*** X														
lateralorbitofrontal	BCH3	3		** X													
lateralorbitofrontal	BCH3	6	**			*** X				***							
medialorbitofrontal	BCH3	2	** X														
middletemporal	XW15	45	**	** X			**										

Table B.5: Gamma responses of electrodes that presented n-since-pair*match as a significant predictor could predict familiarity to the tile’s pair only for match trials. Linear regression results (F-test p-value) using n-since-pair as the independent variable and the gamma power AUC as the dependent variable for match and mismatch trials, separately. Only electrodes that presented n-since-pair*match as a significant predictor were considered.

Region	Subject	Ch	p(match)	p(mismatch)
insula	BCH3	27	0.005	0.978
insula	BCH3	28	0.002	0.343
insula	BCH3	29	0.001	0.856
lateralorbitofrontal	BCH3	3	0.006	0.848
lateralorbitofrontal	BCH3	6	0.003	0.178
lateralorbitofrontal	BCH3	26	0.001	0.408
medialorbitofrontal	BCH3	2	0.012	0.352
middletemporal	XW02	52	0.001	0.701
middletemporal	XW15	45	0.005	0.738
middletemporal	BCH3	110	0.007	0.919
parahippocampal	XW13	7	0.070	0.068
parsopercularis	XW07	83	0.029	0.231
precentral	BCH4	106	0.000	0.698
precuneus	XW01	77	0.010	0.484
supramarginal	XW02	32	0.006	0.331

Table B.6: Second-tile GLM results of gray matter electrodes that presented n-since-last-click and/or first-click as significant predictors. Columns 4-19 represent each predictor in the GLM. ***: p<0.001, **:p<0.01, empty:p>0.01 (not-significant). X indicates the predictor with the biggest t-statistic. Abbreviations: NSLC, n-since-last-click; NTS, n-times-seen; RT: reaction-time.

Region	Subject	Ch	match	NSLC	first.click	NTS	next.match	RT	board.size	x.pos.	y.pos.	distance	animal	food	person	vehicle
fusiform	XW03	11		**	**								*** X			
lateralorbitofrontal	BWH8	22	**	***	***		**							***		*** X
lateralorbitofrontal	BCH3	26	***	**	*** X	***		***								
parsopercularis	XW11	22	***	***	***			*** X	***				***			
postcentral	BCH5	84		**	** X											
precentral	BWH5	24	**	**	** X											
rostralmiddlefrontal	XW11	24	*** X	**	***			***								
Amygdala	XW13	10			** X											
Hippocampus	BCH3	104	*** X		***											
bankssts	BCH3	131	**		**			*** X	**							
fusiform	XW13	37			**											*** X
insula	BCH3	27	*** X		***	**		**								
insula	BCH3	28	*** X		**	**										
lateraloccipital	BCH5	4			** X											
lateraloccipital	BCH5	5			*** X											
lateralorbitofrontal	BCH3	5			** X			**								
lateralorbitofrontal	BCH3	25	***		*** X	***		***								
lingual	XW01	12	**		**							*** X		**		
parahippocampal	XW12	27			**				*** X							
parsopercularis	XW11	23	***		***			*** X	***							
postcentral	BCH5	83			** X					**						
precentral	BCH3	40			** X	**						**				
precuneus	XW01	77			**		*** X									
superiortemporal	BCH3	119			** X						**					
lateralorbitofrontal	BWH52	46		** X												
lateralorbitofrontal	BCH3	9	*** X	**				***	**							

Table B.7: Second-tile GLM results of gray matter electrodes that presented match as significant predictors. Columns 4-19 represent each predictor in the GLM. ***: $p < 0.001$, **: $p < 0.01$, empty: $p > 0.01$ (not-significant). X indicates the predictor with the biggest t-statistic. Abbreviations: NSLC, n-since-last-click; NTS, n-times-seen; RT: reaction-time.

Region	Subject	Ch	match	NSLC	first_click	NTS	next_match	RT	board_size	x_pos.	y_pos.	distance	animal	food	person	vehicle
Amygdala	16	XW07	**				** X									
Amygdala	4	XW08	*** X													
Amygdala	51	XW11	*** X													
Hippocampus	47	XW02	** X			**										
Hippocampus	28	BWH9	*** X													
Hippocampus	102	BCH3	*** X													
Hippocampus	103	BCH3	*** X													
Hippocampus	104	BCH3	*** X		***											
Hippocampus	105	BCH3	*** X													
bankssts	42	BWH9	**										** X			
bankssts	131	BCH3	**	**				*** X	**							
bankssts	132	BCH3	*** X					***	**							
caudalmiddlefrontal	69	BWH6	*** X							**						
caudalmiddlefrontal	73	BWH6	*** X													
entorhinal	2	BCH4	**									** X				
inferioparietal	60	XW03	*** X						**							
inferioparietal	71	XW03	*** X					***					**		***	
inferioparietal	62	BWH9	*** X						**							
inferioparietal	63	BWH9	*** X													
inferiortemporal	65	XW01	** X													
inferiortemporal	66	XW01	**					**							**	** X
inferiortemporal	21	XW08	*** X													
inferiortemporal	37	XW08	** X					**								
inferiortemporal	38	XW08	*** X					***								
insula	50	XW03	*** X													
insula	77	XW07	*** X					**								
insula	79	XW08	*** X													
insula	80	XW08	*** X					**								
insula	27	BCH3	*** X		***	**		**								
insula	28	BCH3	*** X	**	**											
insula	29	BCH3	*** X													
insula	44	BCH3	*** X													
insula	45	BCH3	*** X													
insula	55	BCH4	*** X													
insula	104	BCH4	** X					**								
insula	151	BCH5	** X													
lateraloccipital	81	BWH9	**					*** X								
lateralorbitofrontal	39	XW04	*** X													
lateralorbitofrontal	43	XW04	*** X													
lateralorbitofrontal	45	XW04	*** X													
lateralorbitofrontal	40	XW13	*** X													
lateralorbitofrontal	43	XW13	*** X													
lateralorbitofrontal	46	XW13	*** X													
lateralorbitofrontal	28	BWH6	*** X													
lateralorbitofrontal	29	BWH6	*** X			**										
lateralorbitofrontal	30	BWH6	*** X			***										
lateralorbitofrontal	22	BWH8	**	***	***	**							***			*** X
lateralorbitofrontal	3	BCH3	*** X					***			**					
lateralorbitofrontal	7	BCH3	*** X						***							
lateralorbitofrontal	8	BCH3	*** X					***	***							
lateralorbitofrontal	9	BCH3	*** X	**				***	**							
lateralorbitofrontal	20	BCH3	*** X						**							
lateralorbitofrontal	21	BCH3	*** X													
lateralorbitofrontal	22	BCH3	*** X													
lateralorbitofrontal	25	BCH3	***		*** X	***		***					**			
lateralorbitofrontal	26	BCH3	***	**	*** X	***		***								
lateralorbitofrontal	41	BCH4	** X													
lateralorbitofrontal	54	BCH4	** X													
lingual	12	XW01	**		**							*** X		**		
medialorbitofrontal	2	BCH3	*** X					***	***							
medialorbitofrontal	18	BCH3	*** X													
medialorbitofrontal	19	BCH3	*** X					**								
middletemporal	60	XW01	*** X								**					
middletemporal	52	XW02	*** X													
middletemporal	32	XW12	*** X													
middletemporal	19	BWH6	** X													
middletemporal	45	BWH6	*** X													
middletemporal	22	BWH9	** X													
middletemporal	23	BWH9	** X													
middletemporal	24	BWH9	** X													
middletemporal	108	BCH3	*** X													
middletemporal	109	BCH3	*** X													
middletemporal	133	BCH3	*** X					***			***					
middletemporal	134	BCH3	*** X								***					
middletemporal	135	BCH3	*** X					***			***					
middletemporal	148	BCH3	** X													
parahippocampal	8	XW07	***										**	***	**	*** X
parahippocampal	9	XW07	**										**	***	**	*** X
parsopercularis	78	XW07	*** X					**		***		***				
parsopercularis	22	XW11	***	***	***			*** X	***				***			
parsopercularis	23	XW11	***	***	***			*** X	***							
parsopercularis	30	BCH3	*** X			**			**							
parsopercularis	32	BCH3	** X					*** X	**							
parsopercularis	50	BCH5	** X						**							
parstriangularis	25	XW02	*** X													
parstriangularis	74	XW07	*** X					***								
parstriangularis	75	XW07	*** X					***								
parstriangularis	59	XW13	*** X													
parstriangularis	11	BCH3	** X													
parstriangularis	12	BCH3	*** X					***	**							
parstriangularis	13	BCH3	*** X									**				
parstriangularis	14	BCH3	*** X					***	**							
postcentral	35	BCH3	*** X													
postcentral	39	BWH5	** X													
posteriorcingulate	73	BCH5	** X			**										
precentral	32	BWH52	** X			**										
precentral	33	BWH52	*** X													
precentral	16	BWH8	*** X							**						
precentral	50	BWH9	*** X													
precentral	53	BWH9	*** X													
precentral	36	BCH3	*** X										**			
precentral	24	BWH5	**	**	** X											
rostralanteriorcingulate	34	XW12	*** X					***								
rostralmiddlefrontal	24	XW11	*** X	**	***			***								
superiorfrontal	175	BCH4	*** X					**								
superiorfrontal	6	BWH5	**					*** X								
superiorparietal	61	BWH9	*** X					**	**							
superiorparietal	129	BCH5	*** X													
superiorparietal	130	BCH5	*** X													**
supramarginal	37	XW02	** X													
supramarginal	64	BWH9	*** X													
supramarginal	65	BWH9	*** X													

Table B.8: Second-tile GLM results of gray matter electrodes that presented next-match as significant predictors. Columns 4-19 represent each predictor in the GLM. ***: $p < 0.001$, **: $p < 0.01$, empty: $p > 0.01$ (not-significant). X indicates the predictor with the biggest t-statistic. Abbreviations: NSLC, n-since-last-click; NTS, n-times-seen; RT: reaction-time.

Region	Subject	Ch	match	NSLC	first.click	NTS	next_match	RT	board_size	x_pos.	y_pos.	distance	animal	food	person	vehicle
amygdala	XW07	16	**				** X									
fusiform	BCH4	17					**						** X	**		
inferiortemporal	BCH3	73					**	*** X								
lateralorbitofrontal	BWH6	29	*** X				**									
lateralorbitofrontal	BWH6	30	*** X				***									
lateralorbitofrontal	BWH8	22	**	***	***		**						***			*** X
parsopercularis	XW07	82					** X									
parsopercularis	XW07	83					** X	**								
precuneus	XW01	77			**		*** X									
supramarginal	BWH52	29					**								** X	

Table B.9: First-tile GLM results of gray matter electrodes that were selective for one or more image category. Columns 4-19 represent each predictor in the GLM. ***: $p < 0.001$, **: $p < 0.01$, empty: $p > 0.01$ (not-significant). X indicates the predictor with the biggest t-statistic. Abbreviations: NSP, n-since-pair*match; NSLC, n-since-last-click; NTS, n-times-seen; RT: reaction-time.

Region	Subject	Ch	match	NSP	NSLC	first.click	NTS	next_match	RT	board_size	x_pos.	y_pos.	distance	animal	food	person	vehicle
Amygdala	XW04	15															*** X
Amygdala	BWH8	81				**											*** X
Hippocampus	XW01	50													*** X		
Hippocampus	XW01	51													** X		
bankssts	XW04	36	** X												**		
bankssts	BWH9	41			**									**		*** X	
bankssts	BWH9	42			**									**	**	*** X	
caudalmiddlefrontal	BWH6	69														** X	
caudalmiddlefrontal	BWH6	70						**						**		*** X	
fusiform	XW01	42				**				**							*** X
fusiform	XW03	11			**	**			***					*** X			
fusiform	XW07	10	**														** X
fusiform	XW07	11			*** X	**											**
fusiform	XW08	61						**								** X	
fusiform	XW13	37						**				**					** X
fusiform	BWH52	13												** X		**	
fusiform	BCH4	17												*** X	**		
fusiform	BCH4	68												**	** X	**	
inferioparietal	XW03	71			*** X	***		***								**	
inferioparietal	BCH3	151			*** X	***					**					**	
inferiortemporal	XW08	37									*** X				**		
insula	XW15	72												** X			
lateraloccipital	BCH5	4												*** X		**	
lateraloccipital	BCH5	5				***		*** X			**			**		**	
lateralorbitofrontal	XW04	39	** X											**			
lateralorbitofrontal	BWH8	73			**			***								*** X	
lingual	XW01	12												***	*** X	**	
medialorbitofrontal	BWH52	42										**	**			** X	
middletemporal	XW11	37	**				**									*** X	
middletemporal	XW11	38														*** X	
middletemporal	BWH9	24			**			**						*** X			
middletemporal	BCH3	110	*** X	**		**										**	
parahippocampal	XW01	11												***	*** X	***	
parahippocampal	XW07	8			***												*** X
parahippocampal	XW07	9			***							***					*** X
parahippocampal	XW13	21												** X			
parsopercularis	XW11	22			*** X	***		***						**			
parsopercularis	XW11	23			***	*** X		***								***	
parsopercularis	XW15	78			**	*** X		**						**			**
parstriangularis	XW04	46												** X	**		
parstriangularis	BCH3	11				**				**				** X		**	
posteriorcingulate	BCH4	178														** X	
precentral	BCH4	106	*** X	**												**	
rostralmiddlefrontal	XW11	24			***	*** X		***								**	

Table B.10: Second-tile GLM results of gray matter electrodes that were selective for one or more image category. Columns 4-19 represent each predictor in the GLM. ***: $p < 0.001$, **: $p < 0.01$, empty: $p > 0.01$ (not-significant). X indicates the predictor with the biggest t-statistic. Abbreviations: NSLC, n-since-last-click; NTS, n-times-seen; RT: reaction-time.

Region	Subject	Ch	match	NSLC	first_click	NTS	next_match	RT	board_size	x_pos.	y_pos.	distance	animal	food	person	vehicle
Amygdala	XW07	17														** X
Hippocampus	XW02	48														** X
bankssts	BWH9	42	**											** X		
entorhinal	BWH52	3									** X		**			
fusiform	XW03	11		**	**								*** X			
fusiform	XW07	10											*** X			
fusiform	XW07	11						**					*** X		***	
fusiform	XW08	61											**		*** X	
fusiform	XW13	37			**											*** X
fusiform	XW15	17											*** X			
fusiform	BCH4	17					**							** X	**	
fusiform	BCH4	68												** X		
inferioparietal	XW03	71	*** X					***					**		***	
inferioparietal	BCH3	150						**	*** X		**				**	
inferioparietal	BCH3	152											**		** X	
inferiortemporal	XW01	66	**					**							**	** X
lateralorbitofrontal	XW06	51									** X			**	**	** X
lateralorbitofrontal	BWH8	22	**	***	***		**							***		*** X
lateralorbitofrontal	BWH8	73													** X	
lateralorbitofrontal	BCH3	22	*** X										**			
lingual	XW01	12	**		**								**			
medialorbitofrontal	BWH52	42									*** X		**		*** X	
parahippocampal	XW07	8	***										**	***	**	*** X
parahippocampal	XW07	9	**										**			*** X
parahippocampal	XW07	52													*** X	
parsopercularis	XW11	22	***	***	***			*** X	***				***			
parstriangularis	XW04	46														** X
precentral	BCH3	36	*** X										**			
superioparietal	XW03	112						*** X	***	***						**
superioparietal	BCH5	130	*** X													**
supramarginal	XW02	33				**										** X
supramarginal	BWH52	29					**								** X	

Table B.11: Each row indicates the percentage of electrodes in each brain region that are also VS, NAMS and/or AMS. Only brain region with 2 or more significant Vs, NAMS or AMS electrodes were considered. n indicates the total number of electrodes in each population.

Brain Region	n	% VS	% NAMS	% AMS
amygdala	45	4.44	4.44	0
hippocampus	66	3.03	1.52	3.03
bankssts	7	42.86	42.86	14.29
fusiform	25	36	24	4
inferioparietal	19	10.52	21	0
inferiortemporal	23	4.35	13.04	13.04
insula	28	3.57	17.85	14.28
lateralorbitofrontal	51	3.92	25.49	17.65
medialorbitofrontal	11	9.09	18.18	9.09
middletemporal	91	4.39	7.69	6.59
parahippocampal	23	17.39	17.3	4.35
parsopercularis	16	18.75	31.25	18.75
parstriangularis	32	6.25	12.5	0
precentral	20	5	15	5

Table B.12: Proportion VS, AMS and NAMS electrodes showing gamma and slower frequency interactions after the 1st tile Proportion of VS, AMS and NAMS and 2nd tile match-significant that show a positive or negative time-wise correlation between the gamma and beta band power, and gamma and alpha band power, after the 2nd tile. n indicates the total number of electrode in each population.

	Gamma - Beta		Gamma Alpha	
	Anti-corr. (-)	Positive corr. (+)	Anti-corr. (-)	Positive corr. (+)
VS 1st tile (n = 44)	6.82% (3)	77.27% (34)	15.91% (7)	15.91% (7)
NAMS 1st tile (n = 75)	2.67% (2)	74.77% (56)	13.33% (10)	6.67% (5)
AMS 1st tile (n = 36)	0% (0)	91.67% (33)	8.33% (3)	11.11% (4)
Match-selective 2nd tile (n = 112)	1.79% (2)	76.79% (86)	14.29% (16)	6.25% (7)

Table B.13: Proportion of electrodes in each brain region showing gamma and slower frequency interactions after the 1st tile Proportion of brain regions containing two or more VS, AMS and NAMS electrodes that show a positive or negative time-wise correlation between the gamma and beta band power, and gamma and alpha band power, after the 1st tile. n indicates the total number of electrode in each brain region.

Brain region	# chs.	Gamma - Beta		Gamma Alpha	
		Anti-corr. (-)	Positive corr. (+)	Anti-corr. (-)	Positive corr. (+)
amygdala	3	0	100%	0	66.67%
hippocampus	5	0	100%	0	60%
bankssts	4	0	50%	0	0
fusiform	12	0	83.33%	0	0
inferiorparietal	4	0	0	25%	0
inferiortemporal	5	40%	40%	20%	0
insula	7	0	85.71%	0	0
lateralorbitofrontal	19	0	73.68%	10.53%	0
medialorbitofrontal	4	0	50	50	0
middletemporal	12	0	41.67%	8.33%	0
parahippocampal	7	0	100%	14.29%	14.29%
parsopercularis	8	12.5%	62.5%	12.5%	0
parstriangularis	5	0	60%	40%	0
precentral	4	0	75%	0	25%

Table B.14: Proportion of electrodes in each brain region showing gamma and slower frequency interactions after the 2nd tile Proportion of brain regions containing two or 2nd tile more match-significant electrodes that show a positive or negative time-wise correlation between the gamma and beta band power, and gamma and alpha band power, after the 2nd tile. n indicates the total number of electrode in each brain region.

Brain region	# chs.	Gamma - Beta		Gamma Alpha	
		Anti-corr. (-)	Positive corr. (+)	Anti-corr. (-)	Positive corr. (+)
Amygdala	3	0	100%	0	33.33%
Hippocampus	6	0	83.33%	0	0
bankssts	3	0	33.33%	0	0
inferiorparietal	4	0	25%	50%	0
inferiortemporal	5	20%	60%	20%	0
insula	12	0	100%	0	0
lateralorbitofrontal	21	0	95.23%	9.52%	4.76%
medialorbitofrontal	3	0	66.67%	100%	0
middletemporal	14	0	64.29%	7.14%	0
parsopercularis	6	16.67%	66.67%	16.67%	0
parstriangularis	8	0	50%	37.5%	0
precentral	6	0	100%	0	0
superiorparietal	3	0	66.67%	0	0
supramarginal	3	0	0	100%	0

C Gray matter figures

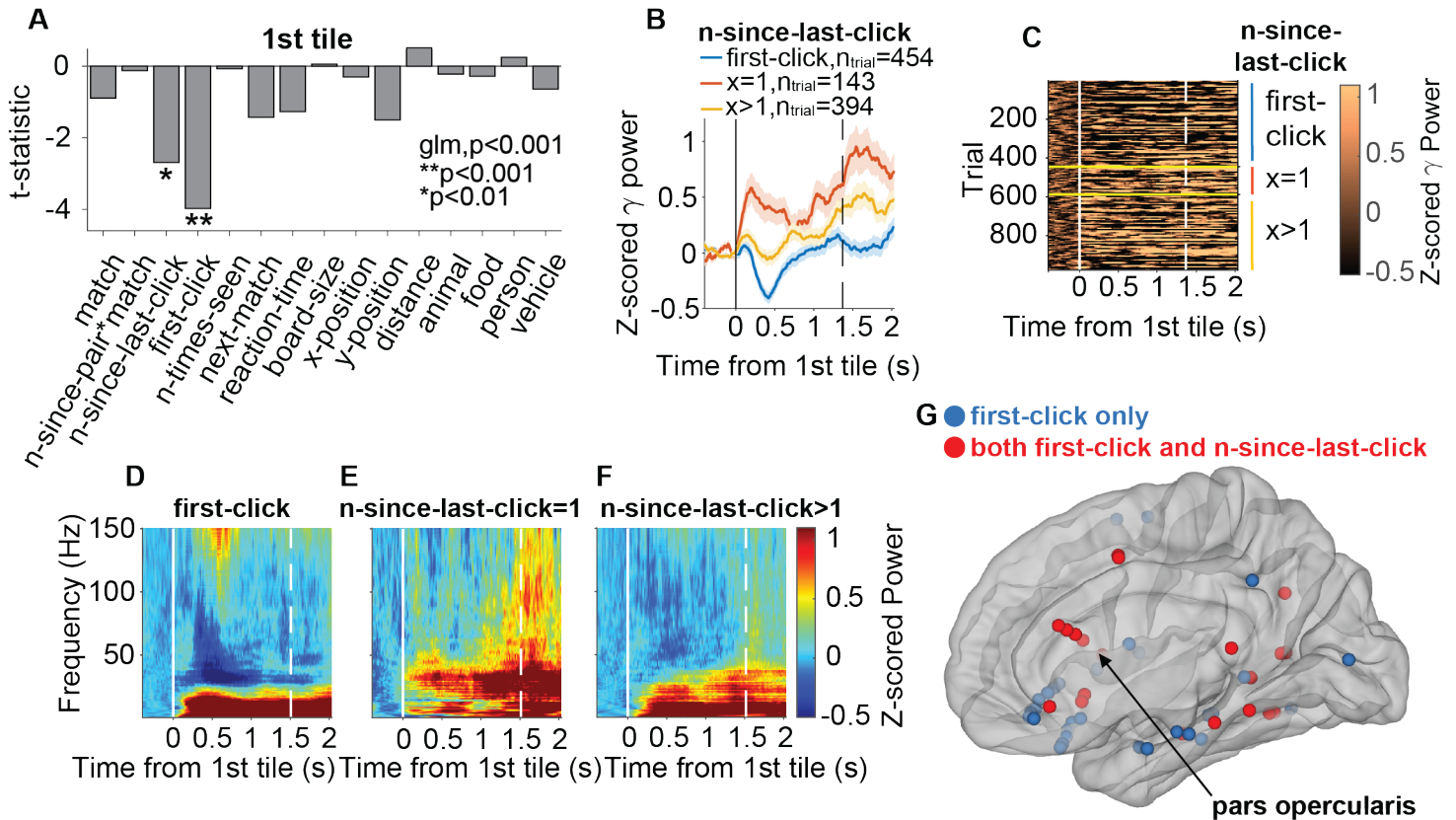


Figure C.1: An example of a pars opercularis electrode where gamma activities decreased for *first-click* and larger *n-since-last-click* tiles. **A.** T-statistic of each predictor in the GLM. Asterisks indicate significant predictors for the gamma power AUC. **B.** Z-scored gamma power aligned to the 1st tile onset for *first-click* (blue line), clicked in the previous tile (red line) or clicked more than one tile ago (yellow line) tiles. Shaded error bars indicate SEM. Dashed line indicates the mean RT. **C:** Raster plots showing the z-scored gamma power in individual trials ordered by *first-click* and then from smaller to larger *n-since-last-click*; division indicated by yellow horizontal lines and colored vertical lines. **D-F.** Spectrograms showing the power aligned to the 1st tile onset during *first-click* (**D**), *n-since-last-click*=1 (**E**), and *n-since-last-click*>1 (**F**). **G.** Locations of all *first-click* electrodes during the 1st tile. Blue: *first-click* only; red: both *first-click* and *n-since-last-click*.

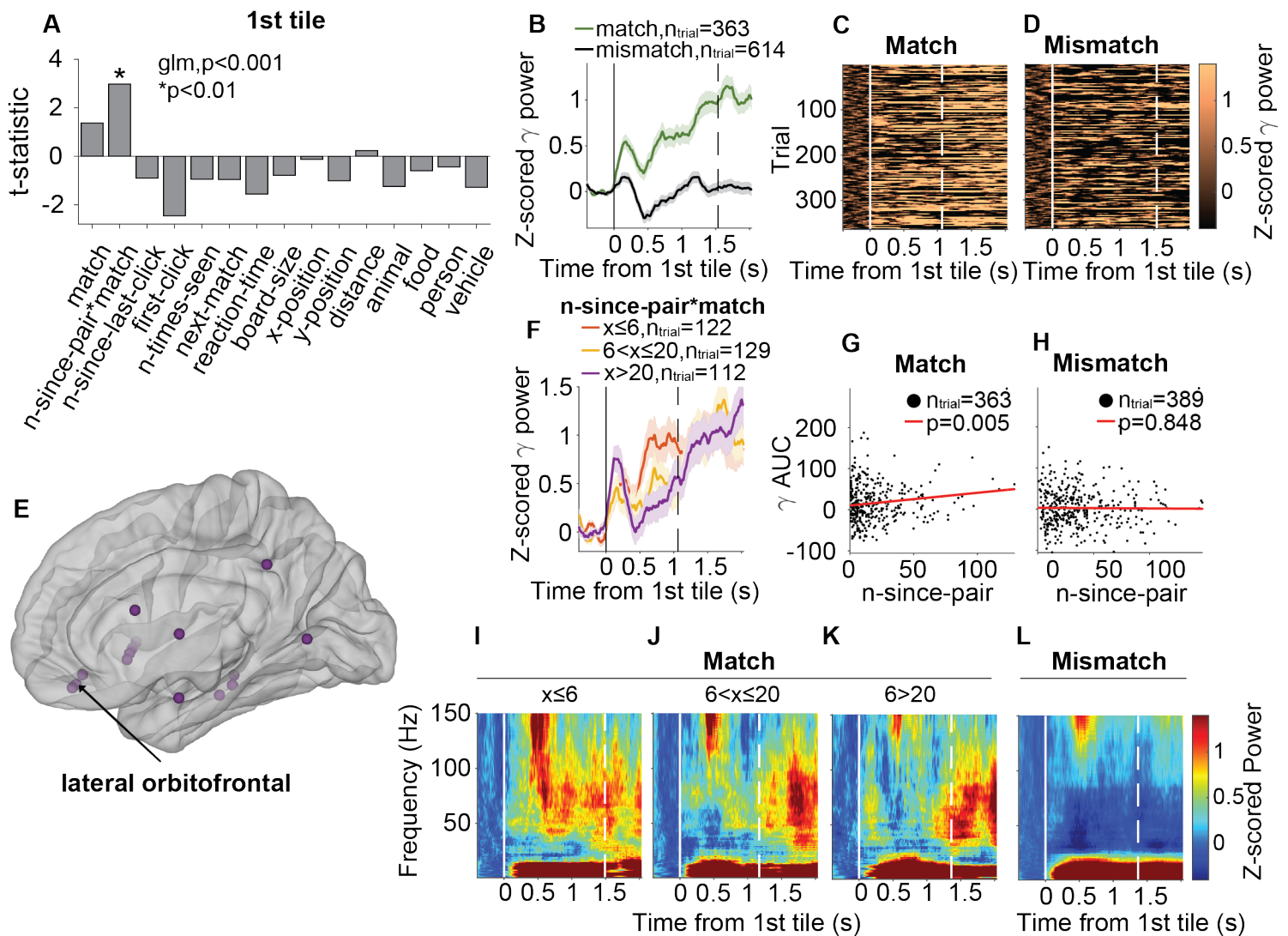


Figure C.2: An example electrode located in the lateral orbitofrontal cortex where *match* and *n-since-pair*match* were significant predictors. **A.** T-statistic of each predictor in the GLM for the 1st tile. Asterisks indicate significant predictors for the gamma power AUC. **B.** Z-scored gamma power during match (green) and mismatch (black) trials aligned to the 1st tile onset (solid line). **C-D.** Raster plots showing the z-scored gamma power in individual trials. For display purpose, trial number of match and mismatch was equalized (Methods). **F.** Z-scored gamma power grouped by different n-since-pair ranges for match trials aligned to the 1st tile onset (solid line). Dashed line indicate the mean reaction time. Shaded error bars indicate SEM. **G-H.** Scatter plots of AUC gamma power vs. n-since-pair for match (**G**) and mismatch (**H**). Each dot represents data from one trial. Red lines represent linear fits of the data. **I-K.** Spectrograms showing the band power aligned to the 1st tile for different n-since-pair ($x=n\text{-since-pair}$) values for match trials. **L.** Spectrogram showing the band power aligned to the 1st tile for mismatch trials. **E.** Locations of all n-since-pair*match electrodes plotted on one hemisphere.

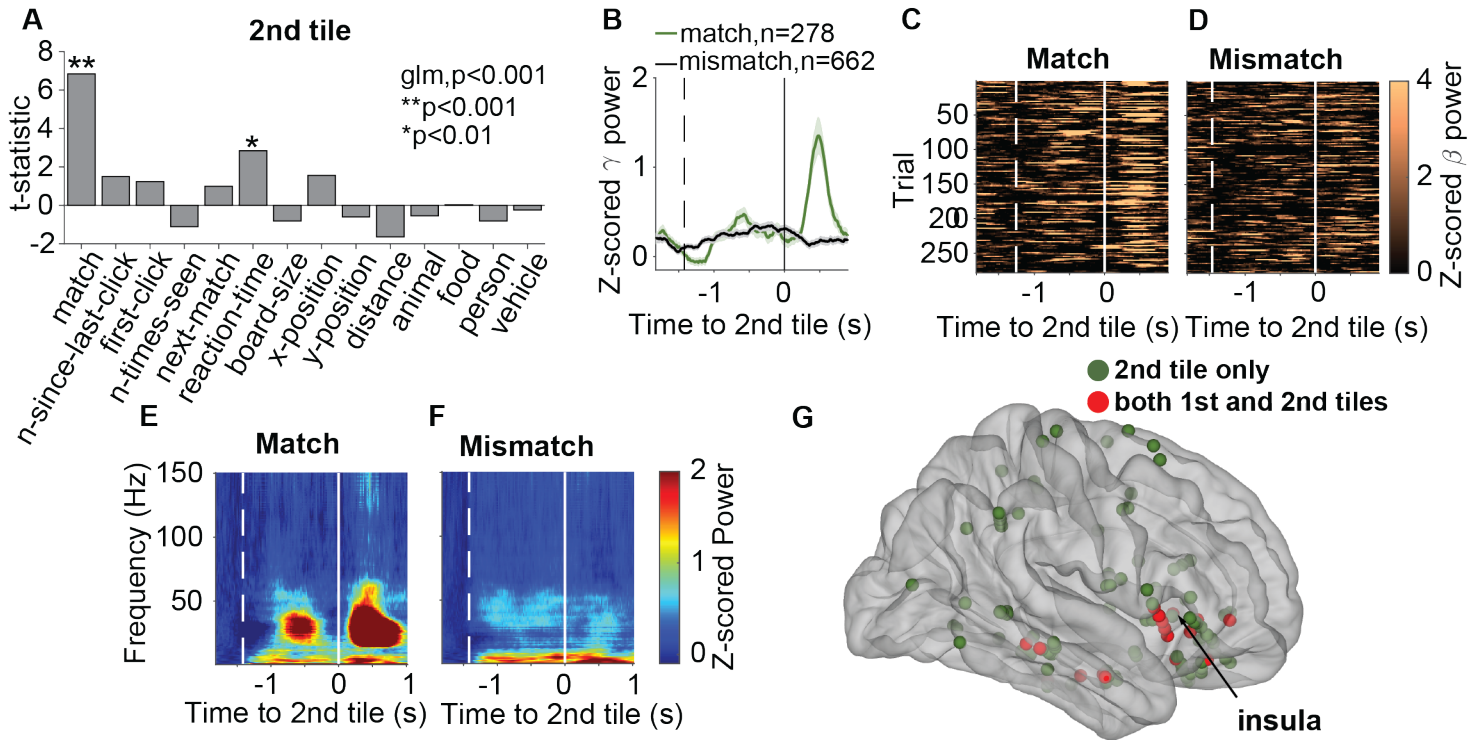


Figure C.3: An example electrode in the insula where *match* was a significant predictor for gamma activities after the 2nd tile. **A.** T-statistic of each predictor in the GLM for the 2nd tile. **B.** Z-scored gamma power during matched and mismatched trials aligned to the 2nd tile onset (solid line). Dashed line indicates the mean onset of the 1st tile. **C-D.** Raster plots showing the z-scored gamma power in individual trials. Number of match and mismatch trials was equalized (Methods). **E-F.** Spectrograms showing the band power during matched and mismatched trials aligned to the 2nd tile onset. **G.** Location of all electrodes where "match" is a significant predictor during the 2nd tile only (green) or during both tiles (red).

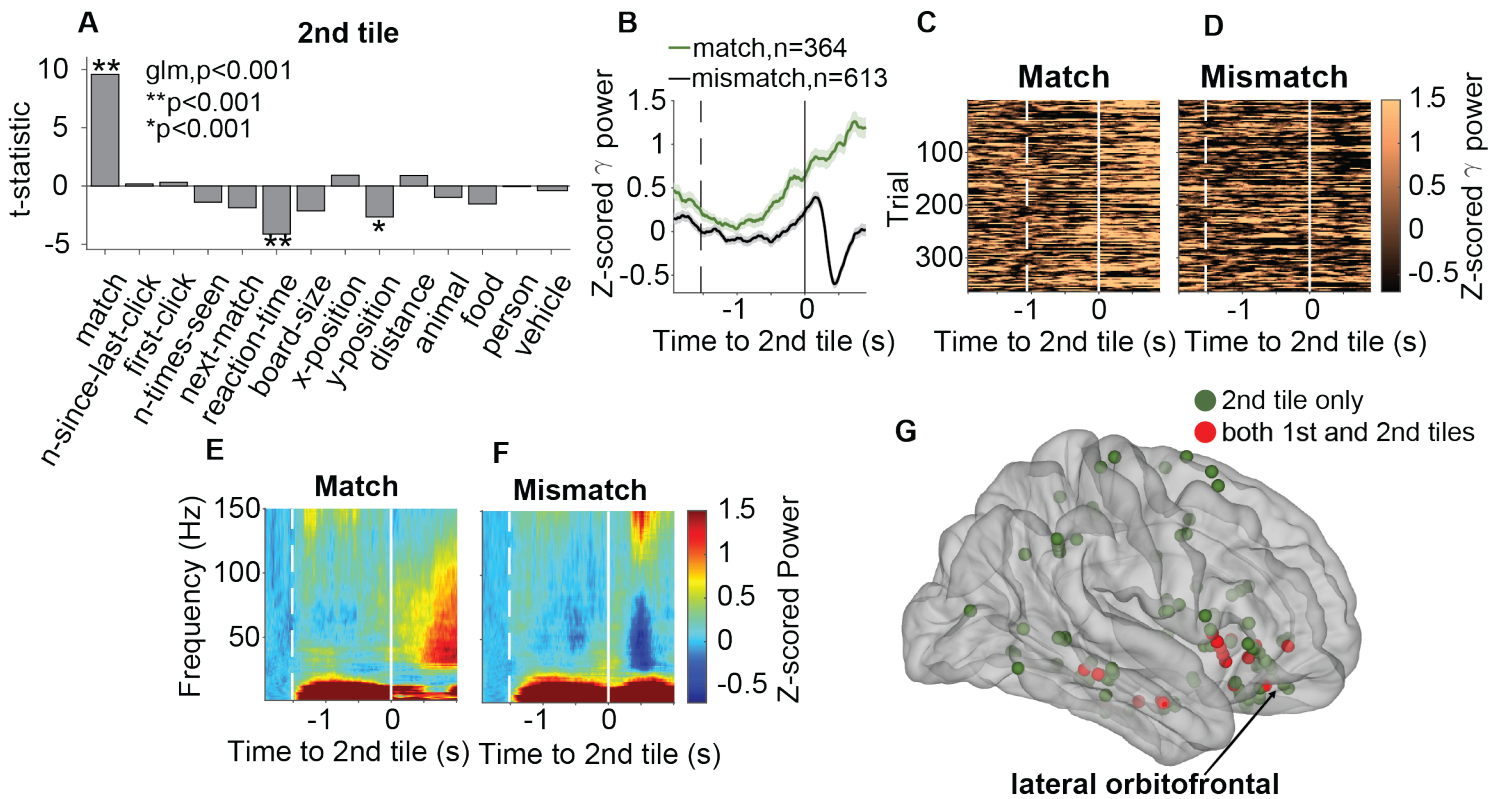


Figure C.4: An example electrode in the LOF cortex where *match* was a significant predictor for gamma activities after the 2nd tile. **A.** T-statistic of each predictor in the GLM for the 2nd tile. **B.** Z-scored gamma power during matched and mismatched trials aligned to the 2nd tile onset (solid line). Dashed line indicates the mean onset of the 1st tile. **C-D.** Raster plots showing the z-scored gamma power in individual trials. Number of match and mismatch trials was equalized (Methods). **E-F.** Spectrograms showing the band power during matched and mismatched trials aligned to the 2nd tile onset. **G.** Location of all electrodes where "match" is a significant predictor during the 2nd tile only (green) or during both tiles (red).

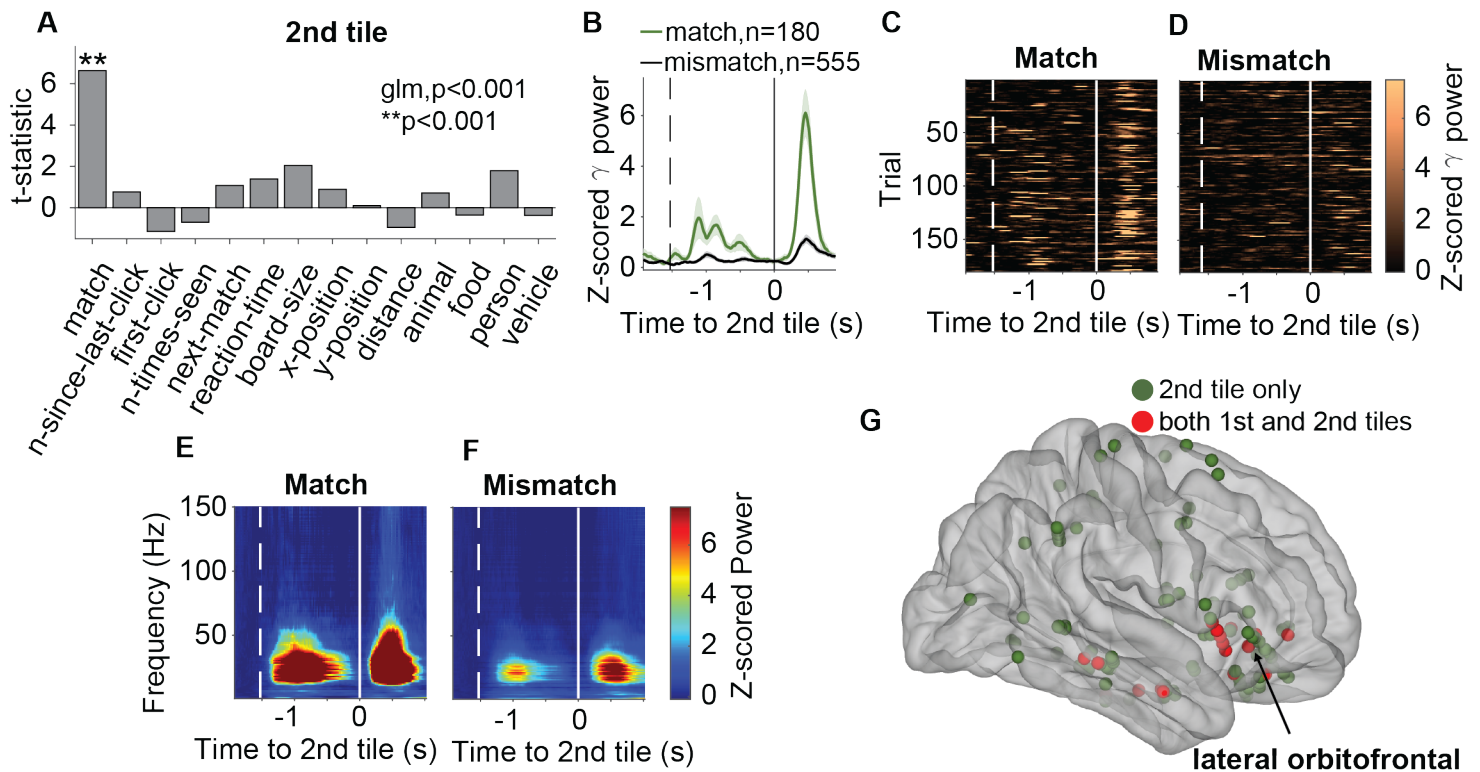


Figure C.5: An example electrode in the lateral orbitofrontal cortex where *match* was a significant predictor for gamma activities for both the 1st the 2nd tiles. See Figure 3.8 for the 1st tile. **A.** T-statistic of each predictor in the GLM for the 2nd tile. **B.** Z-scored gamma power during matched and mismatched trials aligned to the 2nd tile onset (solid line). Dashed line indicates the mean onset of the 1st tile. **C-D.** Raster plots showing the z-scored gamma power in individual trials. Number of match and mismatch trials was equalized (Methods). **E-F.** Spectrograms showing the band power during matched and mismatched trials aligned to the 2nd tile onset. **G.** Location of all electrodes where "match" is a significant predictor during the 2nd tile only (green) or during both tiles (red).

D White matter tables

Table D.1: Number of white matter electrodes that presented each predictor as significant for the 1st tile GLM. Abbreviations: NSP, n-since-pair*match; NSLC, n-since-last-click; NTS, n-times-seen; RT: reaction-time.

Region	# Ch	match	NSP	NSLC	first_click	NTS	next_match	RT	board-size	x-pos.	y-pos.	distance	animal	food	person	vehicle
bankssts	7	0	0	0	0	0	0	0	0	0	0	0	0	0	1	0
caudalanteriorcingulate	1	1	0	1	1	0	0	1	0	0	0	0	0	0	0	0
caudalmiddlefrontal	8	0	0	0	0	0	0	0	1	0	0	0	0	0	0	0
cuneus	2	0	0	0	0	0	0	0	0	0	0	0	0	0	0	0
entorhinal	4	1	0	0	0	0	0	0	0	0	0	0	0	0	0	0
fusiform	35	1	0	9	7	1	0	3	9	3	0	1	5	2	8	1
inferioparietal	10	0	0	0	0	0	0	0	0	0	0	0	0	0	1	0
inferiortemporal	47	3	0	3	6	3	2	3	2	1	0	0	2	2	5	2
insula	23	0	0	0	0	0	0	0	0	1	0	1	0	0	0	0
isthmuscingulate	1	0	0	0	0	0	0	0	0	0	0	0	0	0	0	0
lateraloccipital	5	0	0	0	0	0	0	0	0	2	0	0	2	0	1	0
lateralorbitofrontal	53	6	3	8	6	2	0	4	1	1	0	1	0	1	1	2
lingual	4	1	0	0	0	0	0	0	0	1	1	0	1	0	1	0
medialorbitofrontal	14	1	0	0	0	0	1	0	0	0	0	0	0	0	0	0
middletemporal	52	2	1	1	0	0	0	2	4	0	2	1	0	0	1	0
paracentral	6	0	0	0	0	0	0	1	1	0	0	0	0	0	0	0
parahippocampal	11	1	0	1	1	0	0	1	0	0	0	0	1	1	1	1
parsopercularis	8	1	1	0	1	0	1	0	0	0	0	0	0	0	0	0
parsorbitalis	11	1	0	1	0	0	0	0	0	0	0	0	0	0	0	0
parstriangularis	20	3	2	1	1	0	0	1	0	0	0	1	0	0	1	0
pericalcarine	4	0	0	0	0	0	0	0	0	2	0	1	0	0	0	1
postcentral	6	0	0	0	0	0	0	0	0	0	0	0	0	0	0	0
posteriorcingulate	11	0	0	0	0	0	0	2	0	0	0	1	0	0	0	0
precentral	26	5	1	1	0	0	0	0	0	0	0	0	0	0	0	0
precuneus	15	0	0	0	0	0	0	0	0	0	0	0	0	0	0	0
rostralanteriorcingulate	6	0	0	0	0	0	0	0	0	0	0	0	0	0	0	0
rostralmiddlefrontal	9	0	0	1	2	0	0	0	0	0	0	0	0	0	0	0
superiorfrontal	28	0	0	0	1	0	0	1	0	0	0	1	0	0	0	0
superioparietal	17	1	0	4	5	0	0	3	1	2	0	0	0	0	0	0
superiortemporal	34	1	0	1	2	0	1	0	0	2	0	1	0	0	0	1
supramarginal	8	1	1	0	0	0	0	1	0	0	0	0	0	0	0	0
transversetemporal	6	0	0	0	0	0	0	0	0	0	0	0	0	0	0	0
Total	492	30	9	32	33	6	5	23	19	15	3	9	11	6	21	8

Table D.2: Number of white matter electrodes that presented each predictor as significant for the 2nd tile GLM. Abbreviations: NSLC, n-since-last-click; NTS, n-times-seen; RT: reaction-time.

Region	Ch	match	NSLC	first_click	NTS	next_match	RT	board_size	x_pos.	y_pos.	distance	animal	food	person	vehicle
bankssts	7	0	0	0	0	0	1	0	0	0	0	0	0	0	0
caudalanteriorcingulate	1	1	1	1	0	0	1	0	0	0	0	0	0	0	0
caudalmiddlefrontal	8	0	1	0	0	1	0	0	1	0	0	0	0	0	0
cuneus	2	0	0	0	0	0	0	0	0	0	0	0	0	0	0
entorhinal	4	0	0	0	0	0	0	0	0	0	0	0	0	0	0
fusiform	35	8	7	1	0	0	6	2	4	0	0	4	1	6	1
inferioparietal	10	1	0	1	0	0	0	0	0	0	0	0	0	1	0
inferiortemporal	47	10	0	0	0	4	4	1	1	0	1	1	2	1	0
insula	23	1	0	0	0	0	2	0	0	0	0	0	0	0	0
isthmuscingulate	1	0	0	0	0	0	0	0	0	0	0	0	0	0	0
lateraloccipital	5	0	0	0	0	0	0	0	1	1	0	2	0	1	0
lateralorbitofrontal	53	11	5	3	2	1	2	1	0	1	2	1	0	2	1
lingual	4	1	0	0	0	0	0	0	0	0	0	1	1	1	0
medialorbitofrontal	14	1	0	0	0	0	0	0	0	0	0	0	0	0	0
middletemporal	52	4	3	0	0	1	3	1	0	1	0	1	2	2	0
paracentral	6	1	0	0	0	0	1	1	0	0	0	0	0	0	0
parahippocampal	11	2	1	0	0	0	0	0	0	0	0	1	1	1	0
parsopercularis	8	4	0	0	0	0	3	1	1	0	1	0	0	0	0
parsorbitalis	11	1	2	0	0	0	1	0	0	0	1	0	0	0	1
parstriangularis	20	4	3	2	1	2	0	0	0	1	1	0	0	0	1
pericalcarine	4	1	0	0	0	0	0	0	0	0	0	0	0	0	0
postcentral	6	0	0	0	0	0	0	0	0	0	0	0	0	0	0
posterioingulate	11	0	0	1	0	0	1	0	0	0	0	0	0	0	0
precentral	26	3	0	3	0	4	1	0	0	0	1	1	1	1	0
precuneus	15	0	0	0	0	0	0	0	0	0	0	0	0	0	0
rostralanteriorcingulate	6	0	0	0	0	0	0	0	0	0	0	0	0	0	0
rostralmiddlefrontal	9	2	0	0	0	0	0	0	0	0	0	0	0	0	0
superiorfrontal	28	3	0	0	0	0	1	0	0	0	2	0	0	0	0
superioparietal	17	4	1	0	0	1	1	1	0	0	0	1	0	1	0
superiortemporal	34	1	0	0	0	0	0	0	1	0	0	0	0	0	0
supramarginal	8	1	0	0	0	1	1	0	0	0	0	0	0	0	0
transversetemporal	6	1	0	0	0	0	1	0	0	0	0	0	0	0	0
Total	492	66	24	12	3	15	30	8	9	4	9	13	8	17	4

Table D.3: First-tile GLM results of white matter electrodes that presented n-since-last-click and/or first-click as significant predictors. Columns 4-19 represent each predictor in the GLM. ***: $p < 0.001$, **: $p < 0.01$, empty: $p > 0.01$ (not-significant). X indicates the predictor with the biggest t-statistic. Abbreviations: NSP, n-since-pair*match; NSLC, n-since-last-click; NTS, n-times-seen; RT: reaction-time.

Region	Subject	Ch	match	NSP	NSLC	first.click	NTS	next.match	RT	board-size	x-pos.	y-pos.	distance	animal	food	person	vehicle
caudalanteriorcingulate	XW11	21	***		*** X	***			***								
fusiform	XW03	28			*** X	***			***				**			***	
fusiform	BCH3	138			***	*** X				***	***					**	
fusiform	BCH3	139			***	*** X				**	**						
fusiform	BCH3	140			***	*** X			***	***	**						
fusiform	BCH3	141			***	*** X				**							
fusiform	BCH3	142	**		***	*** X				**							
inferiortemporal	XW08	39			***	**			*** X		**						
lateralorbitofrontal	BWH8	21			*** X	***			**								
lateralorbitofrontal	BWH8	23			*** X	**											
rostralmiddlefrontal	BWH8	3			*** X	***											
superiorparietal	XW03	23			*** X	***			**								
superiorparietal	XW03	70			*** X	***											
superiorparietal	XW03	72			*** X	***			**								
superiorparietal	XW03	73			*** X	***			***		**						
superiortemporal	XW02	43			***	*** X											***
fusiform	BCH3	106				** X											
inferiortemporal	XW01	43				**											*** X
inferiortemporal	XW01	69				** X		**									
inferiortemporal	XW01	82				*** X		**									
inferiortemporal	XW07	58				*** X	***										
inferiortemporal	BCH3	107				*** X											
lateralorbitofrontal	BCH3	4				*** X											
lateralorbitofrontal	BCH3	10				*** X											
lateralorbitofrontal	BCH3	23				*** X											
lateralorbitofrontal	BCH3	24				*** X											
parahippocampal	XW01	10				**			**					*** X	***	***	**
parsopercularis	BCH3	31				*** X	**										
parstriangularis	BWH9	8				*** X							**				
rostralmiddlefrontal	XW03	80				*** X											
superiorfrontal	BWH8	10				**			*** X								
superiorparietal	XW03	20	**			**				** X							
superiortemporal	XW02	40				** X											
fusiform	XW03	12			***				***					*** X		***	
fusiform	XW07	12			**					**				*** X	**	***	
fusiform	XW07	53			*** X											***	***
inferiortemporal	XW08	40			**										***	*** X	
inferiortemporal	XW08	41			**				***					*** X	***	***	
lateralorbitofrontal	XW07	66			** X												
lateralorbitofrontal	XW07	67			***				*** X								
lateralorbitofrontal	XW07	68			**												*** X
lateralorbitofrontal	BWH6	31			** X				**								
lateralorbitofrontal	BWH8	74	**		***									**		*** X	
lateralorbitofrontal	BWH8	75			** X												
middletemporal	XW06	66			** X												
parahippocampal	XW07	50	**		*** X												
parsorbitalis	BWH8	76	*** X		**												
parstriangularis	XW04	49	*** X		**				**								
precentral	XW04	59	** X		**												

Table D.4: First-tile GLM results of white matter electrodes that presented match and/or n-since-pair*match as significant predictors. Columns 4-19 represent each predictor in the GLM. ***: $p < 0.001$, **: $p < 0.01$, empty: $p > 0.01$ (not-significant). X indicates the predictor with the biggest t-statistic. Abbreviations: NSP, n-since-pair*match; NSLC, n-since-last-click; NTS, n-times-seen; RT: reaction-time.

Region	Subject	Ch	match	NSP	NSLC	first.click	NTS	next.match	RT	board-size	x-pos.	y-pos.	distance	animal	food	person	vehicle
lateralorbitofrontal	55	XW13	*** X	***			**										
lateralorbitofrontal	36	BWH7	*** X	**			**										**
parsopercularis	81	XW07	*** X	***													
parstriangularis	82	XW08	*** X	**													
parstriangularis	84	XW08	*** X	***													
precentral	57	XW04	*** X	**													
supramarginal	31	XW02	*** X	***					**								
caudalanteriorcingulate	21	XW11	***		*** X	***			***								
entorhinal	19	XW13	*** X														
fusiform	142	BCH3	**		***	*** X				**							
inferiortemporal	57	XW07	*** X														
inferiortemporal	19	XW08	** X														
inferiortemporal	63	XW08	** X														
lateralorbitofrontal	41	XW04	*** X														
lateralorbitofrontal	44	XW04	** X														
lateralorbitofrontal	34	BWH7	*** X														
lateralorbitofrontal	74	BWH8	**		***									**	*** X	*** X	
lingual	60	XW15	**								***	**		***			
medialorbitofrontal	63	XW15	*** X					**									
middletemporal	24	XW12	*** X														
middletemporal	44	BWH6	**						**			**	*** X				
parahippocampal	50	XW07	**		*** X												
parsorbitalis	76	BWH8	*** X	**													
parstriangularis	49	XW04	*** X	**					**								
precentral	55	XW04	*** X														
precentral	56	XW04	*** X														
precentral	58	XW04	*** X														
precentral	59	XW04	** X	**													
superioparietal	20	XW03	**			**				** X							
superiortemporal	19	XW07	**				**	**			** X		**				
lateralorbitofrontal	6	BWH7	*** X							** X			**				
middletemporal	60	BCH3	**							** X		**					

Table D.5: Second-tile GLM results of white matter electrodes that presented n-since-last-click and/or first-click as significant predictors. Columns 4-19 represent each predictor in the GLM. ***: $p < 0.001$, **: $p < 0.01$, empty: $p > 0.01$ (not-significant). X indicates the predictor with the biggest t-statistic. Abbreviations: NSLC, n-since-last-click; NTS, n-times-seen; RT: reaction-time.

Region	Subject	Ch	match	NSLC	first_click	NTS	next_match	RT	board_size	x_pos.	y_pos.	distance	animal	food	person	vehicle
caudalanteriorcingulate	XW11	21	***	***	**			*** X								
fusiform	BCH3	138	*** X	***	**				***	**					**	
lateralorbitofrontal	XW07	68		**	*** X	**										
lateralorbitofrontal	BWH8	23		**	***											*** X
lateralorbitofrontal	BCH3	24	***	**	*** X	**										
inferiorparietal	BCH5	15			*** X											
parstriangularis	BWH9	7			*** X											
parstriangularis	BWH9	9			*** X											
posteriorcingulate	BCH5	123			*** X			**								
precentral	XW04	54			** X											
precentral	XW04	57			**		** X									
precentral	XW04	58			**		*** X									
caudalmiddlefrontal	XW03	90		*** X		**										
fusiform	XW03	28		***				**							*** X	
fusiform	XW07	12	***	***									*** X	**	**	
fusiform	XW07	53		**				***							*** X	**
fusiform	BCH3	139	*** X	***				**		**						
fusiform	BCH3	140	*** X	**				***		***						
fusiform	BCH3	141	*** X	***				***		**						
lateralorbitofrontal	BWH8	21	*** X	**												
lateralorbitofrontal	BWH8	74		**				*** X							**	
middletemporal	XW08	10		** X												
middletemporal	XW08	66		**									** X	**		
middletemporal	XW08	67	** X	**							**					
parahippocampal	XW07	50	**	*** X												
parorbitalis	XW07	71		** X												
parorbitalis	BWH8	76		**				**								*** X
parstriangularis	XW02	28		** X												
parstriangularis	XW02	29		**												** X
parstriangularis	XW08	83	*** X	**		**										
superiorparietal	XW03	72	*** X	**					**						**	

Table D.6: Second-tile GLM results of white matter electrodes that presented match as significant predictors. Columns 4-19 represent each predictor in the GLM. ***: p<0.001, **:p<0.01, empty:p>0.01 (not-significant). X indicates the predictor with the biggest t-statistic. Abbreviations: NSLC, n-since-last-click; NTS, n-times-seen; RT: reaction-time.

Region	Subject	Ch	match	NSLC	first.click	NTS	next.match	RT	board_size	x_pos.	y_pos.	distance	animal	food	person	vehicle
caudalanteriorcingulate	XW11	21	***	***	**			*** X								
fusiform	XW07	12	***	***									*** X	**	**	
fusiform	XW08	5	*** X													
fusiform	XW08	6	** X													
fusiform	BCH3	106	*** X													
fusiform	BCH3	138	*** X	***	**				***	**					**	
fusiform	BCH3	139	*** X	***				**		**						
fusiform	BCH3	140	*** X	**				***		***						
fusiform	BCH3	141	*** X	***				***		**						
inferioparietal	XW03	59	*** X													
inferiortemporal	XW01	69	*** X				**					**				
inferiortemporal	XW01	81	*** X													
inferiortemporal	XW07	42	*** X				**	***								
inferiortemporal	XW07	57	*** X													
inferiortemporal	XW07	58	*** X													
inferiortemporal	XW07	59	** X													
inferiortemporal	XW07	60	**					** X								
inferiortemporal	XW08	39	*** X					***								
inferiortemporal	BCH3	107	*** X													
inferiortemporal	BCH3	147	** X						**							
insula	XW03	49	*** X													
lateralorbitofrontal	XW04	40	*** X													
lateralorbitofrontal	XW04	41	*** X													
lateralorbitofrontal	XW04	44	*** X													
lateralorbitofrontal	XW07	64	*** X								**					
lateralorbitofrontal	XW07	66	*** X													
lateralorbitofrontal	XW07	67	*** X													
lateralorbitofrontal	XW13	55	*** X				***									
lateralorbitofrontal	BWH6	32	**					*** X				**				
lateralorbitofrontal	BWH8	21	*** X	**												
lateralorbitofrontal	BCH3	23	*** X													
lateralorbitofrontal	BCH3	24	***	**	*** X	**										
lingual	XW15	60	**										*** X	***	***	
medialorbitofrontal	XW15	63	*** X													
middletemporal	XW06	9	** X													
middletemporal	XW08	65	**					**					**	** X		
middletemporal	XW08	67	** X	**							**					
middletemporal	BWH6	44	*** X													
paracentral	XW03	106	**					**	*** X							
parahippocampal	XW01	10	***										*** X	***	***	
parahippocampal	XW07	50	**	*** X												
parsopectularis	XW07	79	*** X									**				
parsopectularis	XW07	80	*** X					**		**						
parsopectularis	XW07	81	*** X					**								
parsopectularis	BWH6	67	*** X													
parsopectularis	XW06	54	*** X													
parstriangularis	XW04	49	** X													
parstriangularis	XW08	82	*** X				**				**					
parstriangularis	XW08	83	*** X	**			**									
parstriangularis	XW08	84	*** X									**				
pericalcarine	BCH5	1	** X													
precentral	XW03	54	** X				**									
precentral	XW03	55	*** X				**						**	***		
precentral	XW04	55	*** X					**								
rostralmiddlefrontal	XW03	80	** X													
rostralmiddlefrontal	BWH8	3	*** X													
superiorfrontal	BCH4	173	*** X													
superiorfrontal	BCH4	174	*** X													
superiorfrontal	BCH4	183	*** X													
superioparietal	XW03	21	**					*** X								
superioparietal	XW03	70	** X				**									
superioparietal	XW03	72	*** X	**					**						**	
superioparietal	XW03	73	** X													
superiortemporal	XW02	43	** X													
supramarginal	XW02	31	*** X				**	***								
transversetemporal	XW11	10	*** X					**								

Table D.7: Second-tile GLM results of white matter electrodes that presented next-match as significant predictors. Columns 4-19 represent each predictor in the GLM. ***: $p < 0.001$, **: $p < 0.01$, empty: $p > 0.01$ (not-significant). X indicates the predictor with the biggest t-statistic. Abbreviations: NSLC, n-since-last-click; NTS, n-times-seen; RT: reaction-time.

Region	Subject	Ch	match	NSLC	first_click	NTS	next_match	RT	board_size	x_pos.	y_pos.	distance	animal	food	person	vehicle
caudalmiddlefrontal	XW03	90		*** X			**									
inferiortemporal	XW01	69	*** X				**					**				
inferiortemporal	XW01	82					** X									
inferiortemporal	XW07	42	*** X				**	***								
inferiortemporal	XW08	40					** X									
lateralorbitofrontal	XW13	55	*** X				***									
middletemporal	XW08	34					***	*** X								
parstriangularis	XW08	82	*** X				**				**					
parstriangularis	XW08	83	*** X	**			**									
precentral	XW03	54	** X				**									
precentral	XW03	55	*** X				**						**	***		
precentral	XW04	57			**		** X									
precentral	XW04	58			**		*** X									
superiorparietal	XW03	70	** X				**									
supramarginal	XW02	31	*** X				**	***								

Table D.8: First-tile GLM results of white matter electrodes that were selective for one or more image category. Columns 4-19 represent each predictor in the GLM. ***: $p < 0.001$, **: $p < 0.01$, empty: $p > 0.01$ (not-significant). X indicates the predictor with the biggest t-statistic. Abbreviations: NSP, n-since-pair*match; NSLC, n-since-last-click; NTS, n-times-seen; RT: reaction-time.

Region	Subject	Ch	match	NSP	NSLC	first_click	NTS	next_match	RT	board_size	x_pos.	y_pos.	distance	animal	food	person	vehicle
bankssts	37	XW04														** X	
fusiform	12	XW03			***				***							***	
fusiform	28	XW03			*** X	***			***				**	*** X		***	
fusiform	12	XW07			**					**				*** X	**	***	
fusiform	53	XW07			*** X											***	***
fusiform	5	XW08					**			**				** X			
fusiform	30	XW08								** X					**		
fusiform	62	XW08												***		*** X	
fusiform	14	BWH52												*** X		***	
fusiform	52	BWH7														** X	
fusiform	138	BCH3			***	*** X				***	***					**	
inferioparietal	14	BCH5														** X	
inferiortemporal	43	XW01				**											*** X
inferiortemporal	55	XW01								**						*** X	
inferiortemporal	55	XW07					**			**						** X	
inferiortemporal	40	XW08			**										***	*** X	
inferiortemporal	41	XW08			**				***					*** X	***	***	
inferiortemporal	42	XW08												***		*** X	**
lateraloccipital	36	XW11									**			**		*** X	
lateraloccipital	3	BCH5									*** X			**			
lateralorbitofrontal	68	XW07			**												*** X
lateralorbitofrontal	36	BWH7	*** X	**			**										**
lateralorbitofrontal	74	BWH8	**		***										**	*** X	
lingual	60	XW15	**								***	**		***		*** X	
middletemporal	39	XW11														*** X	
parahippocampal	10	XW01				**			**					*** X	***	***	**
parstriangularis	47	XW04														*** X	
pericalcarine	1	BCH5									**		**				** X
superiortemporal	43	XW02			***	*** X											***

Table D.9: Second-tile GLM results of white matter electrodes that were selective for one or more image category. Columns 4-19 represent each predictor in the GLM. ***: $p < 0.001$, **: $p < 0.01$, empty: $p > 0.01$ (not-significant). X indicates the predictor with the biggest t-statistic. Abbreviations: NSLC, n-since-last-click; NTS, n-times-seen; RT: reaction-time.

Region	Subject	Ch	match	NSLC	first_click	NTS	next_match	RT	board_size	x_pos.	y_pos.	distance	animal	food	person	vehicle
fusiform	XW03	12							**				** X			
fusiform	XW03	28		***				**							*** X	
fusiform	XW07	12	***	***									*** X	**		
fusiform	XW07	53		**				***							*** X	**
fusiform	XW08	62													*** X	
fusiform	BWH52	14													*** X	
fusiform	BCH3	138	*** X	***	**				***	**					**	
fusiform	BCH4	69											** X			
inferioparietal	BCH5	14													*** X	
inferiortemporal	XW08	41											**	***	*** X	
inferiortemporal	XW08	42						** X		**			**			
lateraloccipital	XW11	36													*** X	
lateraloccipital	BWH9	72											** X			
lateralorbitofrontal	BWH8	23		**	***											*** X
lateralorbitofrontal	BWH8	74		**				*** X							**	
lateralorbitofrontal	BCH3	10											*** X		***	
lingual	XW15	60	**										*** X	***	***	
middletemporal	XW08	65	**					**					**	** X		
middletemporal	XW08	66		**									**	** X	**	
middletemporal	XW11	39													** X	
parahippocampal	XW01	10	***										*** X	***	***	
parorbitalis	BWH8	76		**				**								*** X
parstriangularis	XW02	29		**												** X
precentral	XW03	55	*** X				**						**	***		
precentral	BWH6	66													** X	
superioparietal	XW03	72	*** X	**					**						**	
superioparietal	BWH9	60											*** X			

E White matter figures

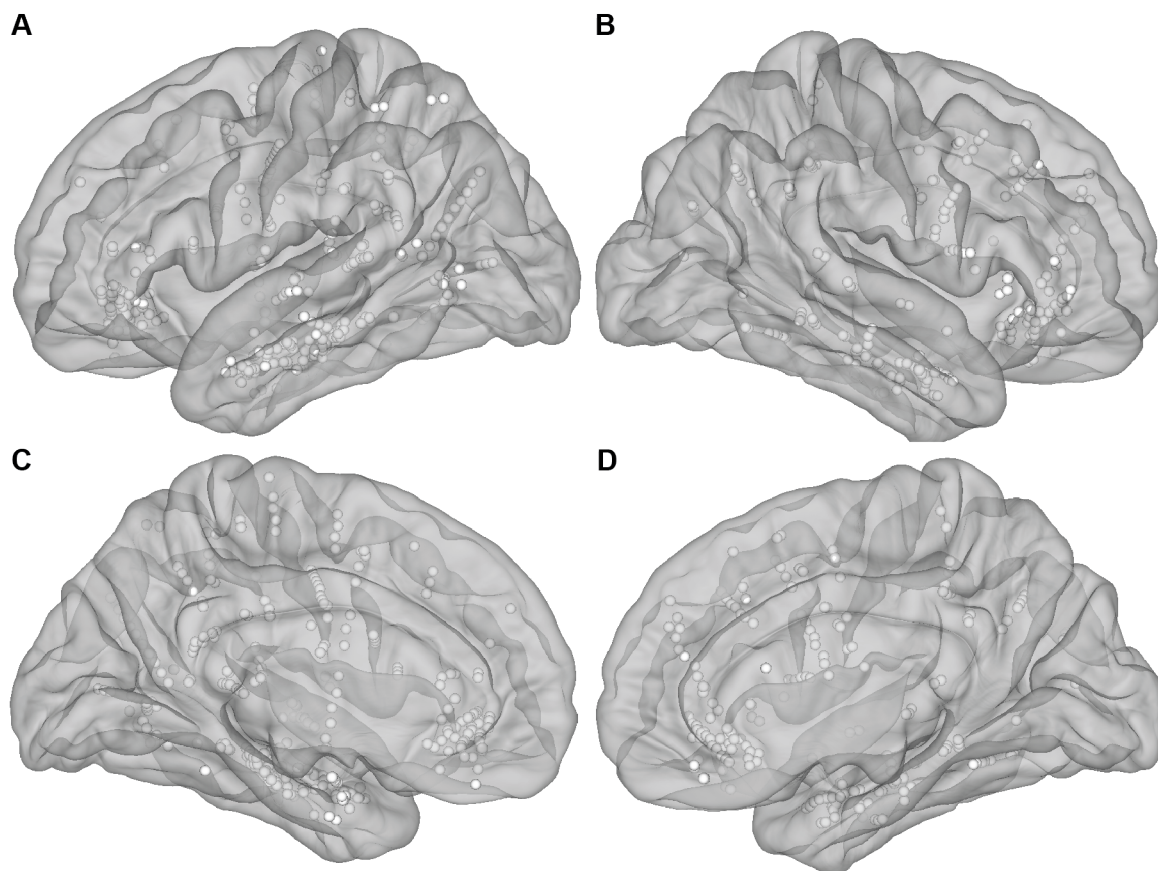


Figure E.1: Locations of electrodes in the white matter. Each sphere reflects one of each pair of nearby electrodes that were bipolarly referenced ($n=493$), with different views: **A**: left lateral; **B**: right lateral; **C**: left medial; **D**: right medial.

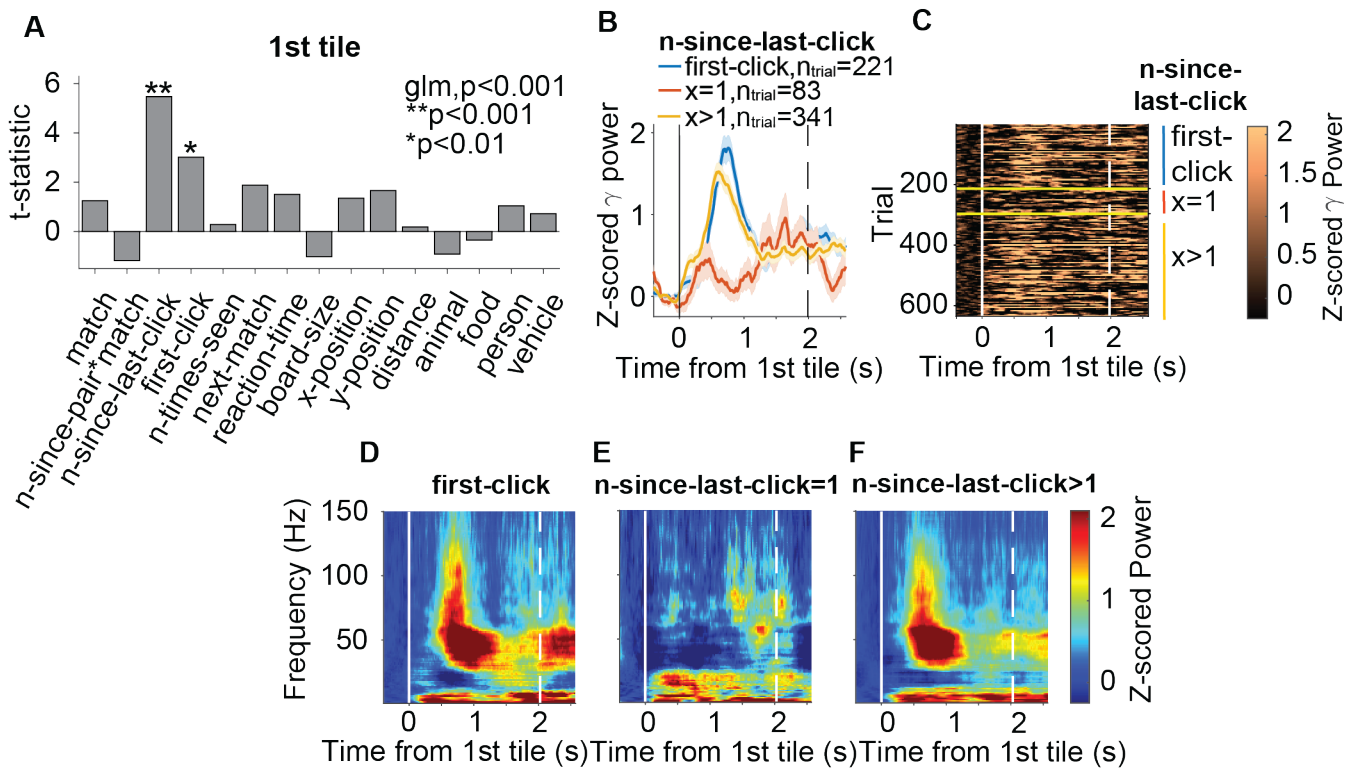


Figure E.2: An example of a white matter electrode located close to the lateral orbitofrontal cortex that presented *first-click* and *n-since-last-click* as significant predictors. **A.** T-statistic of each predictor in the GLM. Asterisks indicate significant predictors for the gamma power AUC. **B.** Z-scored gamma power aligned to the 1st tile onset for *first-click* (blue line), clicked in the previous tile (red line) or clicked more than one tile ago (yellow line) tiles. Shaded error bars indicate SEM. Dashed line indicates the mean RT. **C:** Raster plots showing the z-scored gamma power in individual trials ordered by *first-click* and then from smaller to larger *n-since-last-click*; division indicated by yellow horizontal lines and colored vertical lines. **D-F.** Spectrograms showing the power aligned to the 1st tile onset during *first-click* (**D**), *n-since-last-click*=1 (**E**), and *n-since-last-click*>1 (**F**).

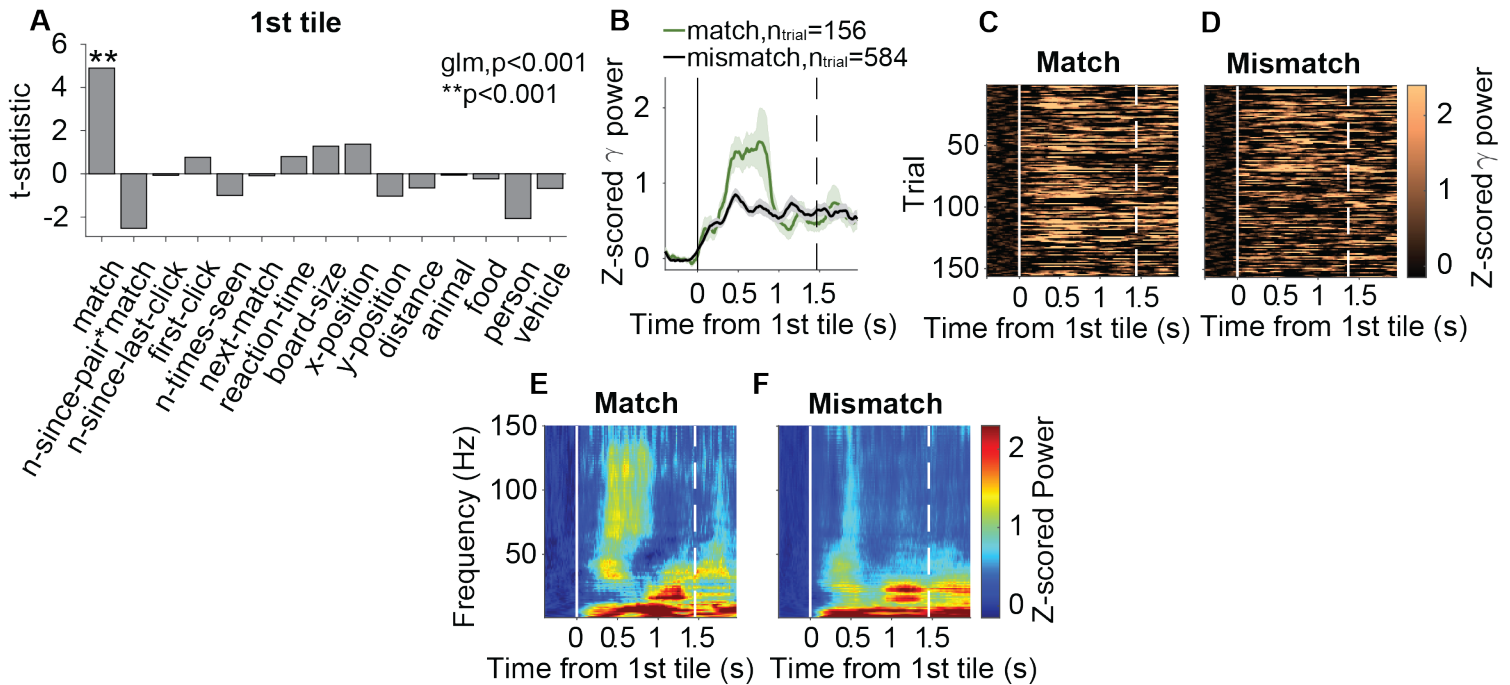


Figure E.3: An example white matter electrode located close to the entorhinal cortex where *match* was a significant predictor for gamma activities during the 1st tile. **A.** T-statistic of each predictor in the GLM for the 1st tile. Asterisks indicate significant predictors for the gamma power AUC. **B.** Z-scored gamma power during match (green) and mismatch (black) trials aligned to the 1st tile onset (solid line). Dashed line indicates the mean reaction time. Legend denotes the number of match and mismatch trials. Shaded error bars indicate SEM. **C-D.** Raster plots showing the z-scored gamma power in individual trials. For display purpose, trial number of match and mismatch was equalized (Methods). **E-F.** Spectrograms showing the band power during match and mismatch trials aligned to the 1st tile onset.

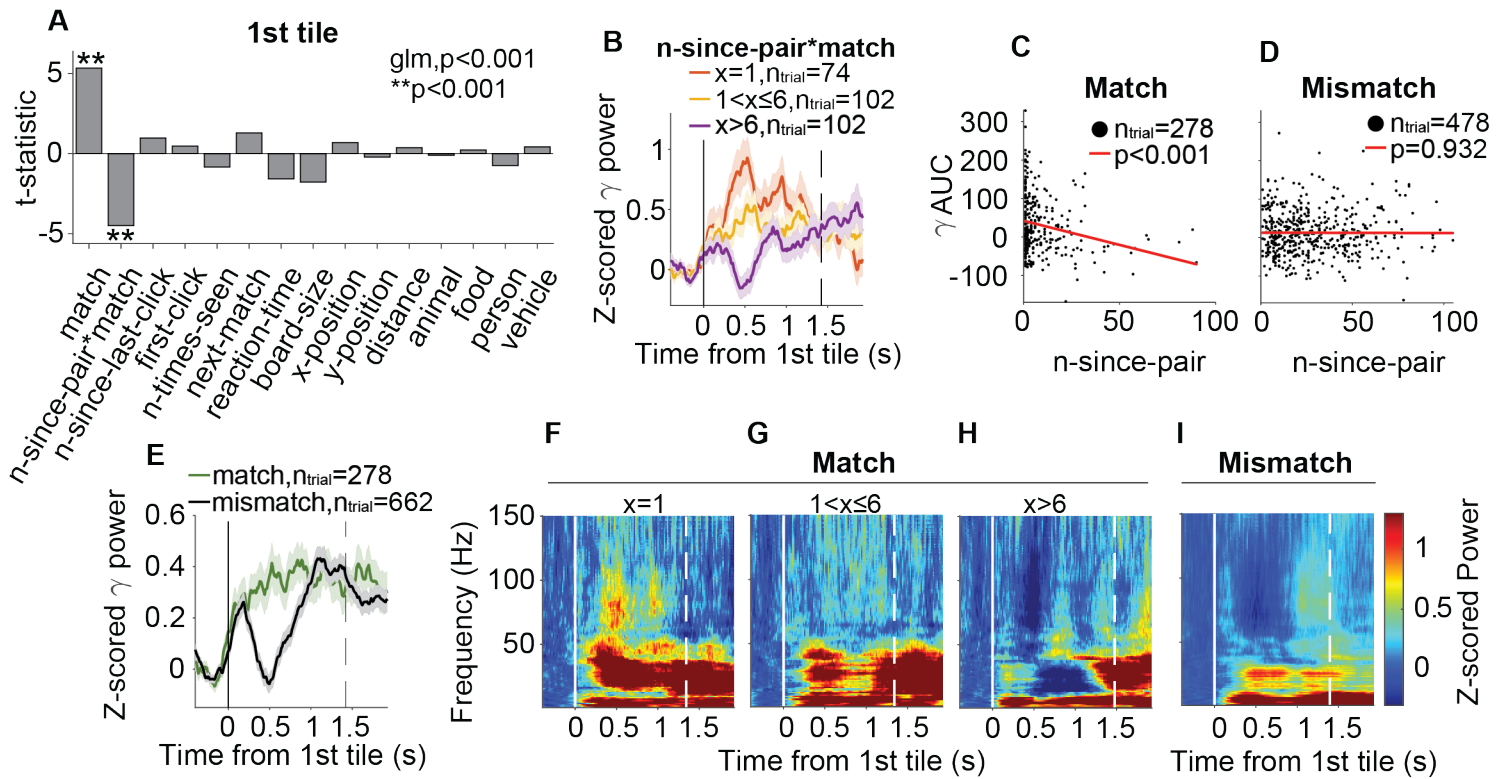


Figure E.4: An example white matter electrode located close to the parsopercularis where n -since-pair*match was a significant predictor for gamma activities during the 1st tile]. **A.** T-statistic of each predictor in the GLM for the 1st tile. Asterisks indicate significant predictors for the gamma power AUC. **B.** Z-scored gamma power grouped by different n -since-pair ranges for match trials aligned to the 1st tile onset (solid line). Dashed line indicate the mean reaction time. Shaded error bars indicate SEM. **C-D.** Scatter plots of AUC gamma power vs. n -since-pair for match (**C**) and mismatch (**D**). **E.** Z-scored gamma power during match (green) and mismatch (black) trials aligned to the 1st tile onset (solid line). Dashed line indicates the mean reaction time. Legend denotes the number of match and mismatch trials. Shaded error bars indicate SEM. **F-G.** Spectrograms showing the band power aligned to the 1st tile for different n -since-pair ($x=n$ -since-pair) values for match trials. **I** Spectrogram for mismatch trials.

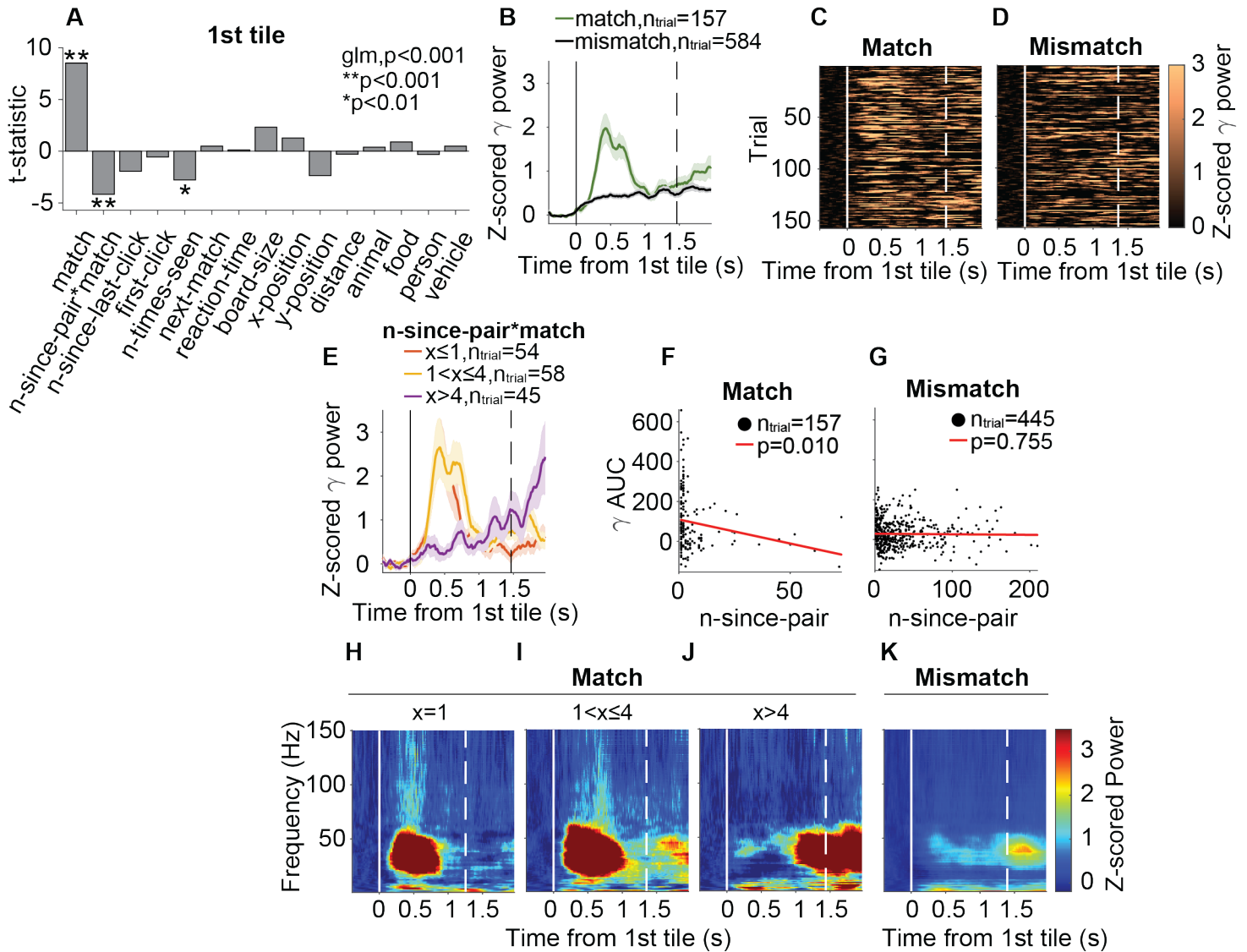


Figure E.5: An example white matter electrode located close to the LOF where *n-since-pair*match* was a significant predictor for gamma activities during the 1st tile]. **A.** T-statistic of each predictor in the GLM for the 1st tile. Asterisks indicate significant predictors for the gamma power AUC. **B.** Z-scored gamma power during match (green) and mismatch (black) trials aligned to the 1st tile onset (solid line). **C-D.** Raster plots showing the z-scored gamma power in individual trials. For display purpose, trial number of match and mismatch was equalized (Methods). **F.** Z-scored gamma power grouped by different *n-since-pair* ranges for match trials aligned to the 1st tile onset (solid line). Dashed line indicate the mean reaction time. Shaded error bars indicate SEM. **G-H.** Scatter plots of AUC gamma power vs. *n-since-pair* for match (**G**) and mismatch (**H**). Each dot represents data from one trial. Red lines represent linear fits of the data. **I-K.** Spectrograms showing the band power aligned to the 1st tile for different *n-since-pair* ($x=n-since-pair$) values for match trials. **L.** Spectrogram showing the band power aligned to the 1st tile for mismatch trials.

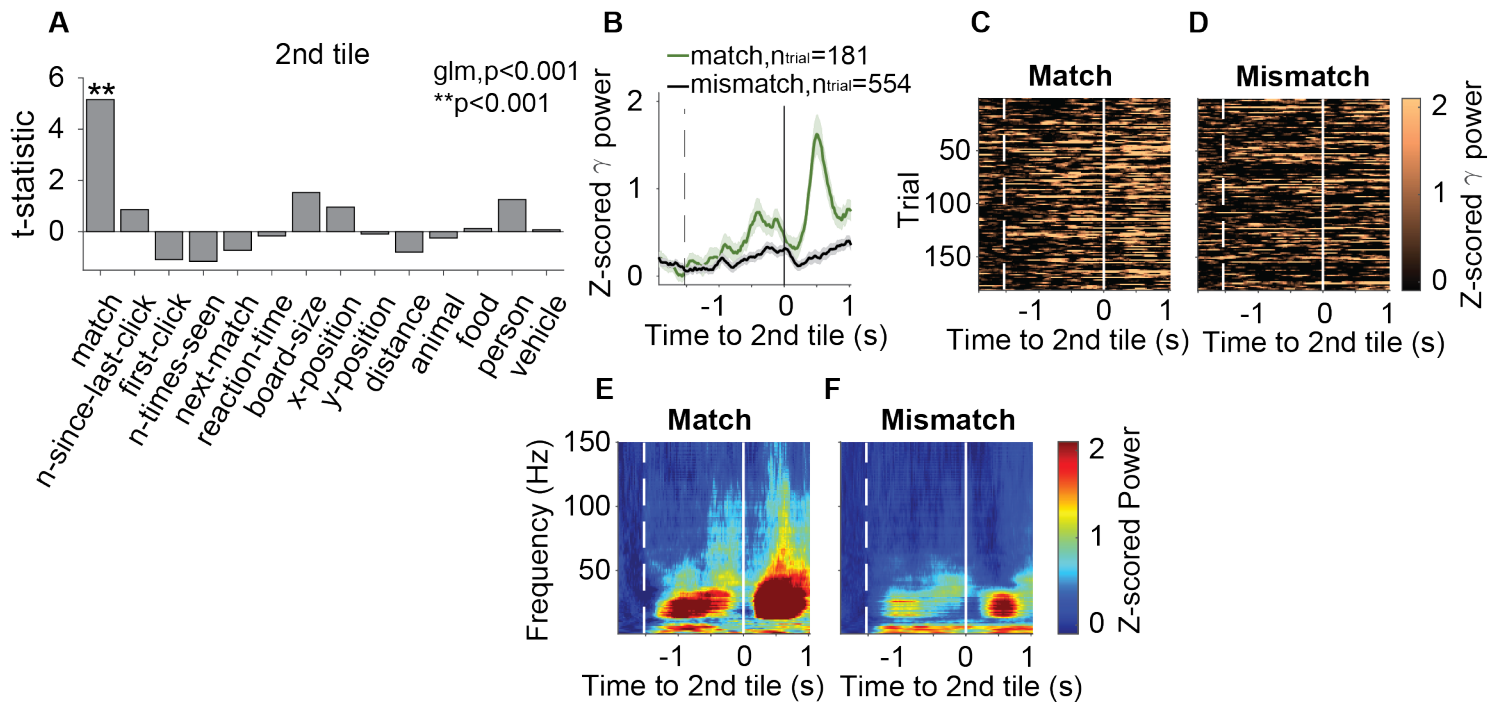


Figure E.6: An example white matter electrode located close to the the lateral orbitofrontal cortex where *match* was a significant predictor for gamma activities after 2nd tile. **A.** T-statistic of each predictor in the GLM for the 2nd tile. **B.** Z-scored gamma power during matched and mismatched trials aligned to the 2nd tile onset (solid line). Dashed line indicates the mean onset of the 1st tile. **C-D.** Raster plots showing the z-scored gamma power in individual trials. Number of match and mismatch trials was equalized (Methods). **E-F.** Spectrograms showing the band power during matched and mismatched trials aligned to the 2nd tile onset.

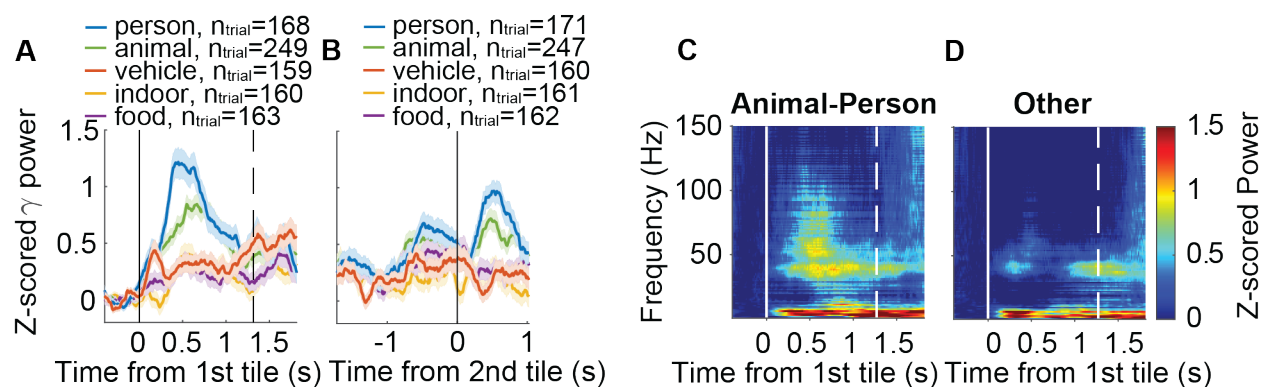


Figure E.7: An example white matter electrode located close to the the fusiform gyrus that was selective for images containing animals and persons. **A, B.** Z-scored gamma power for tiles containing a person (blue), animal (green), vehicle (red), indoor (yellow), food (purple) image category, for the 1st tile (**A**) and the 2nd tile (**B**). **C-D.** Spectrograms aligned to the 1st tile showing the band power for the preferred (animal, person; **C**) and non-preferred (**D**) image categories. 42